AD-A145 626 A GENERALIZED SOLUTION TO A CLASS OF PRINTED CIRCUIT ANTENNAS. (U) CALIFORNIA UNIV LOS ANGELES INTEGRATED ELECTROMAGNETICS LAB P B KATEHI-TSEREGOUNIS 15 JUN 84 1/2

UNCLASSIFIED UCLA-ENG-84-14 DAAG29-83-K-0067 F/G 9/5 NL

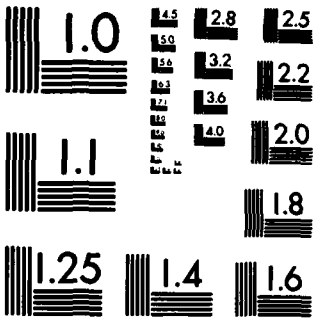

MICROCOPY RESOLUTION TEST CHART
NATIONAL BUREAU OF STANDARDS-1963-A

UCLA School of Engineering and Applied Science

"A Generalized Solution to a Class of Printed Circuit Antennas"

By: Pisti B. Katehi-Tseregounis

Integrated Electromagnetics Laboratory
Report No. 14
UCLA ENG-84-14
June 15, 1984

Sponsored by Research Contracts:
U.S. Army Contract DAAG 29-83-K-0067
U.S. Navy Contract N00014-79-C0856 Mod. P0005

UNCLASSIFIED
SECURITY CLASSIFICATION OF THIS PAGE (When Data Entered)

REPORT DOCUMENTATION PAGE		READ INSTRUCTIONS BEFORE COMPLETING FORM
1. REPORT NUMBER Report No. 14	2. GOVT ACCESSION NO. AD-A145626	3. RECIPIENT'S CATALOG NUMBER
4. TITLE (and Subtitle) "A Generalized Solution to a Class of Printed Circuit Antennas"		5. TYPE OF REPORT & PERIOD COVERED 6. PERFORMING ORG. REPORT NUMBER UCLA-ENG-84-14
7. AUTHOR(s) P. B. Katehi-Tseregounis		8. CONTRACT OR GRANT NUMBER(s) DAAG 29-83-K-0067
9. PERFORMING ORGANIZATION NAME AND ADDRESS Electrical Engineering Department UCLA 7732 Boelter Hall Los Angeles, CA 90024		10. PROGRAM ELEMENT, PROJECT, TASK AREA & WORK UNIT NUMBERS
11. CONTROLLING OFFICE NAME AND ADDRESS U. S. Army Research Office Post Office Box 12211 Research Triangle Park, NC 27709		12. REPORT DATE June 15, 1984 13. NUMBER OF PAGES 133
14. MONITORING AGENCY NAME & ADDRESS(if different from Controlling Office) U.S. Army Research Triangle Park North Carolina 27709 U.S. Navy Naval Weapons Center China Lake CA		15. SECURITY CLASS. (of this report) Unclassified 15a. DECLASSIFICATION/DOWNGRADING SCHEDULE
16. DISTRIBUTION STATEMENT (of this Report) Approved for public release; distribution unlimited.		
17. DISTRIBUTION STATEMENT (of the abstract entered in Block 20, if different from Report) NA		
18. SUPPLEMENTARY NOTES The view, opinions, and/or findings contained in this report are those of the author(s) and should not be construed as an official Department of the Army position, policy, or decision, unless so designated by other documentation.		
19. KEY WORDS (Continue on reverse side if necessary and identify by block number)		

20. ABSTRACT (Continue on reverse side if necessary and identify by block number)

This dissertation deals with the theory and design of antennas excited by a microstrip transmission line or by a gap generator. The antennas and the strip transmission line may be embedded inside or printed on the substrate. A theoretical approach is implemented which accounts accurately for the physical effects involved including surface waves. The Green's function has been obtained by synthesizing the fields of Hertzian dipoles which are oriented in arbitrary directions and which are printed on or embedded in the substrate. The method of solution is based on solving the Pocklington integral equation by employing the method of moments with proper choice of expansion and testing functions. The excitation mechanism is taken into account effectively by considering it as part of the antenna.

DD FORM 1 JAN 73 1473 EDITION OF 1 NOV 65 IS OBSOLETE

UNCLASSIFIED
SECURITY CLASSIFICATION OF THIS PAGE (When Data Entered)

(6)

UNIVERSITY OF CALIFORNIA
Los Angeles

A Generalized Solution to a Class of Printed Circuit Antennas

A dissertation submitted in partial satisfaction of the requirements for the degree Doctor of Philosophy in Engineering

By

Pisti B. Katehi-Tseregounis

1984

The dissertation of Pisti B. Katehi-Tseregounis is approved.

Nicolaos G. Alexopoulos
Committee Chair

Robert S. Elliott

Harold Fetterman

Nathaniel Grossman

Reiner Stenzel

University of California, Los Angeles

1984

This dissertation is dedicated to my husband, Spyros, and my son, Iraklis.

TABLE OF CONTENTS

TABLE OF CONTENTS (CONT'D)

TABLE OF CONTENTS (CONT'D)

LIST OF FIGURES

LIST OF FIGURES (CONT'D)

LIST OF FIGURES (CONT'D)

LIST OF FIGURES (CONT'D)

ACKNOWLEDGMENTS

I wish to express my sincere gratitude to Professor N. G. Alexopoulos for proposing the topic, for his guidance and encouragement which greatly aided me to complete this research.

I also wish to thank Professor R. S. Elliott for his interest, guidance, and many helpful suggestions as well as Professor N. Grossman for his assistance on this research.

I owe a special expression of appreciation to my husband who has been a constant source of encouragement and to my parents for their continuous moral and material support.

I would also like to thank Zonta International for partially supporting my studies.

Finally, I wish to thank Ms. Irene C. Andreadis for typing this manuscript.

VITA

January 29, 1954--Born, Athens, Greece

1977--B.S., National Technical University of Athens, Greece

1977-1979--Field Work, Athens, Greece, under the Naval Research Laboratory

1979-1981--M.S., University of California, Los Angeles

1981-1984--Ph.D., University of California, Los Angeles

PUBLICATIONS

Marcopoulos, D., Katehi P. 1977	Directive Microstrip Antennas 7th European Microwave. Conference, Proceedings, Copenhagen, Denmark.
Uzunoglu, N.K., Katehi, P.B. 1980	Coupled Microstrip Disc Resonators. IEEE Trans. on MTT, Vol. 28, No. 2.
Rana, I.E., Alexopoulos, N.G. Katehi, P.B. 1981	Theory of Microstrip Yagi-Uda Arrays. Radio Science, Vol. 16, Nov.-Dec.
Katehi, P.B., Alexopoulos, N.G. 1983	On the Effect of Substrate Thickness and Permittivity on Printed Dipole Properties. IEEE Trans. on AP-S, Vol. 31, No. 1, January.
Alexopoulos, N.G., Katehi, P.B., Rutledge, D.B. 1983	Substrate Optimization for Integrated Circuit Antennas. IEEE Trans. on MTT, Vol. 31, No. 7, July.

Katehi, P.B., Alexopoulos, N.G.
1983

Real Axis Integration of Sommerfeld Integrals with Application to Printed Circuit Antennas.
Journal of Math. Physics, 24(3), March.

ABSTRACT OF THE DISSERTATION

A Generalized Solution to a Class
of Printed Circuit Antennas

By

Pisti B. Katehi-Tseregounis

Doctor of Philosophy in Engineering

University of California, Los Angeles, 1984

Professor Nicolaos G. Alexopoulos, Chair

This dissertation deals with the theory and design of antennas excited either by a microstrip transmission line or by a gap generator. The antennas and the strip transmission line may be embedded inside or printed on the substrate. A theoretical approach is implemented which accounts accurately for the physical effects involved including surface waves. The Green's function has been obtained by synthesizing the fields of Hertzian dipoles which are oriented in arbitrary directions and which are printed on or embedded in the substrate. The method of solution is based on solving the Pocklington integral equation by employing the method of moments with proper choice of expansion and testing functions. The excitation mechanism is taken into account effectively by considering it as part of the antenna. The current distribution is obtained both on the transmission line and the printed circuit antennas by matrix inversion. The method accounts for conductor thickness and for

arbitrary substrate parameters.

As an example, printed strip dipoles excited by a transmission line embedded in the substrate or by a voltage gap generator are considered. Current distribution, self impedance and reflection coefficient for the case of the transmission line excitation as well as input impedance, resonant length, resonant resistance and radiation patterns for the case of the gap voltage excitation are obtained for a variety of antenna arrangements. A serious amount of effort is also being placed in evaluating the importance of higher order surface wave modes which are determined by the relative dielectric constant and the thickness of the substrate. Comparison of the theoretical results to experimental data for the case of an electromagnetically coupled printed strip dipole to a strip transmission line shows excellent agreement.

CHAPTER 1

INTRODUCTION

Integrated or printed circuit antennas are a natural evolution of integrated circuit components and are finding increased use in the microwave, millimeter and far infrared frequency ranges. Therefore, the development of antennas which are amenable to integration with other printed circuit elements is of significant technological importance.

The microstrip antenna concept dates back about 30 years to work in the United States by Deschamps [1] and in France by Gutton and Baissinot [2]. Shortly thereafter, Lewin [3] investigated radiation from stripline discontinuities. Additional studies were undertaken in the late 1960's by Kaloi [54] who studied basic rectangular and square configurations (patches). However, the inherent advantages of antenna elements (conformality to a given surface, light weight, negligible volume, inexpensiveness), were not put to widespread practice until the 1970's [4]-[21]. The environmental and technological constraints having been resolved, the task remained to develop analytical methods which would provide accurate design criteria. Mathematical modeling of the basic microstrip radiator was carried out initially either by the application of transmission line analogies to simple rectangular patches fed at the center of a radiating wall, or by an open resonator model [9]-[21]. The former approach gives a heuristic explanation of the radiation

properties of the antenna, while the latter provides a more accurate prediction of the antenna characteristics. However, both models apply mainly to the dominant resonator model and their accuracy is questionable for higher order modes, especially because they do not account for the excitation of surface waves.

Surface waves have an important effect on the printed circuit antenna current distribution, as well as input impedance, resonant length, bandwidth and efficiency [34]-[37]. In addition, since surface waves are cylindrical waves in nature, they decay only as the inverse square root of the distance from their source and for this reason they can be significant in mutual impedance computations [26], an important parameter in phased array design. It has been shown that, regardless of the substrate thickness and dielectric permittivity, the dominant surface wave mode is always excited. The power propagating in this mode is a function of the characteristics of the substrate. As more energy is trapped in the substrate, the microstrip antenna becomes less efficient [35]. In many applications, such as in the millimeter or far infrared region [29]-[31], today's technology provides substrates which are several wavelengths thick. This permits the propagation of many TM and TE waves in the substrate, further complicating the design. These modes can also cause impairment of efficiency. It becomes evident from this discussion that a theoretical approach

should be implemented which accounts accurately for all the physical effects involved including surface waves. Such an approach excludes either of the previously mentioned techniques and relies on treating the microstrip element as an antenna rather than a transmission line section or as a resonator.

A microstrip antenna is usually excited either by the inner conductor of a coaxial transmission line [39] (Fig. 1a) or by a microstrip transmission line [41]-[43] printed or embedded in the substrate (Fig. 1b). From these two ways of excitation, the latter has demonstrated that a microstrip antenna electromagnetically (EM) coupled to a microstrip line makes a desirable element for one- and two-dimensional antenna arrays.

Recently, Oltman and Huebner [40], and later, Stern and Elliott [41]-[42] experimentally studied this radiator as an element as well as part of a two-dimensional array and they described a design procedure with the objectives of an input match and a desired radiation pattern.

In this present work, strip dipoles printed or embedded in the substrate excited either by a gap generator or a microstrip transmission line are considered. The thickness of the strips is considered finite and the widths of the dipole and transmission line are assumed to be much smaller than the wavelength so that the transverse components of the current give a second order effect. The current distri-

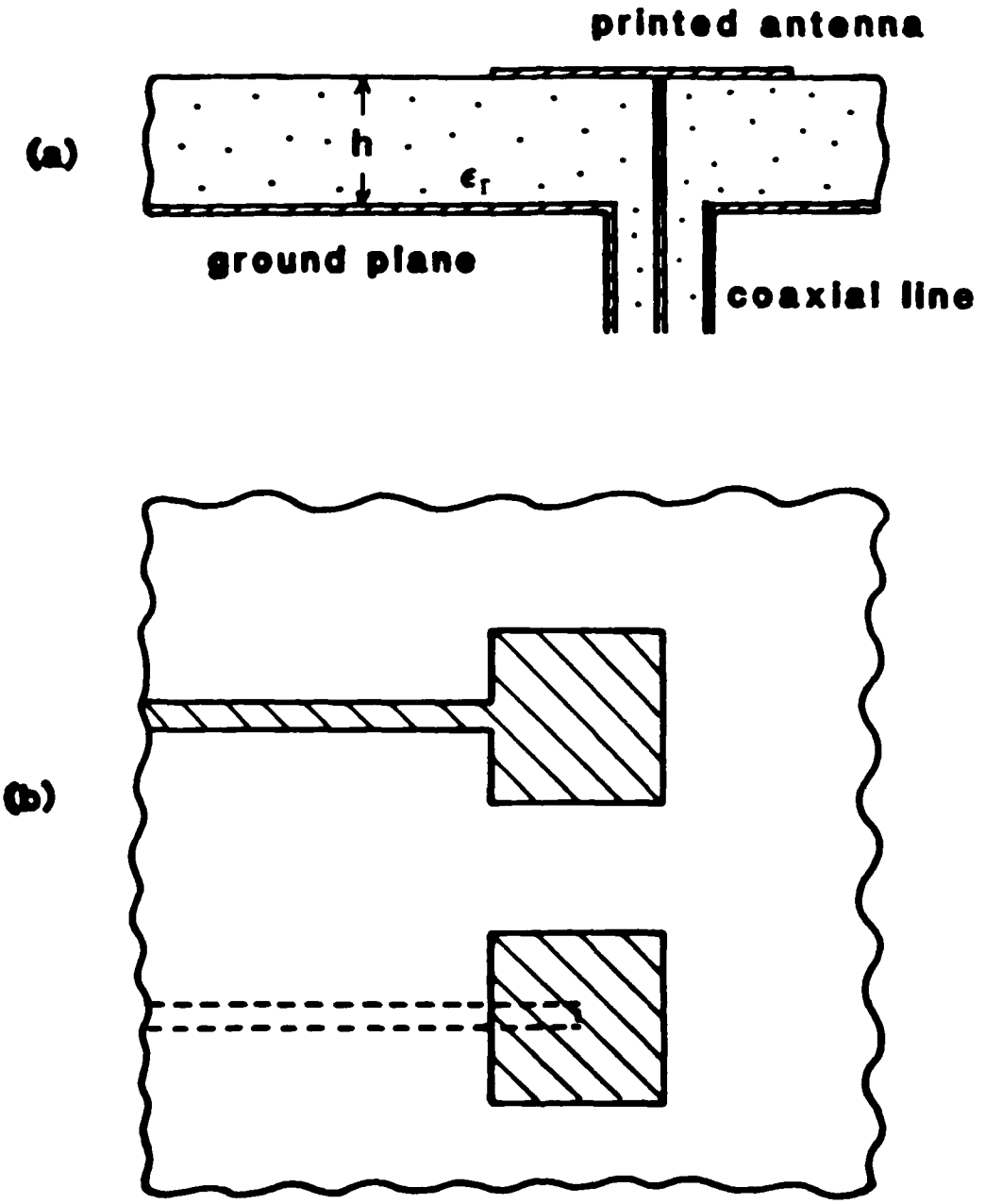

Figure 1

Different Excitation Mechanisms for Printed Antennas

bution on the antenna is obtained first by solving a two-dimensional Pocklington's Integral Equation [38]. The Green's function in this case can be obtained by synthesizing the fields of Hertzian dipoles which are oriented in arbitrary directions and which are printed or embedded in the substrate, therefore accounting properly for all the boundary conditions pertinent to the problem.

An analytical solution of the two-dimensional Pocklington's integral equation is precluded due to the immense complexity of the problem. The use of numerical techniques which discretize the integral equation and obtain the current distribution by matrix inversion is necessary. A numerical method which has found widespread and successful use for the solution of Pocklington type integral equations is the Method of Moments [25]-[28]. For the present application, the Green's function relevant to the problem is given by Sommerfeld-type integrals which require special integration techniques when field and source point coincide [38].

For the case of the antenna excited by a voltage gap generator, the input impedance is defined as the ratio of the applied voltage to the input current and resonant length, resonant resistance, bandwidth and efficiency are evaluated as function of the substrate characteristics. In the case of a dipole EM coupled to a microstrip line, transmission line (T.L.) theory is used to derive a form for the self-

impedance. The application of T.L. theory becomes possible by virtue the fact that the distance of the feeding line from the ground has been kept always very small compared to wavelength in the dielectric so that most of the contribution for the electric field under the microstrip line results from a dominant TEM-like mode. This leads to a design procedure which, for a given substrate, permits determination of the length of the dipole, overlap and offset so that a desired input match is achieved.

A serious amount of effort has also been invested in determining the effect of the substrate thickness and relative permittivity on the radiation properties of printed circuit dipoles (PCD's). A trade-off between substrate thickness and resonant input impedance, bandwidth and radiation efficiency is presented for PTFE glass, quartz and GaAs substrates. The E- and H-plane normalized power patterns are also examined as a function of ε_r and h, and it is shown that even for thin substrates, multiple-beam radiation can result for certain values of ε_r through the excitation of surface waves.

Throughout this work, the cost of the computer programs was kept very low with the application of special analytical and numerical techniques for the evaluation of the elements of the impedance matrix. These techniques will be described since they are quite general and apply to any kind of printed antenna.

CHAPTER 2

THE GREEN'S FUNCTION AND POCKLINGTON'S INTEGRAL EQUATION

2-1. Derivation of the Green's Function

This chapter contains a development of the Green's Function pertinent to the problem of strip or patch antennas printed on and/or embedded in a grounded dielectric substrate of thickness h and relative dielectric constant ε_r.

In order to formulate the Green's function, two elementary horizontal electric dipoles (HED's) are considered to be at the positions $(x_1', y_1', 0)$ and $(x_2', y_2', -b_s)$ as shown in Figure 2.1. The assumed time dependence is $e^{j\omega t}$ and it is suppressed throughout the dissertation. The electromagnetic field at any point due to these two dipoles is the superposition of the fields arising from each one separately

$$\vec{H}^i = \vec{H}_1^i + \vec{H}_2^i \qquad (i = 1,2) \qquad (2.1)$$

$$\vec{E}^i = \vec{E}_1^i + \vec{E}_2^i \qquad (2.2)$$

with $(\vec{H}^1, \vec{E}^1)$ and $(\vec{H}^2, \vec{E}^2)$ the electromagnetic fields in medium (1) and (2) respectively. Maxwell's equations now take the following form:

$$\vec{\nabla} \times \vec{H}_\nu^i = \vec{J}_\nu + j\omega\varepsilon_i \vec{E}_\nu^i \qquad (2.3)$$

$$\vec{\nabla} \times \vec{E}_\nu^i = -j\omega\mu_o \vec{H}_\nu^i \qquad (2.4)$$

$$\vec{\nabla} \cdot \vec{H}_\nu^i = 0 \qquad (2.5)$$

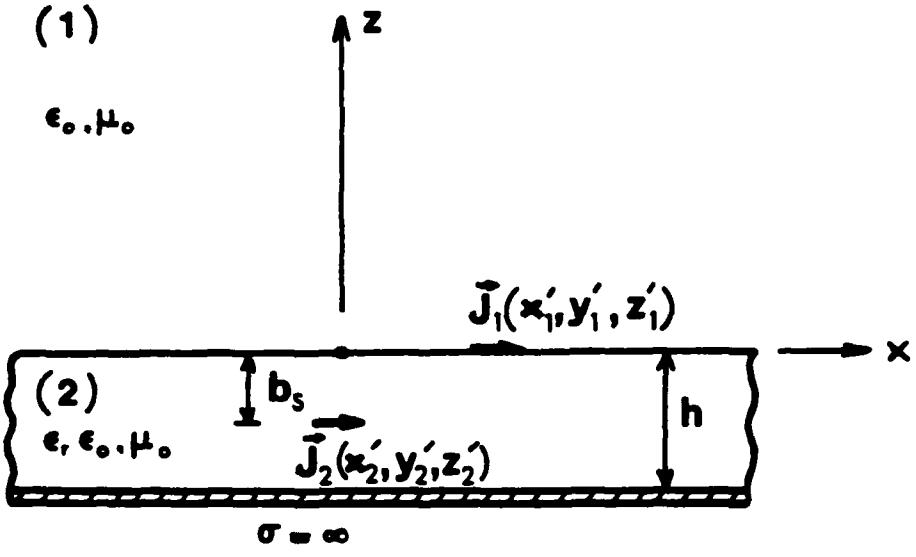

Figure 2.1

HED's Printed on and Embedded in a Grounded Dielectric Slab

$$\vec{\nabla}\cdot\vec{E}_\nu^i = \frac{\rho_\nu}{\varepsilon_i} \tag{2.6}$$

$$\vec{\nabla}\cdot\vec{J}_\nu = -j\omega\rho_\nu \tag{2.7}$$

$$\varepsilon_i = \begin{cases} \varepsilon_o & i=1 \\ \varepsilon_r\varepsilon_o & i=2 \end{cases} \tag{2.8}$$

where the superscript i indicates the medium with the subscript ν indicating the source. The potential function

$$\vec{B}_\nu^i = \mu_o\vec{H}_\nu^i = -\nabla\times\vec{A}_\nu^i \tag{2.9}$$

is now introduced. $\vec{A}_\nu^i$ will turn out to be the vector potential function in medium (i) due to source (ν). A substitution of (2.9) into the curl equation for $\vec{E}_\nu^i$ gives the result

$$\vec{\nabla}\times(\vec{E}_\nu^i - j\omega\vec{A}_\nu^i) = 0 \quad . \tag{2.10}$$

Since $\vec{\nabla}\times(\vec{\nabla}\phi_\nu^i) = 0$, it follows that

$$\vec{E}_\nu^i = j\omega\vec{A}_\nu - \vec{\nabla}\phi_\nu^i \tag{2.11}$$

with ϕ_ν^i the scalar potential in medium (i) due to the source (ν). The relationship between ϕ_ν^i and A_ν^i can be obtained by substituting (2.9) and (2.11) into (2.3), i.e.

$$\vec{\nabla}\times\vec{\nabla}\times\vec{A}_\nu^i = \vec{\nabla}(\vec{\nabla}\cdot\vec{A}_\nu^i) - \nabla^2\vec{A}_\nu^i = -\mu_o\vec{J}_\nu + k_i^2\vec{A}_\nu^i + j\omega\varepsilon_i\mu_o\vec{\nabla}\phi_\nu^i \tag{2.12}$$

If one considers the Lorentz condition

$$\vec{\nabla}\cdot\vec{A}_\nu^i = j\omega\varepsilon_i\mu_o\phi_\nu^i \tag{2.13}$$

equation (2.12) reduces to

$$(\nabla^2 + k_i^2)\vec{A}_\nu^i = \mu_o \vec{J}_\nu \tag{2.14}$$

where

$$\vec{J}_\nu = \hat{x}\delta(\vec{r}-\vec{r}_\nu)$$

The Lorentz condition enables one to write the electromagnetic field in medium (i) due to source (ν), since it follows that

$$\vec{E}_\nu^i = -\frac{1}{j\omega\epsilon_i\mu_o}\{k_i^2\vec{A}_\nu^i + \vec{\nabla}\vec{\nabla}\cdot A_\nu^i\} \tag{2.15}$$

$$\vec{H}_\nu^i = \vec{\nabla}x\vec{A}_\nu^i \tag{2.16}$$

where

$$k_i^2 = \begin{cases} \omega^2\epsilon_o\mu_o & i = 1 \\ \omega^2\epsilon_r\epsilon_o\mu_o & i = 2 \end{cases}$$

For the case of infinitesimally small dipole sources oriented along the x or y axis the solution to the inhomogeneous equation (2.14), when that solution also satisfies the specified boundary conditions, is called Green's function and is given by

$$(\nabla^2 + k_i^2)\vec{F}_\nu^i = \frac{j\omega\mu_o}{k_1^2}\,\delta(\vec{r} - \vec{r}_\nu)\hat{x},\hat{y} \tag{2.17}$$

For an elementary dipole of arbitrary orientation, this vector function becomes dyadic and is the solution of the following inhomogeneous equation

$$(\nabla^2 + k_i^2)\bar{\vec{F}}_\nu^i = \frac{j\omega\mu_o}{k_i^2}\,\bar{\bar{I}}\,\delta(\vec{r} - \vec{r}_\nu) \tag{2.18}$$

where $\bar{\bar{I}}$ is the unit dyadic or idemfactor given by $\hat{x}\hat{x} + \hat{y}\hat{y} + \hat{z}\hat{z}$.

Considering all the equations above, one can prove [45] that for the case of a general current $\vec{J}_\nu$ the electric field is given by

$$\vec{E}^i_\nu(\vec{r}) = \int_{V_\nu} [k_i^2 \bar{\bar{I}} + \vec{\nabla}\vec{\nabla}] \cdot \bar{\bar{F}}^i_\nu(\vec{r}/\vec{r}') \cdot \vec{J}_\nu(\vec{r}')d\tau' \tag{2.19}$$

with the integration extended over the volume which contains all the current sources. One can also deal directly with the equation

$$\vec{\nabla}x\vec{\nabla}x\vec{E}^i_\nu - k_i^2\vec{E}^i_\nu = -j\omega\mu_o\vec{J}_\nu \tag{2.20}$$

which the electric field satisfies. In this case, the the dyadic Green's function can be defined as that solution to the inhomogeneous equation

$$\vec{\nabla}x\vec{\nabla}x\bar{\bar{G}}^i_\nu - k_i^2\bar{\bar{G}}^i_\nu = -j\omega\mu_o\bar{\bar{I}}\delta(\vec{r}-\vec{r}_\nu) \tag{2.21}$$

which also satisfies the specified boundary conditions. Using equations (2.20) and (2.21), one can prove [45], [46] that

$$\vec{E}^i_\nu(\vec{r}) = \int_{V_\nu} \bar{\bar{G}}^i_\nu(\vec{r}/\vec{r}') \cdot \vec{J}_\nu(r')d\tau' \tag{2.22}$$

from equations (2.20) and (2.22) the following relation is true for every $\vec{r}\epsilon V$:

$$\int_{V_\nu} \{\bar{\bar{G}}^i_\nu(\vec{r}/\vec{r}') - (k_i^2\bar{\bar{I}} + \vec{\nabla}\vec{\nabla}) \cdot \bar{\bar{F}}^i_\nu(\vec{r}/\vec{r}')\} \cdot \vec{J}_\nu(\vec{r})d\tau' = 0 \quad \forall \vec{r}\epsilon V \tag{2.23}$$

Therefore, it can be concluded that

$$\bar{\bar{G}}_\nu^i(\vec{r}/\vec{r}') = (k_i^2\bar{\bar{I}} + \vec{\nabla}\vec{\nabla}) \cdot \bar{\bar{F}}_\nu^i(\vec{r}/\vec{r}') \qquad (2.24)$$

$$\forall \vec{r},\vec{r}' \epsilon V$$

For the total field, equations (2.19) and (2.22) can be written as

$$\vec{E}_\nu^i(\vec{r}) = \sum_{\nu=1,2} \int_{V_\nu} \bar{\bar{G}}_\nu^i(\vec{r}/\vec{r}') \cdot \vec{J}_\nu(\vec{r}')d\tau' =$$

$$= \sum_{\nu=1,2} \int_{V_\nu} [k_i^2\bar{\bar{I}} + \vec{\nabla}\vec{\nabla}] \cdot \bar{\bar{F}}_\nu^i(\vec{r}/\vec{r}') \cdot$$

$$\vec{J}_\nu(\vec{r}')d\tau' \qquad (2.25)$$

The solution which satisfies equations (2.18) and the appropriate boundary conditions in medium (i) consists of two parts; the secondary solution which is the solution to the corresponding homogeneous equation and the primary solution which is the particular solution to the wave equation. For the case of a horizontal dipole current along the x direction $\vec{J}_\nu(\vec{r}')$, the dyadic function $\bar{\bar{F}}_\nu^i(\vec{r}/\vec{r}')$ has the form

$$\bar{\bar{F}}_\nu^i(\vec{r}/\vec{r}') = F_{\nu xx}^i \hat{x}\hat{x} + F_{\nu zx}^i \hat{z}\hat{x} \qquad (2.26)$$

where the components $F_{\nu xx}^i(\vec{r}/\vec{r}')$, $F_{\nu zx}^i(\vec{r}/\vec{r}')$ were found to be [33], [37]

$$F_{\nu xx}^i(\vec{r}/\vec{r}') = -2\left(\frac{j\omega\mu_o}{4\pi k_i^2}\right) \int_o^\infty J_o(\lambda\rho)e^{-u_o z^i}\delta_{i1} .$$

$$\cdot \{1 - \delta_{i2}\delta_{\nu 2} + \delta_{i2}\delta_{\nu 2}[u\cosh(uz^{\nu}) + u_o\sinh(uz^{\nu})]\} \cdot$$

$$\cdot \frac{\sinh[u(h-z^{\nu} + z^{\nu}\delta_{i1}\delta_{\nu 1})]}{f_1(\lambda,\varepsilon_r, h)} \lambda d\lambda \qquad (2.27)$$

and

$$F^i_{\nu zx}(\vec{r}/\vec{r}') = -2\left(\frac{j\omega\mu_o}{4\pi k_i^2}\right)(1-\varepsilon_r)\cos\phi \int_o^{\infty} J_1(\lambda\rho)e^{-u_o z^i \delta_{i1}}$$

$$\cdot \frac{\sinh[u(h-z^{\nu} + z^{\nu}\delta_{\nu 1})]}{f_1(\lambda,\varepsilon_r,h)} \cdot$$

$$\cdot \frac{\cosh[u(h-z^i + z^i\delta_{i1})]}{f_2(\lambda,\varepsilon_r,h)} \lambda^2 d\lambda \qquad (2.28)$$

The various parameters involved in equations (2.27) and (2.28) are defined as

$$u \equiv [\lambda^2 - k_2^2]^{1/2} \ , \ u_o \equiv [\lambda^2 - k_1^2]^{1/2} \qquad (2.29)$$

$$\rho = [(x-x')^2 + (y-y')^2]^{1/2} \qquad (2.30)$$

$$f_1(\lambda,\varepsilon_r,h) = u_o\sinh(uh) + u\cosh(uh) \qquad (2.31)$$

$$f_2(\lambda,\varepsilon_r,h) = \varepsilon_r u_o\cosh(uh) + u\sinh(uh) \qquad (2.32)$$

The zeros of $f_1(\lambda,\varepsilon_r,h)$ and $f_2(\lambda,\varepsilon_r,h)$ lead to TE and TM surface wave modes respectively [35], [37]-[39].

2-2 Pocklington's Integral Equation

In this work, the thickness of the metallic strips is considered finite and the widths of the dipole and the transmission line, Fig. (2.2) and (2.3) are assumed to be much smaller than the wavelength in the dielectric so that the transverse components of the current are a second order

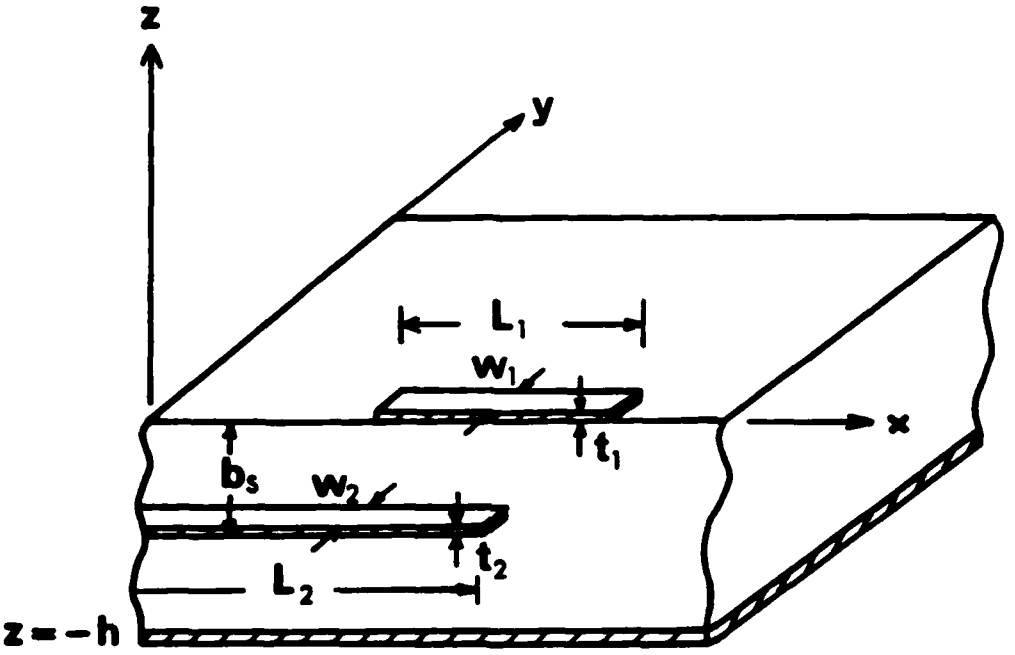

Figure 2.2

Strip Dipole Excited by a Microstrip Transmission Line

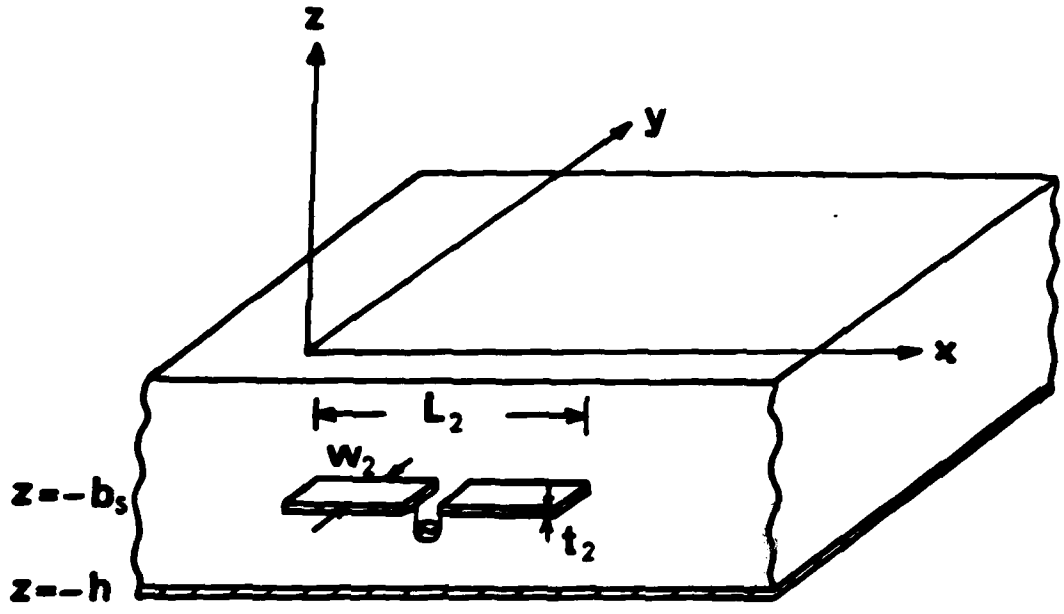

Figure 2.3

Strip Dipole Excited by a Gap Generator

effect. If it is assumed that the current density of the dipole is given by

$$\vec{J}_\nu = \hat{x} J_\nu(\vec{r}') = \hat{x} J_\nu(x', y', z^\nu) \tag{2.33}$$

where $z^\nu = 0$ when $\nu = 1$ and $z^\nu = -b_s$ when $\nu = 2$, then the integral equation takes the form

$$\vec{E}^i(\vec{r}) = \sum_{\nu=1,2} \int_{-w^\nu/2}^{w^\nu/2} dy' \int_0^{L_\nu} dx' [k_i^2 \bar{\bar{I}} + \vec{\nabla}\vec{\nabla}] \cdot$$

$$\cdot \bar{\bar{F}}_\nu^i(\vec{r}/\vec{r}') \cdot \hat{x} J_\nu(\vec{r}') \tag{2.34}$$

If equation (2.26) is substituted into (2.34) the expression for the electric field takes the form

$$\vec{E}^i(\vec{r}) = \sum_{\nu=1,2} \int_{-w^\nu/2}^{w^\nu/2} dy' \int_0^{L_\nu} dx' \cdot$$

$$\left\{ \left(k_i^2 F^i_{\nu xx} + \frac{\partial^2 F^i_{\nu xx}}{\partial x^2} + \frac{\partial^2 F_{\nu zx}}{\partial x \partial z} \right) J_\nu(x', y', z^\nu)\hat{x} + \right.$$

$$+ \left(k_i^2 F^i_{\nu xx} + \frac{\partial^2 F^i_{\nu xx}}{\partial y \partial x} + \frac{\partial^2 F^i_{\nu zx}}{\partial y \partial z} \right) J_\nu(x', y', z^\nu)\hat{y} +$$

$$\left. + \left(\frac{\partial^2 F^i_{\nu xx}}{\partial z \partial x} + \frac{\partial^2 F^i_{\nu zx}}{\partial z^2} \right) J_\nu(x', y', z^\nu)\hat{z} \right| \tag{2.35}$$

From (2.35) it is observed that the electric field consists of three components, namely, E_x^i, E_y^i, and E_z^i. However, only the E_x^i component is needed for the application of the method of Moments along the x-axis. From equation (2.35), the E_x^i component is given by

$$E_x^i(\vec{r}) = \sum_{\nu=1,2} \int_{-w^\nu/2}^{w^\nu/2} dy' \int_0^{L_\nu} dx' \left[k_i^2 F_{\nu xx}^i + \frac{\partial^2 F_{\nu zx}^i}{\partial x^2} + \frac{\partial^2 F_{\nu zx}^i}{\partial x \partial z} \right] J_\nu(x',y',z^\nu) \tag{2.36}$$

A consideration of the following relationship

$$\frac{\partial F_{\nu zx}^i}{\partial z} = - \frac{\partial F_{\nu z}^i}{\partial x} \tag{2.37}$$

leads to

$$E_x^i(\vec{r}) = \sum_{\nu=1,2} \int_{-w^\nu/2}^{w^\nu/2} dy' \int_0^{L_\nu} dx' \left\{ k_i^2 F_{\nu xx}^i + \frac{\partial^2}{\partial x^2} (F_{\nu xx}^i - F_{\nu z}^i) \right\} J_\nu(x',y',z^\nu) \tag{2.38}$$

with $F_{\nu z}^i$ given by (see Appendix A)

$$F_{\nu z}^i = -2\left(\frac{j\omega\mu_o}{4\pi k_i^2}\right) (\varepsilon_r - 1) \int_0^\infty J_o(\lambda\rho) e^{-u_o z^i} \delta_{i1} \frac{\left[\delta_{i1} u_o \cosh(uh) - \delta_{i2} u \sinh[u(h-z^i)]\right]}{f_1(\lambda, \varepsilon_r, h)} \cdot \frac{\left[\delta_{\nu 1} \sinh(uh) + \delta_{\nu 2} \sinh[u(h-z^\nu)]\right]}{f_2(\lambda, \varepsilon_r, h)} \lambda d\lambda \tag{2.39}$$

where

$$\delta_{i1} = \begin{cases} 1 & i = 1 \\ 0 & i \neq 1 \end{cases} \qquad \delta_{\nu 1} = \begin{cases} 1 & \nu = 1 \\ 0 & \nu \neq 1 \end{cases} \tag{2.40}$$

CHAPTER 3

TRANSFORMATION OF THE INTEGRAL EQUATION INTO A MATRIX EQUATION

3-1. Method of Moments

The purpose of this chapter is to present the basic mathematical techniques for reducing functional equations to matrix equations. These techniques are then applied to the specific problem of the strip dipole printed on or embedded in a grounded dielectric substrate and excited either by a microstrip transmission line or by a gap generator. A unifying principle for such techniques is found in the general method of moments, in terms of which most specific solutions can be interpreted.

Throughout this chapter, the width of the strip dipole and transmission line is assumed to be small enough compared to the wavelength in the dielectric, so that the transverse component of the current may be assumed to be a second order effect. It is to be emphasized that in this dissertation the thickness of the conducting strips is finite. The method of moments is a general procedure to solve linear inhomogeneous equations of the type [47]-[52]

$$L_{op}(f) = g \tag{3.1}$$

where L_{op} is a linear operator, g is the source or excitation (known function) and f is the current or response (unknown function to be determined). The term deterministic

means that the solution to equation (3.1) is unique; that is, only one f is associated with a given g. The integral equation (2.37) for the specific problem that is studied here can be transferred into an operator equation as follows:

$$L^i(\vec{J}) = E_x^i \hat{x} \tag{3.2}$$

with L^i given by

$$L^i = \sum_{\nu=1,2} \int_{w^\nu/2}^{w^\nu/2} dy' \int_o^{L_\nu} dx' \left| k_1^2 F^i_{\nu xx} + \frac{\partial^2}{\partial x^2} (F^i_{\nu xx} - F^i_{\nu z}) \right| \tag{3.3}$$

In addition to the above, it is necessary to define the inner product $\langle \vec{J}, (E_x^i \hat{x}) \rangle$, which is a scalar, to satisfy the following relations in Hilbert space

$$\langle \vec{J}, (E_x^i \hat{x}) \rangle = \langle (E_x^i \hat{x}), \vec{J} \rangle \tag{3.4}$$

$$\langle a\vec{J} + \beta(E_x^i \hat{x}), \vec{h} \rangle = a\langle \vec{J}, \vec{h} \rangle + \beta \langle (E_x^i \hat{x}), \vec{h} \rangle \tag{3.5}$$

$$\begin{aligned} \langle \vec{J}^* \vec{J} \rangle \quad &> 0 \quad \text{if } \vec{J} \neq 0 \\ &= 0 \quad \text{if } \vec{J} = 0 \end{aligned} \tag{3.6}$$

where a,β are scalars, $\vec{J} \times \vec{h} = 0$ and * denotes a complex conjugate.

A suitable inner product for this problem is

$$\langle \vec{J}, (E_x^i \hat{x}) \rangle = \int_o^{L_\nu} \vec{J} \cdot (E_x^i \hat{x}) dx \tag{3.7}$$

Furthermore, $\bar{G}^i_\nu(\vec{r}/\vec{r}') = \bar{G}^i_\nu(\vec{r}'/\vec{r})$ (ν=1,2) and using equation (2.25) it can be shown that

$$\langle L^i(J),\ (E_x^i\ \hat{x})\rangle = \langle \vec{J},\ L^i(E_x^i\ \hat{x}) \qquad (3.8)$$

which means that the integral operator is self-adjoint. Consideration of equation (3.8) and of the fact that zero excitation gives no response, it can be proved that there exists a unique solution to functional equation (3.2) and, therefore, the inverse operator $(L^i)^{-1}$ exists such that

$$\vec{J} = (L^i)^{-1}\ (E_x^i\ \hat{x}) \qquad (3.9)$$

In order to obtain a solution for equation (3.2) in the form (3.9), we have to follow the procedure described below:

1) Expand the unknown vector $\vec{J}$ in a series of basis functions spanning $\vec{J}$ in the domain of L^i.
2) Determine a suitable inner product and define a set of weighting functions.
3) Consider the inner products of these functions with both sides of functional equation (3.2) and transform it into a matrix equation.
4) Solve the matrix equation for the unknown vector $\vec{J}$.

3-2. Galerkin's Method

For the evaluation of the current distribution on printed circuit antennas, a specialization of the general method of moments is particularly convenient. At first, the

unknown current is expanded in a series of functions in the domain L^i as follows

$$\vec{J}(\vec{r}) = \sum_{n} I_n^{\nu} \vec{J}_n^{\nu}(\vec{r}) \qquad \begin{matrix} \nu=1,2 \\ n\epsilon N \end{matrix} \tag{3.10}$$

where the I_n's are constants. The functions $\vec{J}_n^{\nu}(\vec{r})$ are called expansion or basis functions. For exact solutions, (3.10) is an infinite summation while for approximate solutions it is usually a finite summation. Substituting (3.10) into (3.2) and using the linearity of L^i, one can have

$$\sum_{n} I_n \, L^i\left(\vec{J}_n^{\nu}(\vec{r})\right) = (E_x^i \, \hat{x}) \tag{3.11}$$

Furthermore, a set of weighting functions, or testing functions, is chosen to be identical with the basis functions, i.e.,

$$\{W_m^i(\vec{r})\} = \{\vec{J}_n^{\nu}(\vec{r})\} \qquad m, \, n\epsilon N \tag{3.12}$$

and then the inner product

$$\sum_{n} I_n^{\nu} \langle \vec{W}_m^i, \, L^i(\vec{J}_n^{\nu}) \rangle = \langle \vec{W}_m^i, \, (E_x^i \, \hat{x}) \rangle \tag{3.13}$$

is formulated. This set of equations can be written in matrix form as

$$[Z_{mn}^{i\nu}] \, [I_n^{\nu}] = [V_m^i] \tag{3.14}$$

where

$$Z_{mn}^{i\nu} = \langle \vec{W}_m^i, \, L^i(\vec{J}_n^{\nu}) \rangle \tag{3.15}$$

and

$$[V_m^i] = \langle \vec{W}_m^i, \, (E_x^i \, \hat{x}) \rangle \tag{3.16}$$

Since the matrix $[Z_{mn}^{i\nu}]$ (as it will be shown in the following chapters) is nonsingular, its inverse exists and equation (3.14) gives

$$[I_n^\nu] = [Z_{mn}^{i\nu}]^{-1} [V_m^i] \tag{3.17}$$

The vector $[\vec{J}_n^\nu]$ is written as

$$[\vec{J}_n^\nu]^T = [\vec{J}_1^1, \vec{J}_2^1, \ldots, \vec{J}_1^2, \vec{J}_2^2, \ldots] \tag{3.18}$$

and, therefore, the solution to equation (3.2) is given by

$$\vec{J}(\vec{r}) = [\vec{J}_n^\nu]^T [Z_{mn}^{i\nu}]^{-1} [V_m^i] \tag{3.19}$$

One of the main tasks in any specific problem is the choice of the functions $\vec{J}_n^\nu$. They should be linearly independent and selected so that some combination (3.10) can approximate $\vec{J}(\vec{r})$ reasonably well. Additional factors which affect the choice of $\vec{J}_n^\nu$ are:

i) The desired accuracy of the solution.

ii) The ease of evaluation of the matrix elements.

iii) The size of the matrix that can be inverted.

iv) The convergence of the solution.

3-3 Impedance Matrix Element Formulation

As mentioned previously, the choice of the basis functions is determined by many factors dictated by the problem under consideration. For the case of a printed or embedded strip dipole electromagnetically coupled to a microstrip transmission line or excited by a gap generator the basis functions were chosen to be of the form

$$\vec{J}_n^{\nu}(\vec{r}') = \hat{x}J_n^{\nu}(\vec{r}') = \hat{x}J_{nx}(x')J_y^{\nu}(y')\delta(z'-z^{\nu}) \qquad (3.20)$$

The $J_{nx}^{\nu}(x')$ are overlapping piecewise sinusoidal functions [38] of the form (Fig. 3.1),

$$J_{nx}(x') = \left| P_{n-1}\frac{\sin[k(x'-x_{n-1})]}{\sin(k\ell_x)} + P_n\frac{\sin[k(x_{n+1}-x')]}{\sin(k\ell_x)}\right| \qquad (3.21)$$

with

$$P_{n-1} = \begin{cases} 1 & x_{n-1} \le x' \le x_n \\ 0 & \text{elsewhere} \end{cases} \qquad (3.22)$$

$$P_n = \begin{cases} 1 & x_n \le x' \le x_{n+1} \\ 0 & \text{elsewhere} \end{cases}$$

and

$$k = \alpha k_1 \qquad \alpha \epsilon R^+ \qquad (3.23)$$

$J_y^{\nu}(y')$ gives the correct transverse variation of the current density on the strips taking into account finite conductor thickness. The expression for the function $J_y^{\nu}(y')$ is given by (Fig. 3.2)

$$J_y^{\nu}(y') = \frac{1}{\left[1-\left(\frac{2y'}{w_e^{\nu}}\right)^2\right]^{\frac{1}{2}}} \qquad (3.24)$$

Here, W_e^{ν} is the effective strip width given by $W_e^{\nu} = W^{\nu} + 2\delta^{\nu}$. The parameter δ^{ν} is the excess half width, and it accounts for fringing effects due to conductor thickness [53]. Interpretation of the choice for the current density dependence in y', indicates that the edge condition is satisfied at $y' = \pm W_e^{\nu}/2$, which is an equivalent strip of

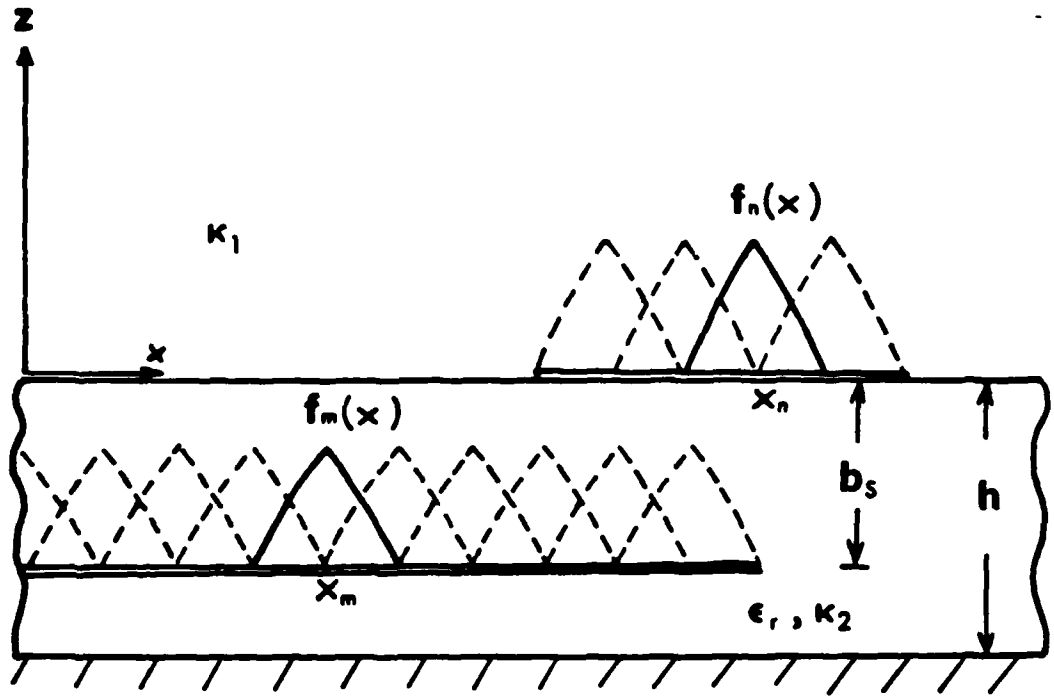

Figure 3.1

Piecewise-Sinusoidal Currents on the Printed Dipole and the Embedded Microstrip Line

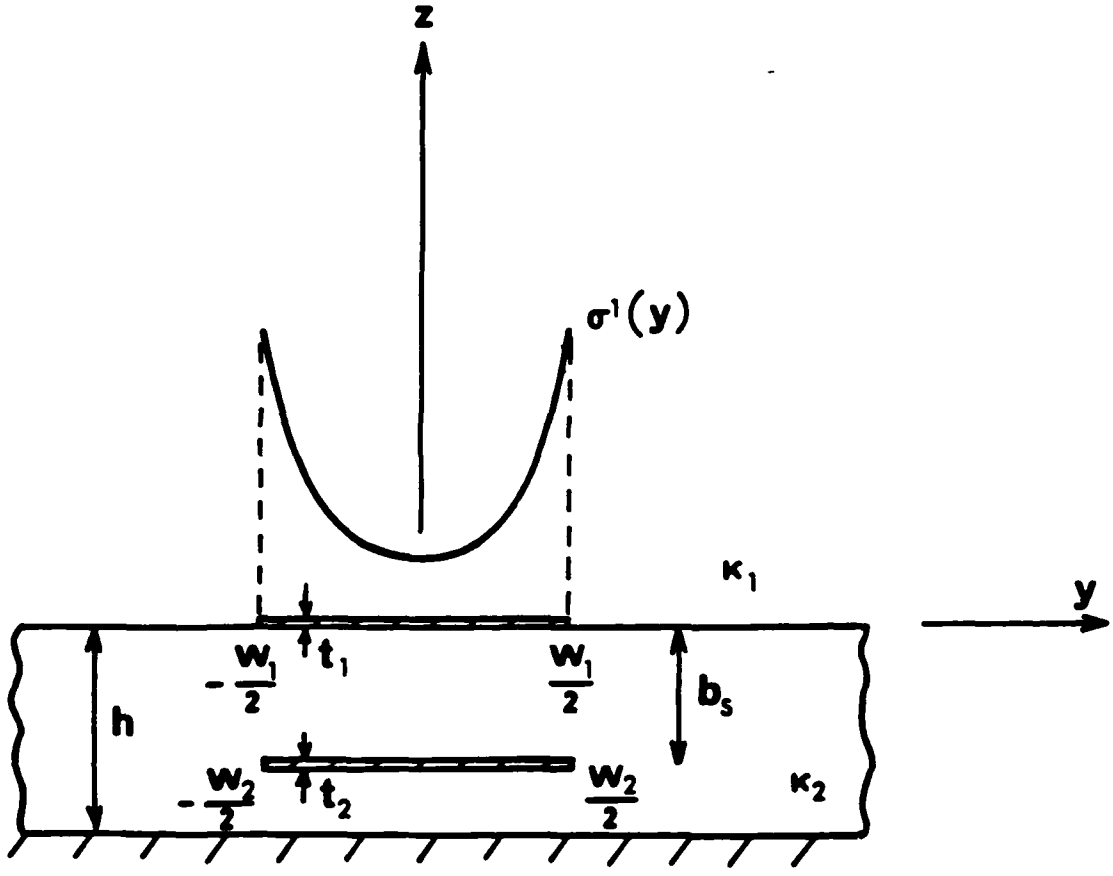

Figure 3.2

Current Distribution on the Dipole in the Transverse Direction

zero thickness. At $y' = \pm\frac{w^\nu}{2}$, the current density remains finite, as is the case for nonzero thickness conductors. This choice of dependence in y' for the current density yields, as will be shown, very accurate results for microstrip dipole resonant length.

If one substitutes (3.20) and (3.10) into (2.38), then it can be found that the expression for the electric field is

$$E_x^i(\vec{r}) = \sum_{\nu=1,2} \sum_n \frac{I_n^\nu}{\sin(k\ell x)} \int_{-w^\nu/2}^{w^\nu/2} \frac{dy'}{\left[1+\left(\frac{2y'}{w_e^\nu}\right)^2\right]^{\frac{1}{2}}} \delta(z'-z^\nu)$$

$$\left[\int_0^{\ell_x} dx' \Big\{(k_i^2 - k^2)\,[F^i_{\nu xx}(x+x',x_n) + \right.$$

$$+ F^i_{\nu xx}(x-x',x_n)] + k^2[F^i_{\nu z}(x+x',x_n) +$$

$$\left. + F^i_{\nu z}(x-x',x_n)]\Big\} \sin[k(\ell_x-x')] +$$

$$+ k[F^i_{\nu xx}(x+x',x_n) - F^i_{\nu z}(x+x',x_n)]\,[\delta(x'+\ell_x) +$$

$$\left. + \delta(x'-\ell_x) - 2\cos(k\ell_x)\delta(x')\right] \qquad (3.25)$$

Now, the following inner produce is defined

$$\langle \vec{W}_m^i, (E_x^i\,\hat{x})\rangle = \int_{x_{m-1}}^{x_m} J_{mx}(x)\; E_x^i(\vec{r})\delta(y-y^i)\delta(z-z^i) \qquad (3.26)$$

Equation (3.26) combined with (3.25) and (3.15) gives the following form for the elements of the impedance matrix

$$Z^i_{mn} = \frac{\delta(y-y^i)\delta(z-z^i)\delta(z'-z^\nu)}{[\sin(k\ell_x)]^2} \int_{-w^\nu/2}^{w^\nu/2} \frac{dy'}{\left[1-\left(\frac{2y'}{w_e^\nu}\right)^2\right]^{1/2}}$$

$$\int_0^{\ell_x} dx \int_0^{\ell_x} dx' \Big| (k_i^2-k^2)\,[F^i_{\nu xx}(x+x',x_n,x_m) +$$

$$+ F^i_{\nu xx}(x-x',x_n,x_m) + F^i_{\nu xx}(-x+x',x_n,x_m) +$$

$$+ F^i_{\nu xx}(-x-x',x_n,x_m)] + k^2[F^i_{\nu z}(x+x',x_n,x_m) +$$

$$+ F^i_{\nu z}(x-x',x_n,x_m) + F^i_{\nu z}(-x+x',x_n,x_m)] +$$

$$+ F^i_{\nu z}(-x-x',x_n,x_m)]\Big| \cdot \sin[k(\ell_x-x)] \cdot \sin[k(\ell_x-x')]$$

$$+ \int_0^{\ell_x} dx\,[F^i_{\nu xx}(x+x',x_n,x_m) + F^i_{\nu xx}(-x+x',x_n,x_m) -$$

$$- F^i_{\nu z}(x+x',x_n x_m) - F^i_{\nu z}(-x+x',x_n,x_m)] \cdot$$

$$\cdot \sin[k(\ell_x-x)]\,[\delta(x'+\ell_x) + \delta(x'-\ell_x) -$$

$$- 2\cos(k\ell_x)\delta(x')] \qquad (3.27)$$

with

$$F^i_{\nu xx}(x+x',x_n,x_m) = F^i_{\nu xx}\Big|_{\rho=\{[(x+x')+(x_m-x_n)]^2+(y-y')^2\}^{1/2}} \qquad (3.28)$$

and

$$F^i_{\nu z}(x+x',x_n,x_m) = F^i_{\nu z}\Big|_{\rho=\{[(x+x')+(x_m-x_n)]^2+(y-y')^2\}^{1/2}} \qquad (3.29)$$

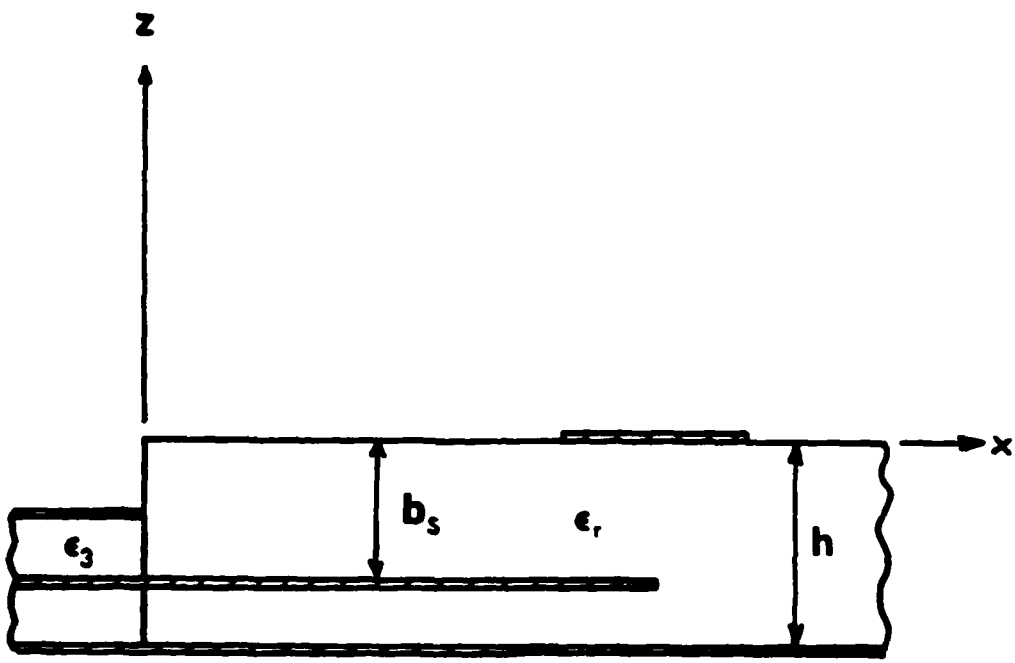

Figure 3.3

Printed Strip Dipole EM Coupled to an Embedded Microstrip Line which is Fed by a Coaxial T.L.

A_s mentioned in previous chapters, the strip dipole is excited either by a voltage gap generator or by a microstrip transmission line embedded in the dielectric. In the first case, the gap generator is considered at the feed point and all the elements of the excitation vector become zero except the one which corresponds to the infinitesimally small gap. In the case of the electromagnetically coupled strip dipole, the problem of the excitation of the transmission line has to be resolved. In practice, the microstrip line is excited by the inner conductor of a grounded coaxial line as shown in figure (3.3). Since the theoretical analysis for such an excitation is very difficult, other possible models were studied such as a voltage or current generator at the end of the microstrip or a voltage gap generator two subsections from this end. From these models the only one that gave very good results was the gap generator but with the condition that the length of the microstrip line is chosen to be more than three wavelengths in the dielectric. This model has been used for the derivation of the results which will be presented in following chapters.

CHAPTER 4

EVALUATION OF THE SOMMERFELD TYPE INTEGRALS

4-1. Singular Points and Related Surface Waves

As shown in Chapter 3, the elements of the generalized impedance matrix are given by

$$z_{mn}^{i\nu} = \int_0^\infty \sum_{\nu=1,2} \mathcal{L}_{mn}^{\nu} \{J_0(\lambda\rho)\} \cdot \left[\frac{A^{i\nu}(\lambda,\varepsilon_r,h;z^i,z^\nu)}{f_1(\lambda,\varepsilon_r,h) \cdot f_2(\lambda,\varepsilon_r,h)} \right] d\lambda \qquad (4.1)$$

where $\mathcal{L}_{mn}^{\nu}$ is a multiple space integral operator acting on the zeroth order Bessel function, $A^{i\nu}(\lambda,\varepsilon_r,h;z^i,z^\nu)$ is a complicated expression of transcendental functions without singularities and $f_1(\lambda,\varepsilon_r,h)$, $f_2(\lambda,\varepsilon_r,h)$ are given by (2.30) and (2.31). The integral in equation (4.1) is a Sommerfeld type [44] and the existence of essential singularities in its integrand necessitates very careful treatment. In this chapter, the computation of this integral will be shown explicitly and the approximations employed will be justified with estimation of the introduced error.

In equation (4.1), the integrand is a function of parameter λ through the radicals

$$u = [\lambda^2 - k_2^2]^{\frac{1}{2}} \qquad (4.2)$$

$$u_o = [\lambda^2 - k_1^2]^{\frac{1}{2}} \qquad (4.3)$$

where k_1, k_2 are the vacuum and substrate wavenumbers respectively. The sign of the radical u does not affect the single value of the integrals, as the terms involving the radicals are even functions of u. For this reason, only the branch cut contribution by the radical u_o is considered and its direction is determined by the requirement that the radiating field is a wave receding from the source. As a result, the restrictions on λ are:

$$\mathrm{Re}(\lambda) > 0 \tag{4.4}$$

$$\mathrm{Im}(\lambda) > 0 \tag{4.5}$$

which in turn impose the following behavior for u and u_o:

$$\mathrm{Re}(u_o) > 0 \qquad \mathrm{Im}(u_o) > 0 \tag{4.6}$$

$$\mathrm{Re}(u) > 0 \qquad \mathrm{Im}(u) > 0 \tag{4.7}$$

A possible position of the branch cuts governed by these inequalities is shown in Fig. (4.1).

The integrand in (4.1) has poles whenever either one of the functions $f_1(\lambda,\varepsilon_r,h)$, $f_2(\lambda,\varepsilon_r,h)$ becomes zero. The zeros of these two functions correspond to surface-wave modes. Particularly the zeros of $f_1(\lambda,\varepsilon_r,h)$ correspond to TE surface waves and the zeros of $f_2(\lambda,\varepsilon_r,h)$ to TM surface waves. In the case of a lossless dielectric, these TE and TM poles are the roots of the equations $u_o = u\coth(uh)$ and $\varepsilon_r u_o = -u\tanh(uh)$. Furthermore, these poles lie within the range $k_1 \leq \mathrm{Re}(\lambda) \leq k_2$.

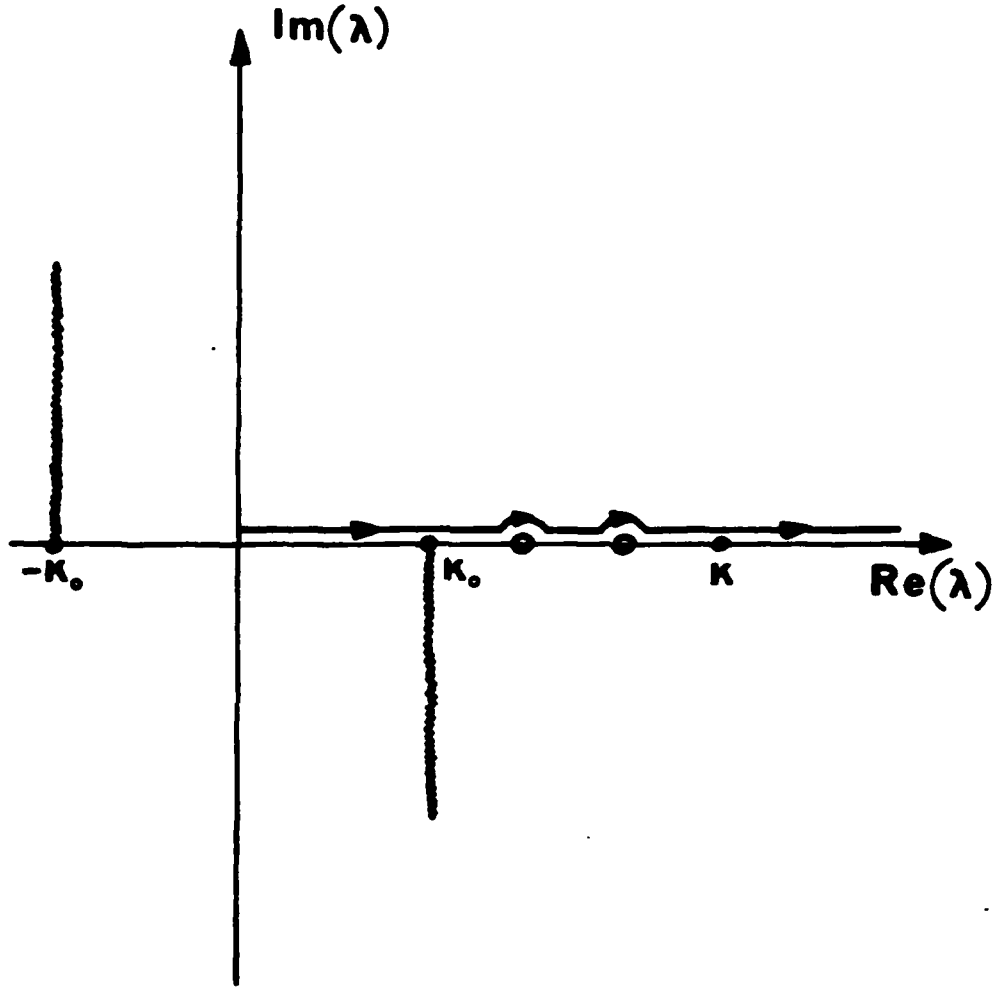

Figure 4.1

Path of Integration

The semi-infinite integration in equation (4.1) is performed along the real axis and is completed in two steps.

(i) Numerical integration over the interval [0,A] where A satisfies the relationship $\coth[(A^2-k_2^2)^{\frac{1}{2}}] \doteq 1$.

(ii) Combination of numerical and analytical integration for the evaluation of the tail contribution which is actually the integration over the path $[a,\infty)$.

Subsequently, it is concluded that the (m,n)/(i,ν) element of the impedance matrix can be split into two parts, viz.,

$$Z_{mn}^{i\nu} = Z_{mn}^{i\nu}(A) + Z_{mn}^{i\nu}(\infty) \tag{4.8}$$

where

$$Z_{mn}^{i\nu}(A) = \int_0^A \sum_{\nu=1,2} \mathcal{L}_{mn}^{\nu}\{J_o(\lambda\rho)\} \cdot \left[\frac{A^{i\nu}(\lambda,\varepsilon_r,h;z^i,z^\nu)}{f_1(\lambda,\varepsilon_r,h)\cdot f_2(\lambda,\varepsilon_r,h)}\right] d\lambda \tag{4.9}$$

and

$$Z_{mn}^{i\nu}(\infty) = \int_A^\infty \sum_{\nu=1,2} \mathcal{L}_{mn}^{\nu}\{J_o(\lambda\rho)\} \left[\frac{A^{i\nu}(\lambda,\varepsilon_r,h;z^i,z^\nu)}{f_i(\lambda,\varepsilon_r,h)\cdot f_2(\lambda,\varepsilon_r,h)}\right] d\lambda \tag{4.10}$$

4-2. Numerical Integration λε[0,A]

The first part of each element of the generalized impedance matrix is given by

$$Z_{mn}^{i\nu}(A) = \int_0^A \sum_{\nu=1,2} \left[\frac{A^{i\nu}(\lambda,\varepsilon_r,h;z^i,z^\nu)}{f_1(\lambda,\varepsilon_r,h)\cdot f_2(\lambda,\varepsilon_r,h)}\right] \mathcal{L}_{mn}^{\nu}\{J_o(\lambda\rho)\}\, d\lambda \tag{4.11}$$

and is evaluated numerically. The operator $\mathcal{L}^{\nu}_{mn}$ is of the form

$$\mathcal{L}^{\nu}_{mn} = \int_{-w^{\nu}/2}^{w^{\nu}/2} dy' J_y^{\nu}(y') \int_o^{\ell_x} dx J_{mx}(x) \left\{ \int_o^{\ell_x} dx' J_{nx}(x') \cdot \right.$$

$$\cdot [\delta(\rho-\rho_1) + \delta(\rho-\rho_2) + \delta(\rho-\rho_3) + \delta(\rho-\rho_4)] +$$

$$+ [\delta(x'+\ell_x) + \delta(x'-\ell_x) - 2\cos(k\ell_x)\delta(x')] \cdot$$

$$\left. \cdot [\delta(\rho-\rho_1) + \delta(\rho-\rho_3)] \right\} \qquad (4.12)$$

where

$$\rho_1 = \{(x+x'+x_m-x_n)^2 + (y-y')^2\}^{\frac{1}{2}} \qquad (4.13)$$

$$\rho_2 = \{(x-x'+x_m-x_n)^2 + (y-y')^2\}^{\frac{1}{2}} \qquad (4.14)$$

$$\rho_3 = \{(-x+x'+x_m-x_n)^2 + (y-y')^2\}^{\frac{1}{2}} \qquad (4.15)$$

$$\rho_4 = \{(-x-x'+x_m-x_n)^2 + (y-y')^2\}^{\frac{1}{2}} \qquad (4.16)$$

$J_{mx}(x)$, $J_{nx}(x')$ belong to the set of basis functions which have been used for the application of the moments method. In the integral of equation (4.11), it has been found that the space integral operator can make the integrand a slowly varying function of λ thereby minimizing the error of integration. Therefore, for the evaluation of $z^{i\nu}_{mn}$, the function

$$S^{\nu}_{mn}(\lambda) = \mathcal{L}^{\nu}_{mn}\{J_o(\lambda\rho)\} \qquad (4.17)$$

is transformed into a rapidly converging series of the form (Appendix B)

$$S_{mn}^{\nu}(\lambda) = \sum_{\sigma=0}^{\infty} \left| A_{2\sigma}\left(\frac{\ell_x}{\lambda_o}\right)^{2\sigma} \frac{d^{2\sigma}}{d|x|^{2\sigma}} J_o(\lambda x_{mn}) + \right.$$

$$+ B_{\sigma}\left(\frac{\ell_x}{\lambda_o}\right)^{\sigma} \frac{d^{\sigma}}{d|x|^{\sigma}} \left[J_o(\lambda x_{m(n+1)}) + J_o(\lambda x_{mn}) + \right.$$

$$\left. \left. + J_o(\lambda x_{m(n-1)}) \right] \right| \qquad (4.18)$$

where ℓ_x is the subsection length ($\ell_x < 0.02\lambda_o$), $J_o(\lambda x_{mn})$ is an expression involving Bessel functions and x_{mn} is given by

$$x_{mn} = (x_m - x_n) \qquad (4.19)$$

For the integration with respect to λ, because of the existence of the poles in the strip $k_1 \leq \mathrm{Re}(\lambda) \leq k_2$, a further division of the integration integral into sub-intervals takes place as is shown below:

i) $0 \leq \lambda \leq k_1$, the integration with respect to λ is performed numerically using a Gaussian-Quadrature method with fixed points.

ii) $k_1 \leq \lambda \leq k_2$; for the integration along this interval a singularity extraction technique is used [37]-[38] which transforms the integral into a finite series plus an integral of a slowly varying function. This finite series gives the contribution of the surface wave modes with the number of its terms dependent on the thickness of the dielectric as well as the dielectric constant.

iii) $k_2 \leq \lambda \leq A$; numerical integration is invoked here

in exactly the same manner as it is performed in the first subinterval.

4-3. Evaluation of the Tail Contribution

In this case, the integration with respect to λ is extended along the interval $[A,\infty]$. The integrals which have to be computed are given by

$$Z_{mn}^{i}(\infty) = \int_{A}^{\infty} \sum_{\nu=1,2} \left[\frac{A^{i\nu}(\lambda,\varepsilon_r,h;z^i,z^\nu)}{f_1(\lambda,\varepsilon_r,h)\cdot f_2(\lambda,\varepsilon_r,h)} \right] \mathcal{L}_{mn}^{\nu}\{J_o(\lambda\rho)\} \tag{4.20}$$

where

$$\begin{aligned} A^{i\nu}(\lambda,\varepsilon_r,h;z^i,z^\nu) = 2\left(\frac{j\omega\mu_o}{4\pi k_i^2}\right) e^{-u_o z^i}\delta_{i1} \Big\{ & [E_1(k_1^2-k^2)+E_2 k]\cdot \\ & \cdot \left(1-\delta_{i2}\delta_{\nu 2} + \delta_{i2}\delta_{\nu 2}[u\cosh(uz^\nu) + u_o\sinh(uz^\nu)]\right)\cdot \\ & \cdot \sinh[u(h-z^\nu + z^\nu\delta_{i1}\delta_{\nu 1})]\cdot f_2(\lambda,\varepsilon_r,h) + \\ & + [E_1 k^2 - E_2 k]\cdot \left[\delta_{i1}u_o\cosh(uh) - \delta_{i2}u\sinh[u(h-z^i)]\right]\cdot \\ & \cdot (\varepsilon_r-1)\cdot \left[\delta_{\nu 1}\sinh(uh) + \delta_{\nu 2}\sinh[u(h-z^\nu)]\right] \Big\} \lambda \end{aligned} \tag{4.21}$$

with E_1, E_2 constants which take the values 1,0. When the source point and the observation point coincide, $\rho\to 0$, $z^i = z^\nu$ and the integral above takes the form,

$$Z_{mn}^{i\nu}(\infty) = C\int_{A}^{\infty} \sum_{\nu=1,2} \left[\frac{A^{i\nu}(\lambda,\varepsilon_r,h;z^i,z^\nu)}{f_1(\lambda,\varepsilon_r,h)\cdot f_2(\lambda,\varepsilon_r,h)} \right] d\lambda \tag{4.22}$$

where C is a constant. For the integrand in (4.22), it can be proved that, when $A \ll \lambda$,

$$\frac{A^{i\nu}(\lambda,\varepsilon_r,h;z^i,z^\nu)}{f_1(\lambda,\varepsilon_r,h)\cdot f_2(\lambda,\varepsilon_r h)} =$$

$$= \frac{E_1 Q_1(\lambda,\varepsilon_r,h)e^{-u_0|z^i-z^\nu|} + E_2 Q_2(\lambda,\varepsilon_r h)e^{-u|z^i-z^\nu|}}{f_1(\lambda,\varepsilon_r,h)\cdot f_2(\lambda,\varepsilon_r,h)} =$$

$$= \frac{E_1 Q_1(\lambda,\varepsilon_r,h)+E_2 Q_2(\lambda,\varepsilon_r,h)}{f_1(\lambda,\varepsilon_r,h)\cdot f_2(\lambda,\varepsilon_r,h)} = O(\lambda^{-a}) \quad (a<1) \qquad (4.23)$$

where $Q_1(\lambda,\varepsilon_r,h)$ and $Q_2(\lambda,\varepsilon_r,h)$ are nonsingular functions of λ,ε_r,h as a consequence of which becomes infinite. In order to avoid this $Z_{mn}^{i\nu}(\infty)$ difficulty, which arises in the computation of the diagonal elements of the impedance matrix, the conducting strips are assumed to have a very small but finite thickness, t, with the source current flowing on the bottom surface and the observation points located on the top surface. As a result, the distance between source and observation points is prevented from becoming zero; the minimum value it can take is equal to the thickness of the strip. Since A has already been chosen in such a way that

$$\coth[(A^2-k_2^2)^{1/2}h] \doteq 1 \qquad (4.24)$$

equation (4.20) can be approximated as (Appendix C),

$$Z_{mn}^{i\nu}(\infty) = \left(\frac{j\omega\mu_o}{4\pi k_i^2}\right) \sum_{\nu=1,2} \left\{ D_1(A) \int_{(A^2-k_1^2)^{1/2}}^{\infty} e^{-u_o t} \mathcal{L}_{mn}^{\nu} \{J_o(u_o\rho_1^*)\} \cdot \right.$$

$$\cdot du_o + D_2(A) \int_{(A^2-k_2^2)^{1/2}}^{\infty} e^{-ut^*} \mathcal{L}_{mn}^{\nu} \{J_o(u\rho_2^*)\}\, du +$$

$$\left. + D_3(A) \int_{(A^2-k_2^2)^{1/2}}^{\infty} e^{-u(2b_s-t)} \mathcal{L}_{mn}^{\nu} \{J_o(u\rho_2^*)\}\, du \right\} +$$

$$+ \text{Error} \qquad (4.25)$$

where

$$D_1(A) = \left\{ [E_1(k_1^2-k^2) + E_2 k] \frac{\delta_{i1}\delta_{\nu 1}}{1-e_2(A)} + [E_1 k^2 - E_2 k] \cdot \delta_{i1}\delta_{\nu 1} \right.$$

$$\left. \left(\frac{1}{1-e_2(A)} - \frac{2}{\varepsilon_r - 1} \cdot \frac{1}{1-e_3(A)}\right) \right| \qquad (4.26)$$

$$D_2(A) = \left| [E_1(k_1^2-k^2)+E_2 k] \frac{\delta_{i1}\delta_{\nu 2}+\delta_{i2}\delta_{\nu 1}+(1+e_4(A))\delta_{i2}\delta_{\nu 2}}{1+e_4(A)} + \right.$$

$$+ [E_1 k^2 - E_2 k]\ (\delta_{i1}\delta_{\nu 2}+\delta_{i2}\delta_{\nu 1}) \left(\frac{1}{1+e_4(A)} - \frac{2}{\varepsilon_r+1} \cdot \right.$$

$$\left. \left. \cdot \frac{1}{1+e_6(A)}\right) \right| \qquad (4.27)$$

$$D_3(A) = \left\{ -[E_1(k_1^2-k^2) + E_2 k] \frac{e_4(A)\delta_{i2}\delta_{\nu 2}}{1+e_4(A)} + \delta_{i2}\delta_{\nu 2} \cdot \right.$$

$$\left. \left(\frac{1}{1+e_4(A)} - \frac{2\varepsilon_r}{1+\varepsilon_r} \cdot \frac{1}{1+e_6(A)}\right) \right| \qquad (4.28)$$

and

$$e_1(A) = \frac{1}{2} \frac{k_1^2}{A^2-k_1^2} \qquad (4.29)$$

$$e_2(A) = \frac{1}{4}\frac{k_2^2-k_1^2}{A^2-k_1^2} \tag{4.30}$$

$$e_3(A) = \frac{1}{2(\epsilon_r+1)}\frac{k_2^2-k_1^2}{A^2-k_1^2} \tag{4.31}$$

$$e_4(A) = \frac{1}{4}\frac{k_2^2-k_1^2}{A^2-k_2^2} \tag{4.32}$$

$$e_5(A) = \frac{1}{2}\frac{k_2^2}{A^2-k_2^2} \tag{4.33}$$

$$e_6(A) = \frac{\epsilon_r}{2(1+\epsilon_r)}\cdot\frac{k_2^2-k_1^2}{A^2-k_2^2} \tag{4.34}$$

$$\rho_1^* = \rho[1+e_1(A)] \tag{4.35}$$

$$\rho_2^* = \rho[1+e_5(A)] \tag{4.36}$$

$$t^* = b_s + t[1+2e_4(A)] \tag{4.37}$$

The error made by the approximation in equation (4.25) depends on A. It has been found that

$$\text{Error} = 0(A^{-2}|Z_{mn}^{i\nu}|) \tag{4.38}$$

and for this reason A always takes values larger than 10^2. Therefore, the approximation considered here is a very good one since the overall error made in the computation of the input impedance is of the order of 0.1%. In equation (4.25), the integrals can be put in the general form,

$$I_i = \int_{(A^2-k_i^2)^{1/2}}^{\infty} e^{-v_i\sigma} \mathcal{L}_{mn}^{\nu} \{J_o(v_i\rho_i^*)\}dv_i \quad (i=1,2) \tag{4.39}$$

where $v_i = (\lambda^2 - k_i^2)^{1/2}$; σ can take either one of the positive values t, t*, $2b_s$-t. If one interchanges the order of the operator and the integration, the integral I_i can be written as

$$I_i = \mathcal{L}_{mn}^{\nu} \left| \int_{(A^2-k_1^2)^{1/2}}^{\infty} e^{-v_i\sigma} J_o(v_i\rho_i^*) dv_i \right| =$$

$$= \mathcal{L}_{mn}^{\nu} \left\{ \frac{1}{g_i(A)} \cdot \frac{1}{\left\{ \rho^2 + \left[\frac{\sigma}{g_i(A)} \right]^2 \right\}^{1/2}} \right\} -$$

$$= -\int_o^A \left(\frac{e^{-(\lambda\sigma/g_i(A))}}{g_i(A)} \right) \cdot \mathcal{L}_{mn}^{\nu} \{J_o(\lambda\rho)\} \delta\lambda \qquad (4.40)$$

where

$$g_i(A) = \left\{ 1 + \frac{k_i^2}{A^2 - k_i^2} \right\}^{1/2} \qquad (i = 1,2) \qquad (4.41)$$

If one substitutes (4.40) into (4.25), $Z_{mn}^{i\nu}(\infty)$ becomes

$$Z_{mn}^{i\nu}(\infty) = \sum_{\nu=1,2} \left\{ \frac{D_1(A)}{g_1(A)} \mathcal{L}_{mn}^{\nu} \left| \left(\rho^2 + \left[\frac{t}{g_1(A)} \right]^2 \right)^{-1/2} \right| + \right.$$

$$+ \frac{D_2(A)}{g_2(A)} \mathcal{L}_{mn}^{\nu} \left| \left(\rho^2 + \left[\frac{t^*}{g_2(A)} \right]^2 \right)^{-1/2} \right| +$$

$$\left. + \frac{D_3(A)}{g_2(A)} \mathcal{L}_{mn}^{\nu} \left| \left(\rho^2 + \left[\frac{2b_s - t}{g_2(A)} \right]^2 \right)^{-1/2} \right| \right\} -$$

$$- \sum_{\nu=1,2} \int_o^A \left| D_1(A) \left(\frac{e^{-(\lambda t/g_1(A))}}{g_1(A)} \right) + D_2(A) \left(\frac{e^{-(\lambda t^*/g_2(A))}}{g_2(A)} \right) + \right.$$

$$+ D_3(A)\left(\frac{e^{-\lambda(2b_s-t)/g_2(A)}}{g_2(A)}\right)\Bigg] \mathcal{L}_{mn}^{\nu}\{J_o(\lambda\rho)\}\, d\lambda \qquad (4.42)$$

From equations (4.8), (4.11) and (4.42), it can be seen that the elements of the impedance matrix can be split into two other parts so that the evaluation of each is simplified

$$Z_{mn}^{i\nu} = \mathcal{Z}_{mn}^{i\nu}(A) + \mathcal{Z}_{mn}^{i\nu}(\infty) \qquad (4.43)$$

where

$$\mathcal{Z}_{mn}^{i\nu}(A) = \int_0^A \sum_{\nu=1,2} \left[\frac{B^{i\nu}(\lambda,\varepsilon_r,h;z^i,z^\nu)}{f_1(\lambda,\varepsilon_r,h)\cdot f_2(\lambda,\varepsilon_r h)}\right] \mathcal{L}_{mn}^{\nu}\{J_o(\lambda\rho)\}d\lambda \qquad (4.44)$$

$$\mathcal{Z}_{mn}^{i\nu}(\infty) = \sum_{\nu=1,2} \left\{\frac{D_1(A)}{g_1(A)} \mathcal{L}_{mn}^{\nu}\left\{\left(\rho^2 + \left[\frac{t^2}{g_1(A)}\right]^2\right)^{-\frac{1}{2}}\right\} + \right.$$

$$+ \frac{D_2(A)}{g_2(A)} \mathcal{L}_{mn}^{\nu}\left\{\left(\rho^2 + \left[\frac{t^*}{g_2(A)}\right]^2\right)^{-\frac{1}{2}}\right\} +$$

$$\left. + \frac{D_3(A)}{g_2(A)} \mathcal{L}_{mn}^{\nu}\left\{\left(\rho^2 + \left[\frac{2b_s-t}{g_2(A)}\right]^2\right)^{-\frac{1}{2}}\right\}\right\} \qquad (4.45)$$

and

$$B^{i\nu}(\lambda,\varepsilon_r,h;z^i,z^\nu) = A^{i\nu}(\lambda,\varepsilon_r,h;z^i z^\nu) -$$

$$-\left\{D_1(A)\left(\frac{e^{-(\lambda t/g_i(A))}}{g_1(A)}\right) + D_2(A)\left(\frac{e^{-(\lambda t^*/g_2(A))}}{g_2(A)}\right) + \right.$$

$$\left. + D_3(A)\left(\frac{e^{-\lambda(2b_s-t)/g_2(A)}}{g_2(A)}\right)\right\} \qquad (4.46)$$

The first term on the RHS of equation (4.43) is evaluated with the technique which was described in Part 4.2 of this chapter, while for the evaluation of the second term a more careful treatment is necessary in order to keep the error of integration within acceptable limits. The operation of $\mathcal{L}_{mn}^{\nu}$ on the function $\left(\rho^2 + \left[\frac{\sigma}{g_i(A)}\right]^2\right)^{-\frac{1}{2}}$ (Eq. 4.40) can be written in the final form

$$\mathcal{L}_{mn}^{\nu}\left\{\left(\rho^2 + \left[\frac{\sigma}{g_i(A)}\right]^2\right)^{-\frac{1}{2}}\right\} = \int_{-w^{\nu}/2}^{w^{\nu}/2} \frac{dy'}{\sqrt{1-\left(\frac{2y'}{w_e^{\nu}}\right)^2}} \cdot$$

$$\left\{\sum_{\tau=-2}^{2} a_t \sin(kx_t)\, \ell_n\left(2\sqrt{x_\tau^2 + y'^2 + \left(\frac{\sigma}{g_i(A)}\right)^2} + 2x_\tau\right) + \right.$$

$$\left. + \mathcal{L}_{mn}^{\nu}\left\{\mathcal{R}\left(\rho, \frac{\sigma}{g_i(A)}\right)\right\}\right\} \qquad (4.47)$$

where a_τ = constant, $x_\tau = \tau\ell_x + x_m - x_n$ and $\mathcal{R}\left(\rho, \frac{\sigma}{g_i(A)}\right)$ is a slowly varying function of ρ. In equation (4.47) all the remaining integrals are evaluated numerically by using the

Gaussian Quadrature method of integration and in this manner the error introduced is of the order of $\left(10^{-6}.\underset{mn}{Z}^{i\nu}(\infty)\right)$.

CHAPTER 5

NUMERICAL RESULTS FOR SELF AND INPUT IMPEDANCE OF PRINTED STRIP DIPOLES

5-1. A Printed Strip Dipole Excited by a Microstrip Transmission Line Embedded in the Dielectric

In this case, the excitation mechanism is provided by a strip transmission line embedded inside the substrate (see Figures 5.1, 5.2) which couples energy parasitically to the microstrip dipole. Since the radiation mechanism of a microstrip dipole is very similar to that of a microstrip patch [55], the model developed in this dissertation is applicable to the analysis and design of microstrip elements which are rectangularly shaped but with a width smaller than the element length. Reference to Figures 5.1 and 5.2 gives reinforcement to the assertion that the parameters of the problem are arbitrary in the development of the model, including substrate thickness and relative permittivity to account for previously recognized substrate effects [33] - [38]. In addition, the thickness of the metallic conductors is included, strip transmission line and microstrip antenna widths may differ and the effects of the microstrip dipole overlap and offset with respect to the transmission line on the current distribution are investigated. If one determines the current distribution by applying the method of moments (see Chapter 3), then transmission line theory is invoked to evaluate at the chosen reference plane, the self impedance Z_s of the microstrip dipole. This leads to a

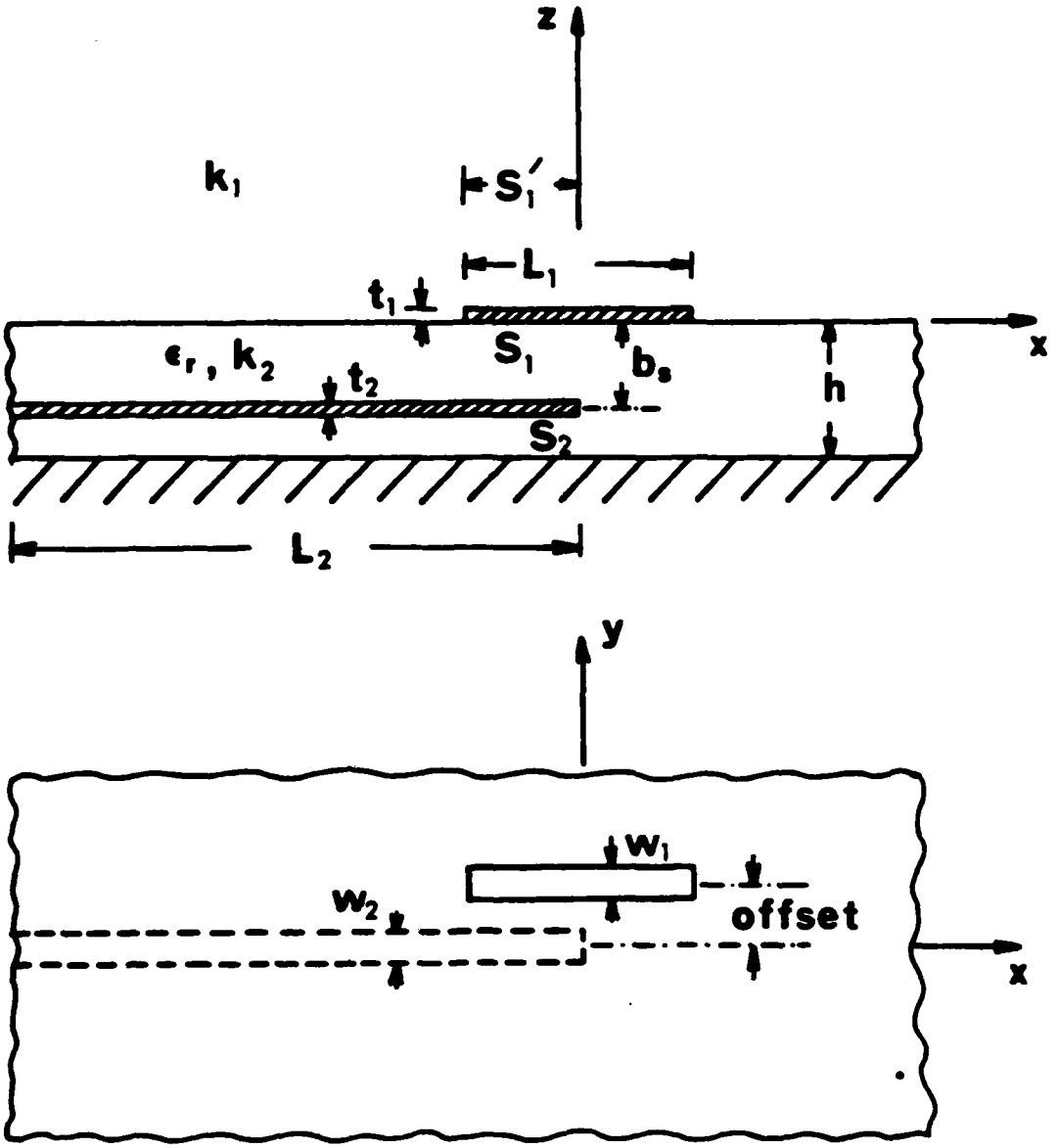

Figure 5.1

Side and Top View of a Printed Strip Dipole Excited by a Transmission Line Embedded in the Dielectric

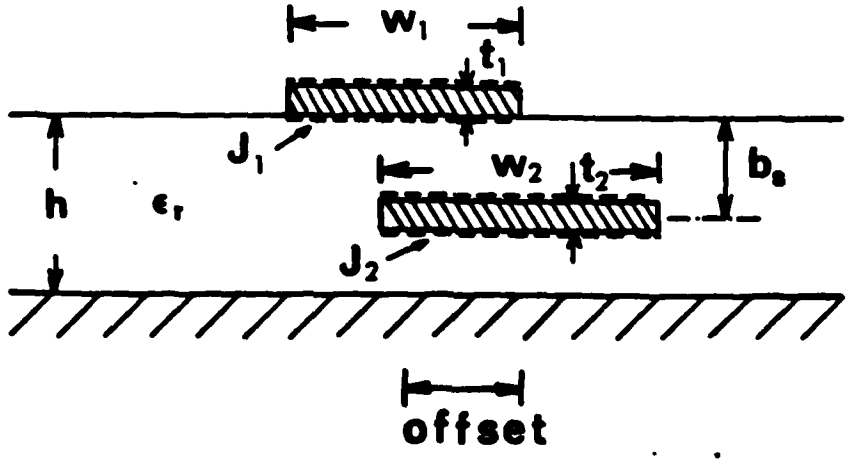

Figure 5.2

Cross Section of a Printed Strip Dipole Excited by a Transmission Line Embedded in the Dielectric

design procedure which yields the microstrip dipole length, overlap and offset so that a desired input match can be achieved for a given substrate. In all the results which are going to be presented below, the operating frequency is 10 GHz.

A. Self-Impedance Evaluation

For the evaluation of the microstrip dipole self-impedance, transmission line theory is applied and, because of this, unimodal behavior of the field far from the strip/dipole coupling region is essential. In order to satisfy this requirement, the transmission line is kept very close to the ground plane giving a ration $w_2/(h-b_s) > 2.0$.

For the particular geometry considered here, a unimodal field is excited under the transmission line and, as a result, the amplitude of the current distribution beyond an appropriate reference plane looks like a standing wave which is due to TEM waves traveling in opposite directions. For this reason, the microstrip line is approximsted by an ideal transmission line of characteristic impedance Z_o which is terminated in an unknown impedance (see Figure 5.3). This Quasi-TEM mode has a wavenumber β and a standing wave ratio SWR equal to the average values evaluated from the original current.

If the origin of x coordinates is taken at the position of Z_s, then the voltage and current waves on the ideal transmission line, with respect to this plane of reference, are given by:

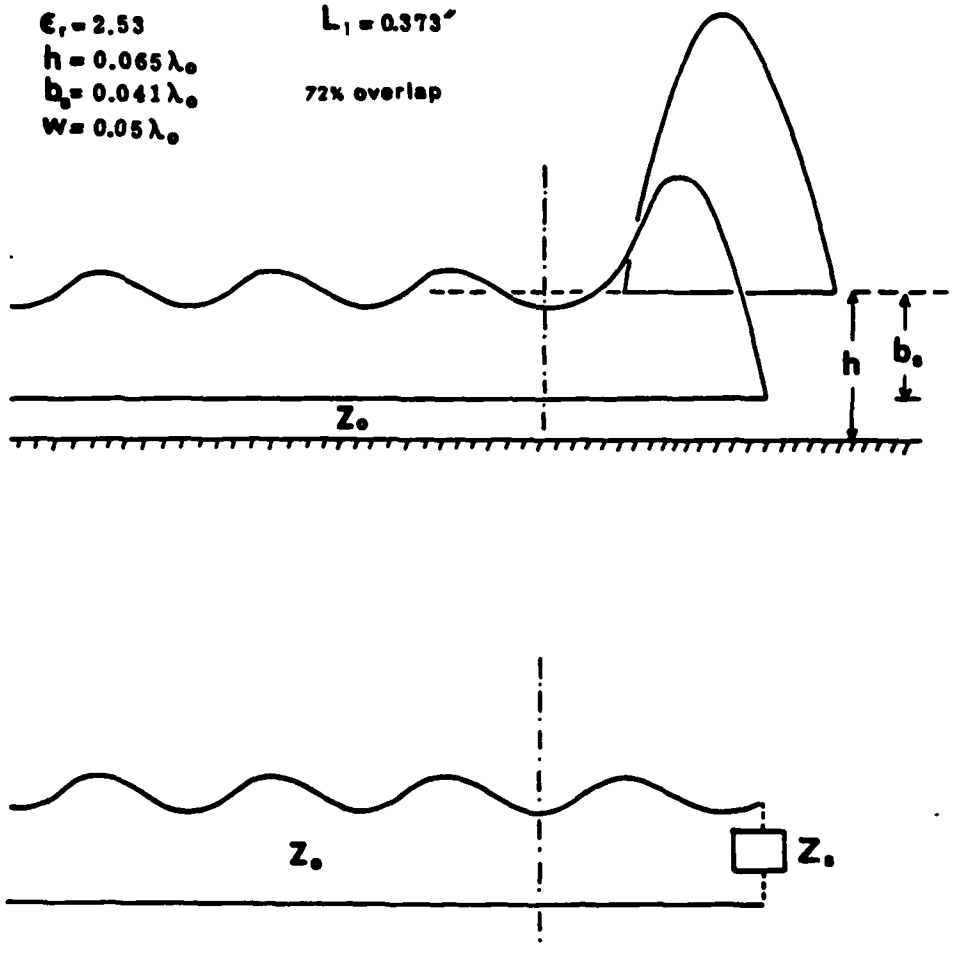

Figure 5.3

Current Amplitude on the Strip Dipole and Microstrip Transmission Line

$$V(x) = Ae^{-j\beta x} + Be^{j\beta x} \tag{5.1}$$

and

$$I(x) = \frac{1}{Z_o}[Ae^{-j\beta x} - Be^{j\beta x}] \tag{5.2}$$

If one considers the positions x_{max} and x_{min} of two consecutive maxima and minima, equation (5.1) gives

$$\frac{I_{max}}{I_{min}} = \frac{1 - \frac{B}{A}e^{j2\beta x_{max}}}{1 - \frac{B}{A}e^{j2\beta x_{min}}} e^{-j\beta(x_{max}-x_{min})} \tag{5.3}$$

Since the absolute difference between x_{max} and x_{min} is equal to one-fourth of the wavelength of the guided wave ($x_{max}-x_{min} = \lambda g/4$), then equation (5.3) can be written as

$$\frac{I_{max}}{I_{min}} = \frac{1 - \frac{B}{A}e^{j2\beta x_{max}}}{1 - \frac{B}{A}e^{j2\beta x_{min}}} e^{\pm j\frac{\pi}{2}} \tag{5.4}$$

The reflection coefficient Γ is defined as

$$\Gamma(x) = \frac{B}{A}e^{j2\beta x} = \Gamma(0)e^{j2\beta x} \tag{5.5}$$

If one considers that

$$\gamma = \frac{I_{max}}{I_{min}} e^{\pm j\frac{\pi}{2}} \tag{5.6}$$

then equation (5.3) gives the following expression for the reflection coefficient,

$$\Gamma(0) = -\frac{\gamma - 1}{\gamma + 1} e^{-j2\beta x_{max}} \qquad (5.7)$$

From (5.1) and (5.2) an expression for the self impedance Z_s evaluated at the position x_o can be written as follows:

$$\frac{Z_s(x_o)}{Z_o} = \frac{1 + \Gamma(x_o)}{1 - \Gamma(x_o)} \qquad (5.8)$$

If now this plane of reference is considered at the position of the first current maximum d_{max} from the end of the open circuited transmission line, then the self impedance measured with respect to this plane is given by

$$\frac{Z_s(d_{max})}{Z_o} = \frac{1 + \Gamma(d_{max})}{1 - \Gamma(d_{max})} = \frac{1 + \Gamma(0)e^{j2\beta d_{max}}}{1 - \Gamma(0)e^{j2\beta d_{max}}} \qquad (5.9)$$

Since for the evaluation of $\Gamma(d_{max})$, the method of moments together with transmission line theory has been applied, equation (5.9) indicates that the evaluated self impedance depends on the characteristics of the substrate (ε_r,h) as well as on the embedding distance of the transmission line, the overlap, the offset and the length of the dipole.

The fundamental design procedure is now revealed. One wants to choose, for a given substrate, the right position of the dipole so that optimum resonance (in other words, perfect match) is obtained. The condition for optimum resonance is characterized by the relation

$$\frac{Z_s(d_{max})}{Z_o} = 1 \qquad (5.10)$$

which combined with (5.9) gives

$$\Gamma(d_{max}) = 0 \qquad (5.11)$$

or

$$\Gamma(x) = 0 \qquad (5.12)$$

This means that one wishes to find the geometry which perfectly matches the dipole to the transmission line.

B. Dipole Length and Overlap Variation

The self impedance is evaluated using equation (5.9) as a function of the length L_d of the dipole and the overlap κ_{ovp}

$$\kappa_{ovp} = \frac{S_1'}{S_1} \% \qquad (5.13)$$

where S_1' is the part of the surface S_d of the dipole which is over the transmission line (Fig. 5.1). The real and the imaginary parts of the normalized self impedance are plotted (Fig. 5.4) for a substrate thickness h = 0.077", dielectric constant ε_r = 2.53 and embedding distance b_s = 0.0485". The width of the strips is w = 0.060" and the thickness t = 0.00025". The length of the dipole is varying between 0.373" and 0.349" and the overlap takes values between 38% and 86%. Figure 5.4 implies that as the overlap becomes larger, the dipole length curves approach

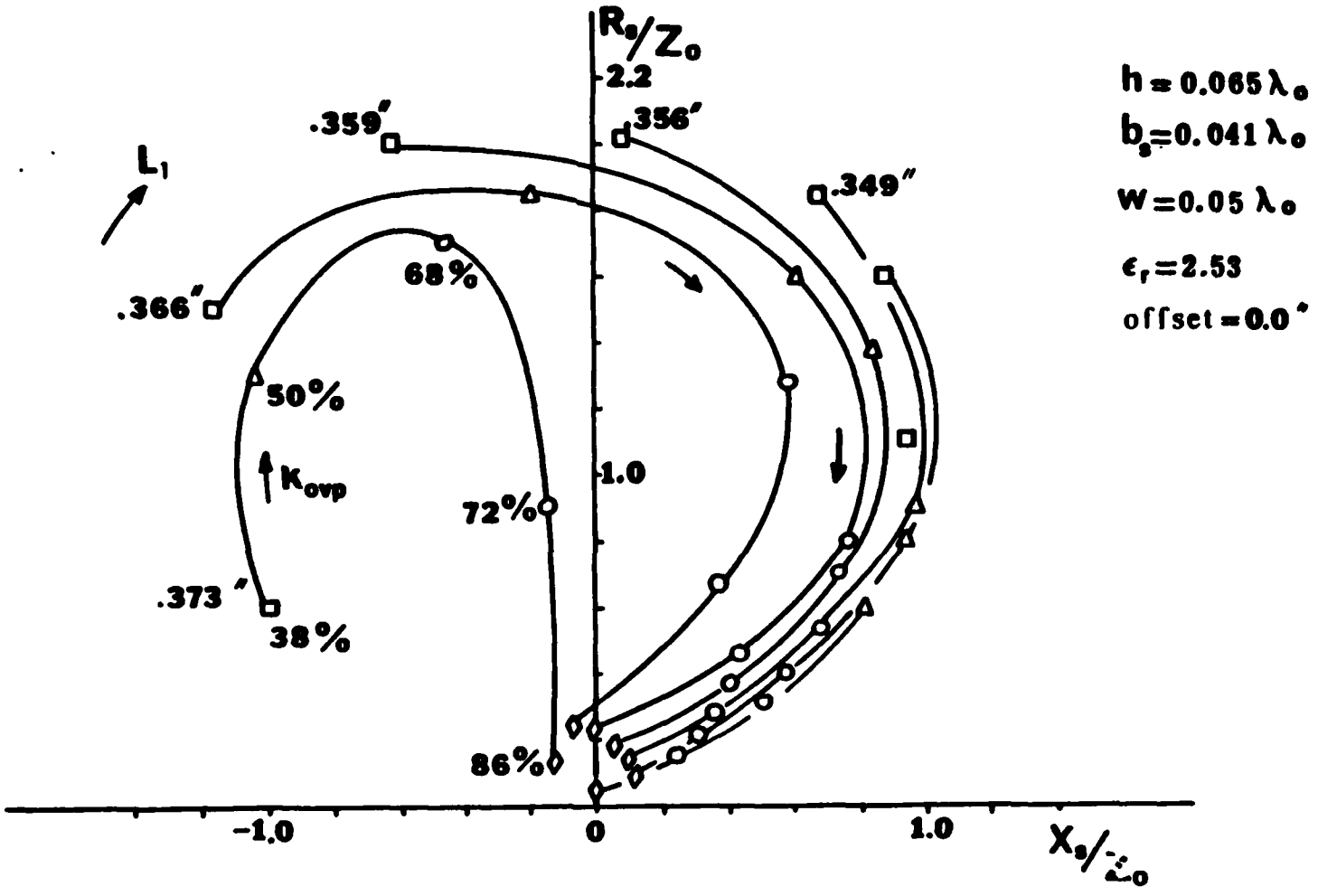

Figure 5.4

Z_s/Z_o as a Function of κ_{ovp} and L_1

the origin of the axis, which means that as the dipole moves to the left from the end of the transmission line, the coupling weakens and the reflection coefficient on the microstrip line approaches its value at open circuit. However, there exists a particular overlap for which the curve of the dipole lengths goes through the point $\frac{Z_s}{Z_o} = 1$; in other words, for the geometry considered above, there is one value for the overlap and a specific dipole length so that the dipole is perfectly matched to the transmission line.

C. Dipole Length and Offset Variation

It is of interest to investigate now the dependence of the normalized self impedance on the offset and the dipole length. Again, the real and imaginary parts of the normalized self impedance are plotted (Figure 5.5) for a substrate thickness h = 0.077", dielectric constant ε_r = 2.35 and embedding distance b_s = 0.0485". The width of the strips is w = 0.060", the thickness t = 0.00025" and the overlap κ_{ovp} = 50%. The length of the dipole varies between 0.373" and 0.349" and the offset takes the values 0.00", 0.02", 0.04", and 0.08". From Figure 5.6 one can see that as the offset becomes larger, the coupling weakens and the dipole length curves are shifted to smaller values for the self impedance. Also, the resonant length of the dipole, or in other words the dipole length for which the self impedance becomes real, is a monotonically descending

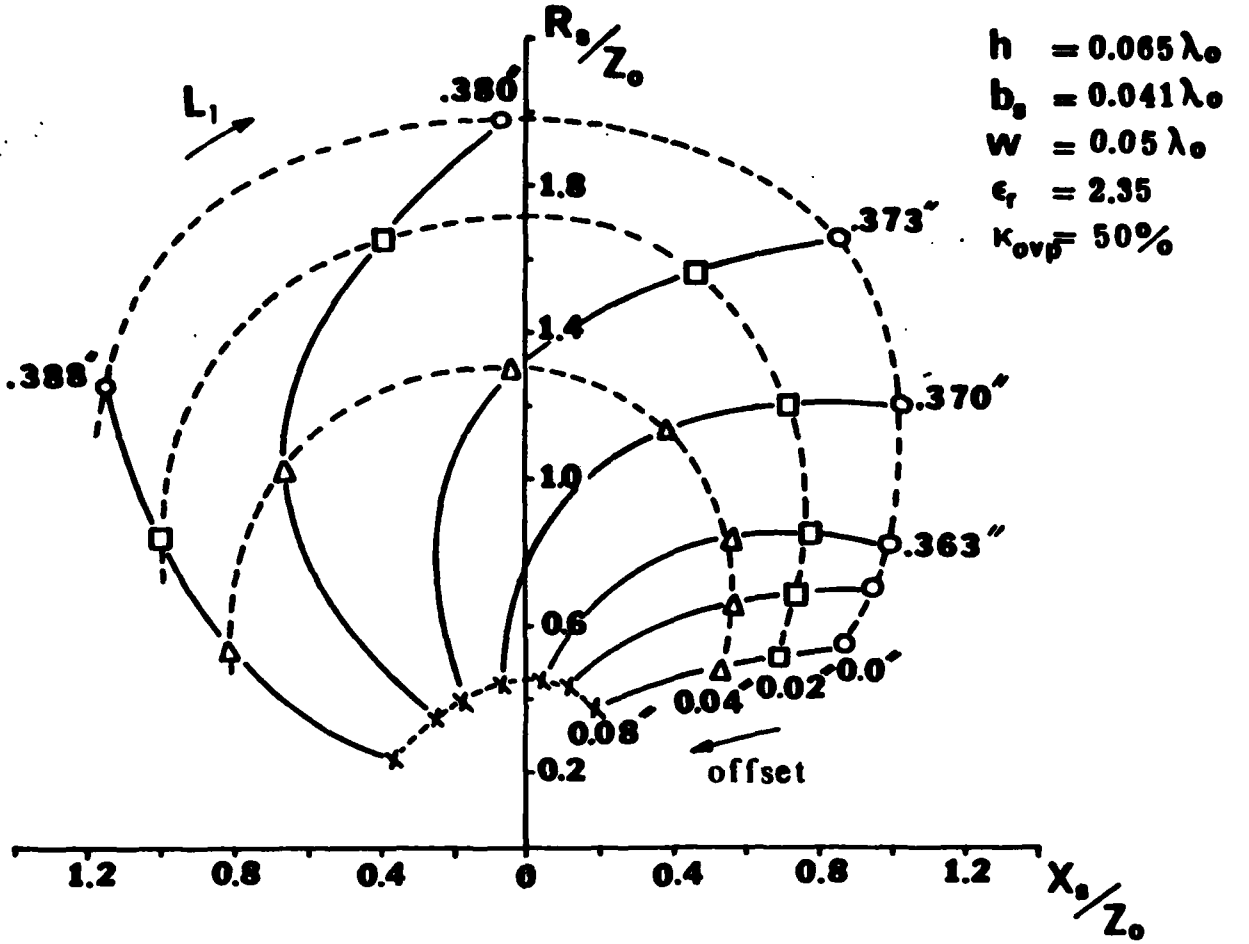

Figure 5.5

Z_s/Z_o as a Fuction of the Offset and L_1

of the offset, which means that as the offset changes to larger values, the dipole self impedance becomes more capacitive. Again, as happened in the case of the overlap variation, one can see that there exists a specific offset which can give optimum resonance if the dipole length is changed appropriately.

D. Dipole Length and Substrate Thickness Variation

As mentioned before, the normalized self impedance is also a function of the substrate characteristics and the position of the transmission line. In order to examine this dependence, the width, thickness, overlap and the distance of the transmission line from the ground plane are kept constant at the values given above, the dielectric constant becomes equal to 2.53, the dipole length is varied again between 0.373" and 0.349", and the substrate thickness takes the values 0.0645", 0.0765", 0.0825", and 0.0945". Figure 5.6 indicates that as the substrate thickness takes larger values, the coupling between the dipole and the transmission line becomes smaller, the dipole resonant length decays monotonically and the self impedance for a given dipole length becomes more capacitive. Also, as happened in the two previous cases of the overlap and offset variation, there is a unique value for the embedding distance which combines with the appropriate dipole length to give a perfect match.

It is also interesting to see how the current dis-

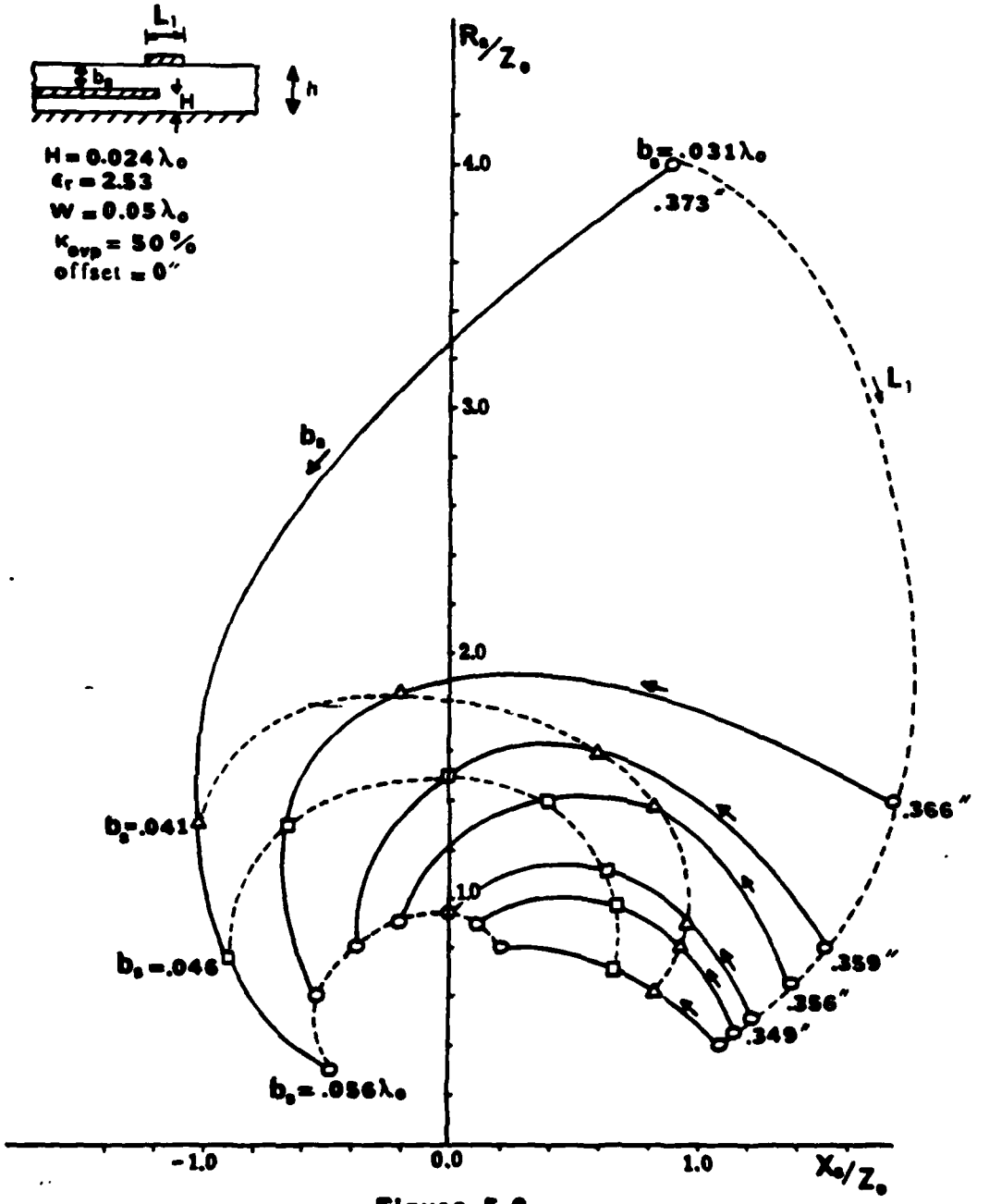

Figure 5.6

Z_s/Z_0 as a Function of b_s and L_1

tribution changes as a function of the substrate thickness h around optimum resonance. Figure 5.7 displays the current distribution normalized to the incident current on the transmission line for h = 0.099" (undercoupled), h=0.093" (perfectly matched) and h=0.082" (overcoupled). The substrate is duroid (ε_r = 2.53), the distance of the transmission line to the ground plane is 0.0285" and the length of the dipole L_1 = 0.353". As shown in the figure, the current on the dipole takes its maximum value when it is perfectly matched.

E. Comparison with Experimental Results

The theoretical analysis of a printed strip dipole electromagnetically coupled to an embedded microstrip line is tested by comparing theoretical results to experimental ones. Stern and Elliott [43] measured experimentally the self impedance of strip dipoles with rounded corners (Figure 5.8) printed on duroid boards (ε_r = 2.35) of substrate thickness h=0.077", excited by a microstrip transmission line in the dielectric at a distance from the ground plane equal to 0.0285". The width of the strips was w = 0.060" and the thickness t = 0.00025". The self impedance was measured for different dipole lengths and its normalized values are shown on a Smith chart (triangles) in Figure 5.9. The solid line corresponds to the theoretical results. From Figure 5.8 one can see that the experi-

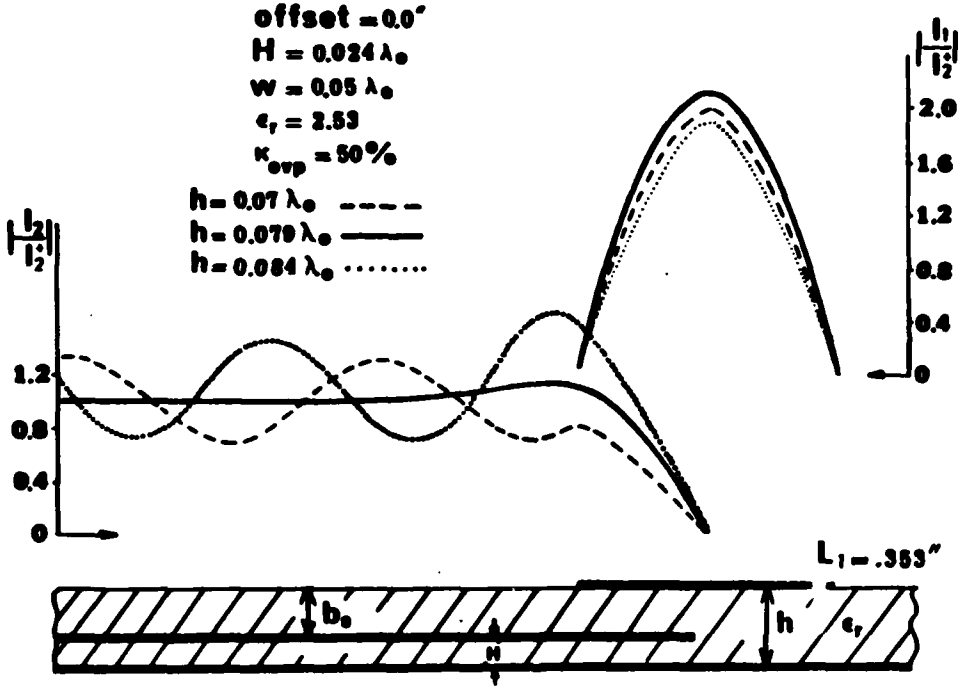

Figure 5.7

Current Amplitude on the Strip Dipole and Transmission Line

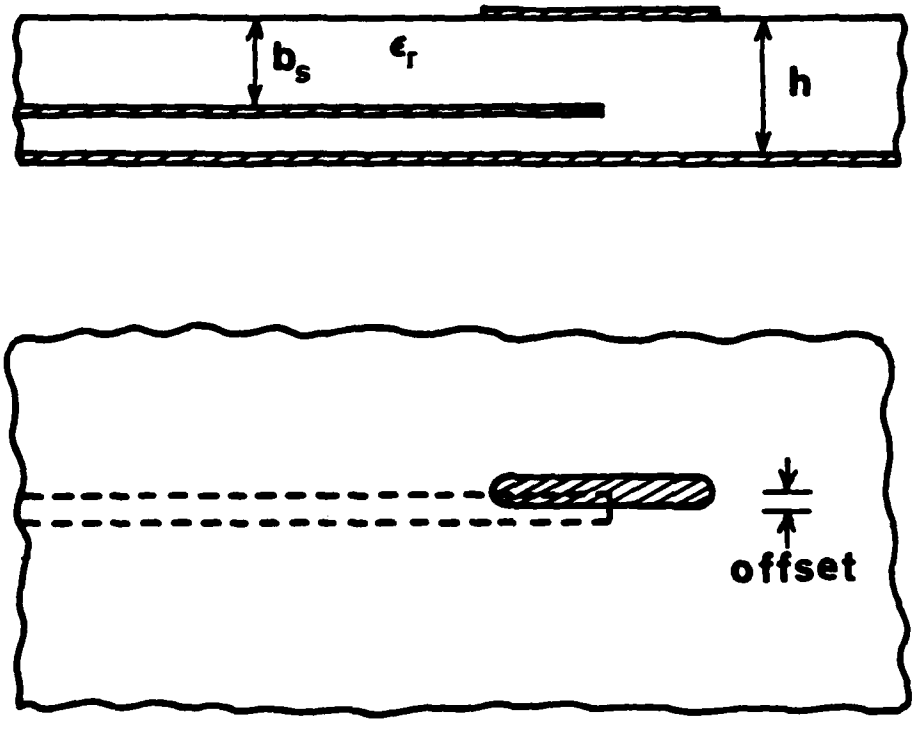

Figure 5.8

Printed Strip Dipole with Round Corners EM Coupled to a Microstrip T.L.

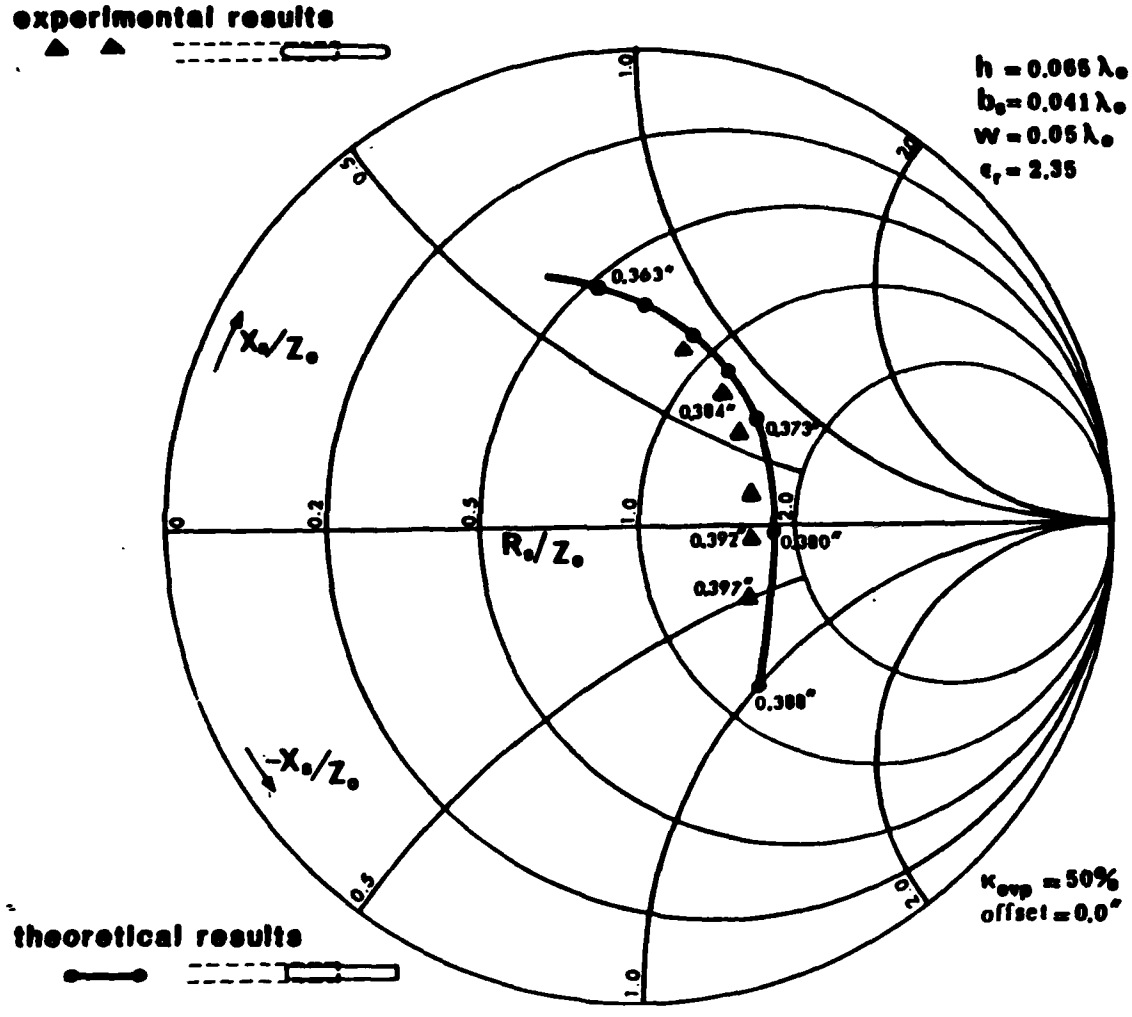

Figure 5.9 Comparison of Theoretical to Experimental Results

mental resonant length is about 0.390" while the theoretical one is 0.379". Therefore, there is a difference of 2.75% with approximately 2% resulting from the different shapes of the dipoles. Those which were studied analytically h a rectangular shape whereas those measured experimentally had round corners [56].

The difference between the theoretical and experimental values of the self impedance has two attributions:

i) Different shapes of the dipoles

ii) The fact that in the theoretical evaluation of the current, the hybrid nature of the modes propagating in the microstrip was taken into account while for the experiments only an equivalent TEM mode was measured.

5-2. Strip Dipoles Excited by a Gap Generator

This section of Chapter 5 presents design procedures for microstrip dipoles printed on or embedded in the dielectric substrate. The dipoles are center-fed by an in phase unit voltage delta gap generator. All the dimensions presented are normalized with respect to the free space wavelength λ_o. Due to an assumed time dependency of $e^{j\omega t}$, inductive reactance is positive in all plots. The dipole is considered either alone or in the presence of parasitic dipoles printed or embedded in the dielectric. The material given here relates the antenna geometry (dipole

length, substrate thickness, dipole-ground plane distance, position and length of the parasitics) to antenna characteristics (resonant length and resonant resistance). The presentation of the numerical results is completed in three steps: At first, a dipole embedded in the substrate is considered and its characteristics are discussed in terms of the embedding distance. After that, this dipole is considered in the presence of one printed parasitic dipole and the change in its performance is studied. Finally, the same dipole is considered in the presence of two parasitics, one printed on the interface, the other embedded in the dielectric. Its characteristics are studied in terms of the relative positions of the parasitics as well as their overlap.

A. One Dipole Printed or Embedded in the Substrate

One of the most important characteristics of a dipole is its input impedance (Fig. 5.10). Figures 5.11 and 5.12 show the real and the imaginary parts of the input impedance when the strip dipole is printed on a duroid board ($\varepsilon_r = 2.45$) with substrate thickness h equal to $0.2\ \lambda_o$ and for different strip widths ($w = 0.0002\lambda_o$, $0.001\lambda_o$, $0.01\lambda_o$). Figure 5.11 shows that the input resistance around resonance is insensitive to width variation while its value far from resonance becomes lower as the width increases. The effect on the resonant length is also very small as Figure 5.12 reveals. However, the input reactance is very sensi-

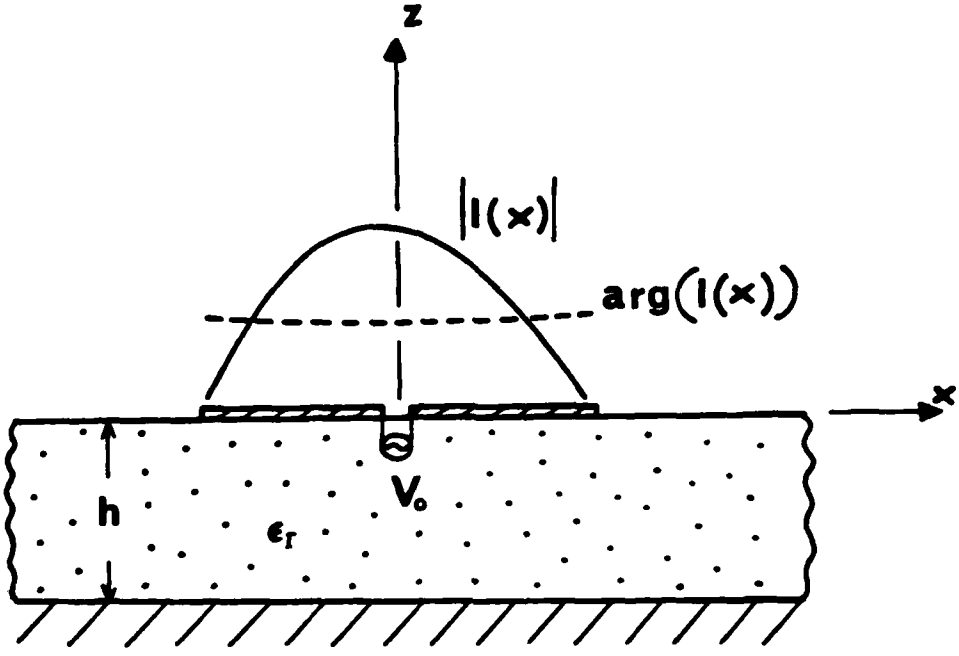

$$Z_{in} = \frac{V_o}{I(0)}$$

Figure 5.10

The Input Impedance of a Printed Strip Dipole Excited by a Voltage Gap Generator

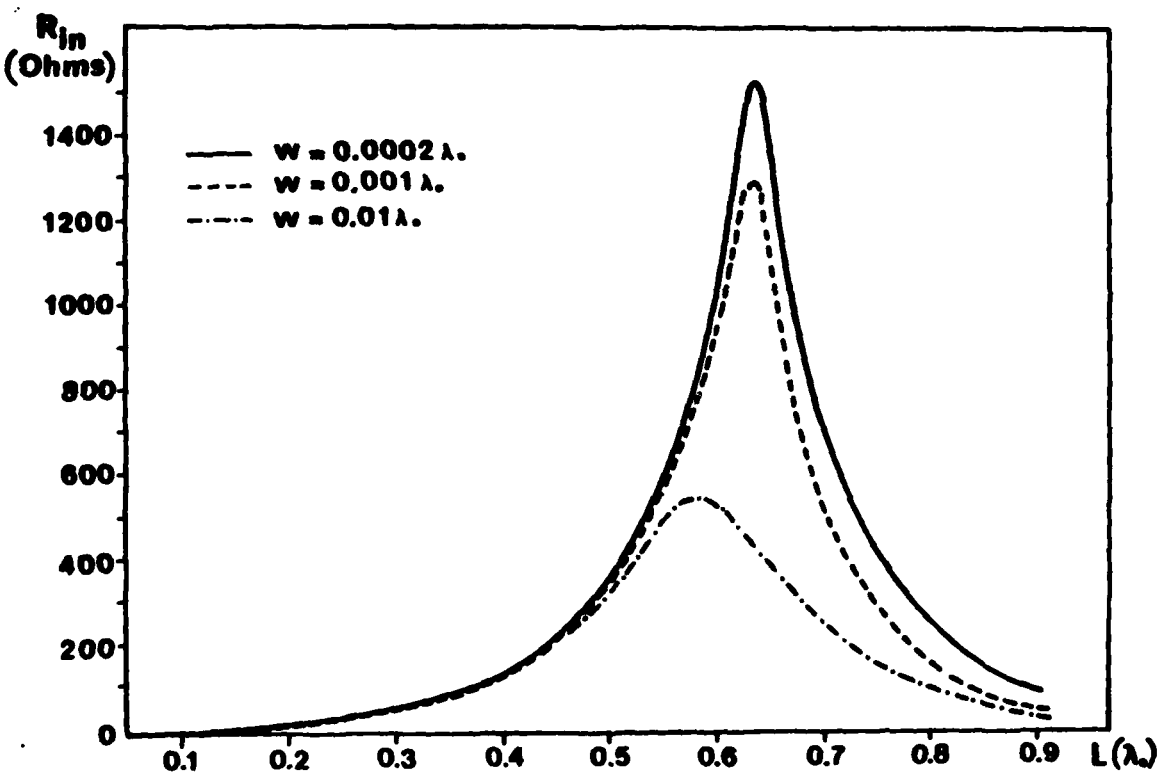

Figure 5.11

Real Part of the Input Impedance of a Printed Strip Dipole with ϵ_r=2.45, h=0.2λ. and t= 0.0001λ.

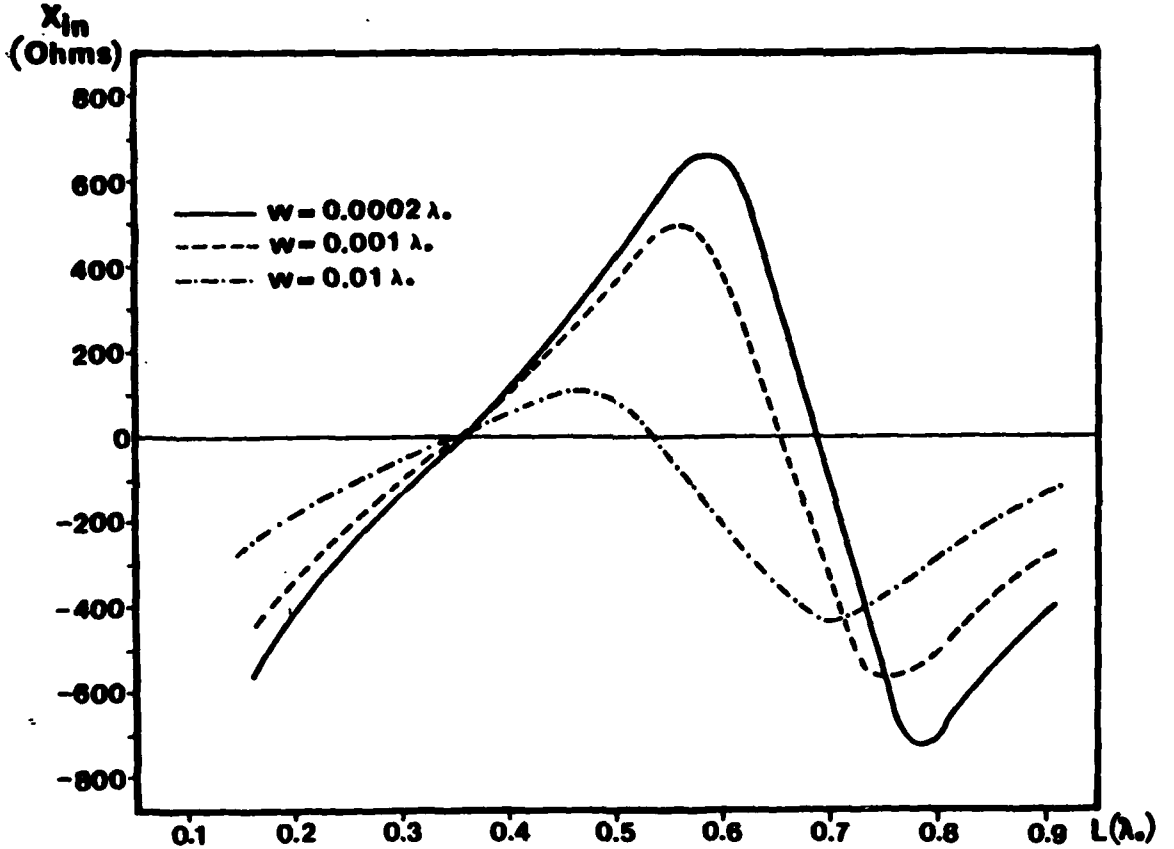

Figure 5.12

Imaginary Part of the Input Impedance of a Printed Strip Dipole with ϵ_r=2.45, h = 0.2 λ. and t = 0.0001 λ.

tive to changes in the width taking much lower values as the width becomes larger. From the figures one can conclude that the behavior of the input impedance of a printed strip dipole as the strip width is varied is similar to that of a free-space wire dipole as its radius is varied. Figure 5.13 shows the current distribution in amplitude and phase on a strip dipole printed on duroid ($\varepsilon_r = 2.45$) with substrate thickness $h = 0.2\lambda_o$, $w = 0.01\lambda_o$, $t = 0.0001\lambda_o$ and for L equal to $0.62\lambda_o$, $0.347\lambda_o$, and $0.248\lambda_o$.

Consider now the dipole shown in Figure 5.10 for duroid of dielectric constant $\varepsilon_r = 2.53$, substrate thickness $h = 0.065\lambda_o$, thickness of strip $t = 0.0001\lambda_o$ and width $w = 0.05\lambda_o$. Figure 5.14 shows how the resonant length L_r and the resonant resistance R_r vary as a function of the embedding distance b_s. It is interesting to note that as the strip dipole enters the dielectric substrate and moves closer to the ground plane, the resonant length decreases to a minimum value when the dipole is at an embedding distance equal to the half of the substrate thickness, and after that increases to a maximum value when the dipole approaches the ground plane. However, the behavior of the resonant resistance is different. It takes its maximum value when the dipole is printed on the interface and decreases to zero as the dipole enters the interface and moves close to the ground plane. The reson-

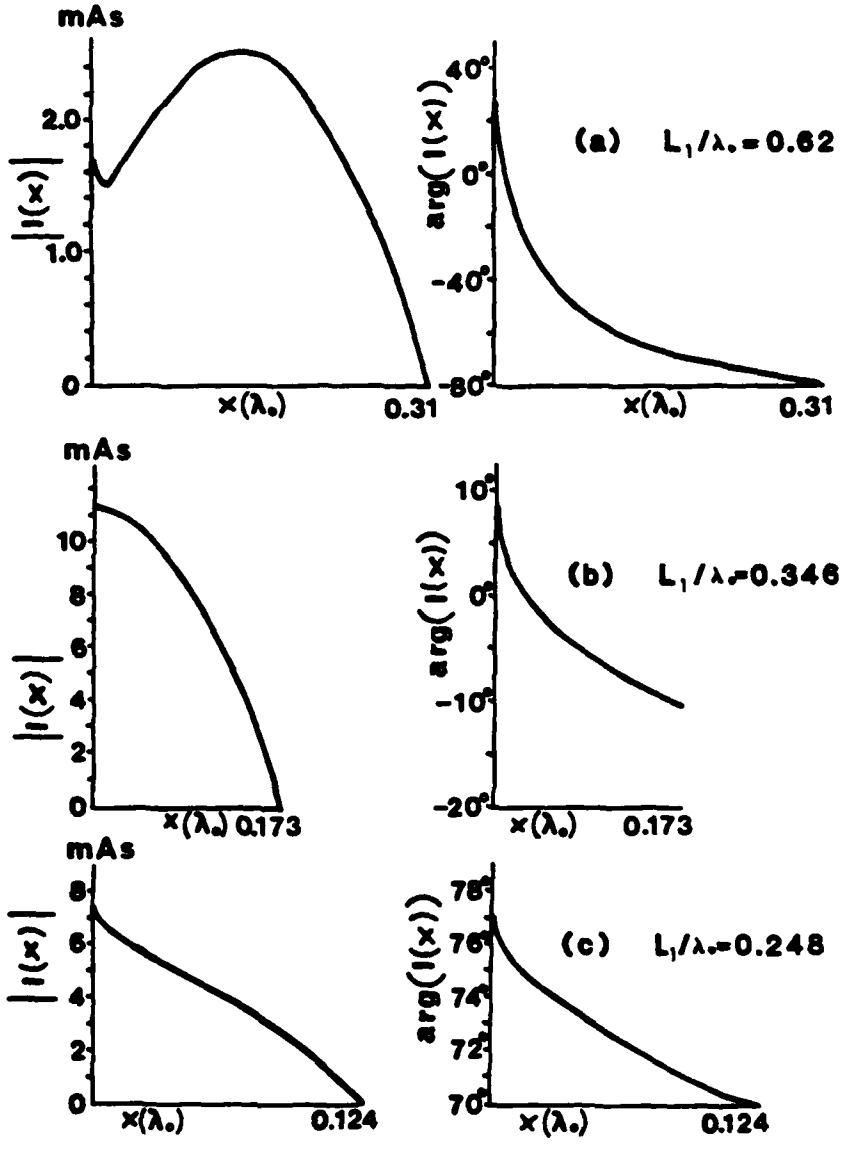

Figure 5.13

Current Distribution on a Printed Strip Dipole with ϵ_r=2.45, h = 0.2 λ_0 , w = 0.01 λ_0

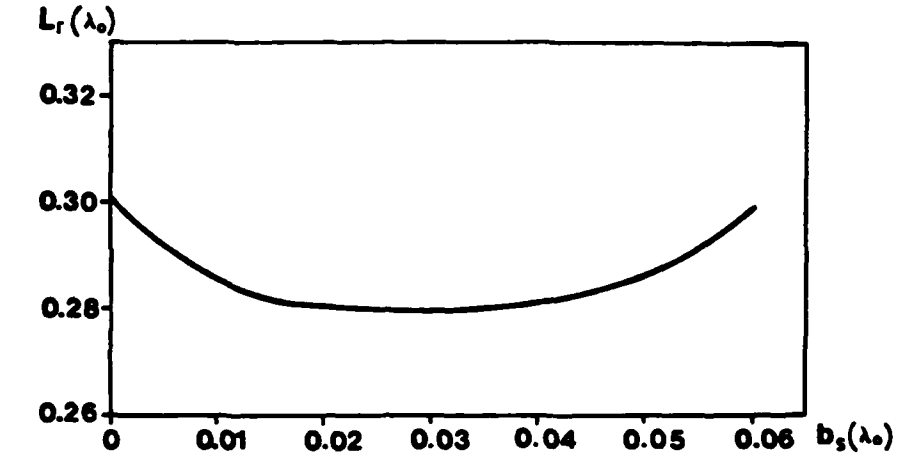

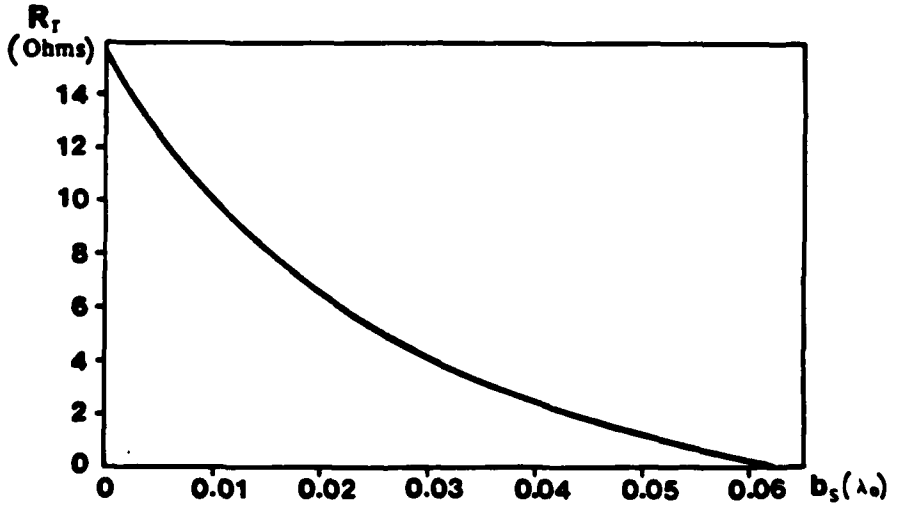

Figure 5.14

Resonant Length and Resonant Resistance of a Strip Dipole as Functions of the Embedding Distance. $\epsilon_r = 2.53, h = 0.065\lambda_o$, $t = 0.0001\lambda_o$ and $w = 0.05\lambda_o$.

ant resistance when the dipole is on the interface takes such a small value because the substrate is thin and the strip dipole is wide.

B. One Embedded Strip Dipole Excited by a Gap Generator in the Presence of a Printed Parasitic Dipole

The dipole of Figure 5.15 is now considered. In this case, the relative dielectric constant for the substrate is 2.35, the substrate thickness h is equal to $0.065\lambda_o$, the strip thicknesses are $t_1 = t_2 = 0.0001$, the strip widths are $w_1 = w_2 = 0.05\lambda_o$ and the overlap is 23%. As shown in Figure 5.16, the resonant length of the excited dipole as a function of the embedding distance does not go through a minimum as happened in the case of the single dipole but decreases monotonically as the exciter approaches the ground plane. The behavior of the resonant resistance is not that much different. For values of b_s smaller than half of the substrate thickness, it oscillates around a value of 15 ohms and for b_s larger than h/2 it decreases monotonically to zero as the exciter goes very close to the ground plane. It is interesting to compare the variation of the resonant length and resonant resistance as functions of the embedding distance for the cases of the single dipole and the dipole in the presence of a parasite (Figures 5.14, 5.16). One can observe that the parasitic not only changes the behavior of the resonant length and resonant resistance, but also

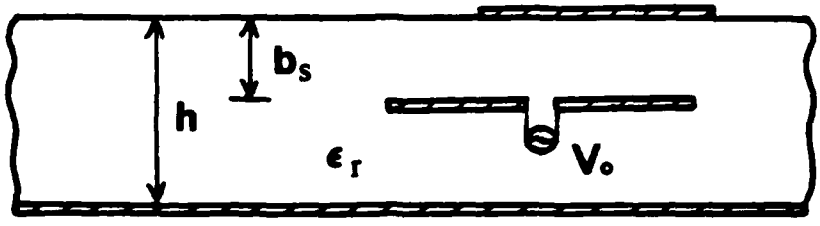

Figure 5.15

Embedded Strip Dipole Excited by a Voltage Gap Generator in the Presence of a Parasitic

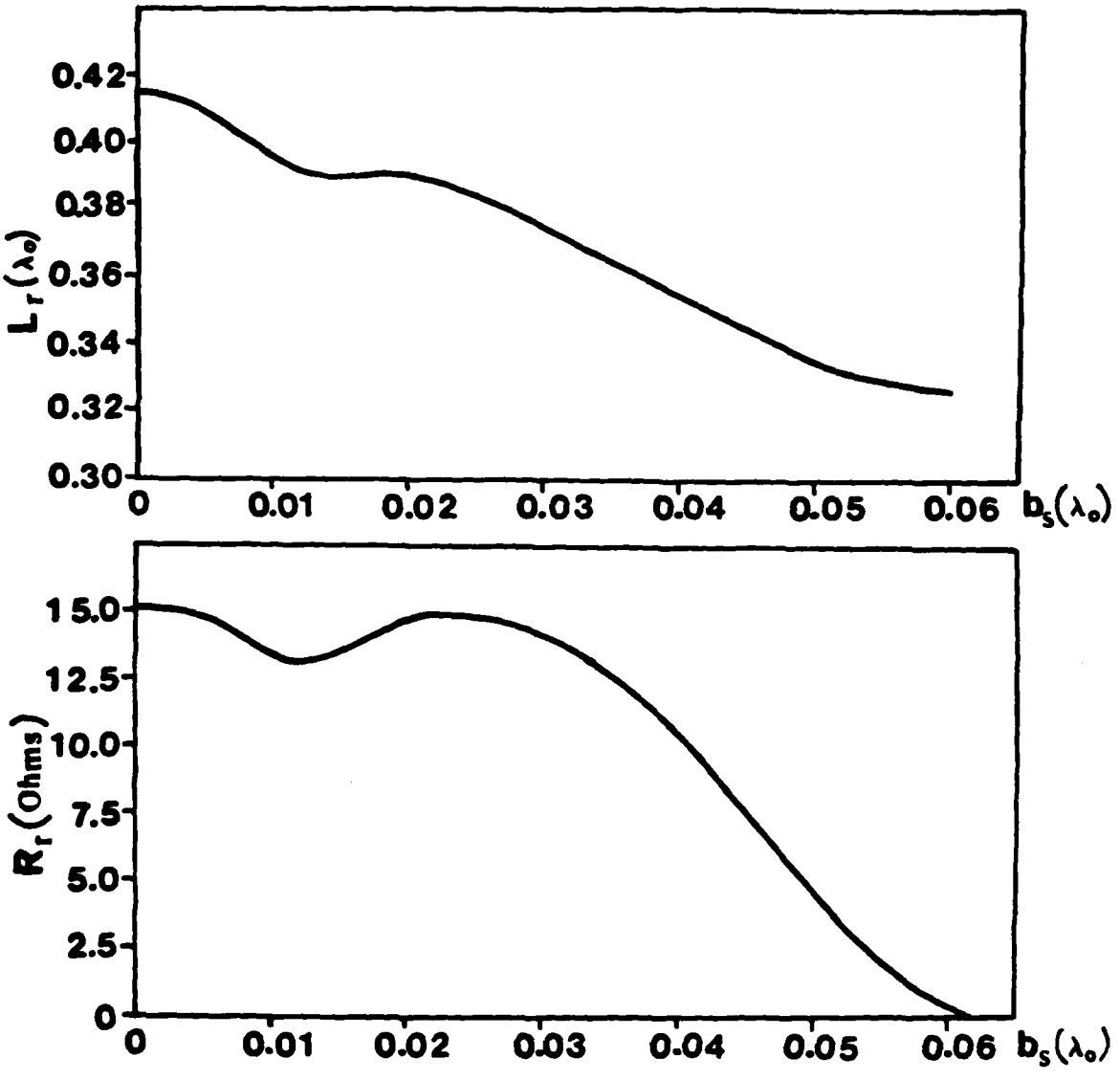

Figure 5.16

Resonant Length and Resonant Resistance of the Excited Dipole as Functions of its Embedding Distance ϵ_r=2.53 , h = 0.065λ_o w = 0.05λ_o. κ_{ovp} = 23% and t = t = 0.0001λ_o.

makes their values larger. This means that the bandwidth and the efficiency of the antenna are increased. It is also interesting to see how the resonant length and resonant resistance change as functions of the substrate thickness when the distance of the exciter from the ground plane is held constant. In Figures 5.17 and 5.18, the resonant length and resonant resistance are shown as functions of h when $\varepsilon_r = 2.35$, $w_1 = w_2 = 0.05\lambda_o$, $t_1 = t_2 = 0.0001\lambda_o$ and $h-b_s = 0.1\lambda_o$, $0.2\lambda_o$ respectively. In the first of these two figures, the substrate thickness takes values between $0.15\lambda_o$ to $0.25\lambda_o$ while in the second one h varies between $0.065\lambda_o$ and $0.075\lambda_o$. Except for the difference in values the behavior of L_r, R_r is the same in both cases. From Figures 5.17 and 5.18 one can see that as the parasitic dipole moves to greater distances from the exciter the coupling weakens and the resonant length and resonant resistance of the embedded dipole asymptotically tend, as one would expect to the values they have in the case of the single excited dipole (Figure 5.14).

C. An Embedded Strip Dipole Excited by a Gap Generator in the Presence of Two Parasitic Dipoles

The geometry for this antenna is shown in Figure 5.19. For this arrangement, with $\varepsilon_r = 2.35$, $h = 0.065\lambda_o$, $b_s = 0.041\lambda_o$, $t_1 = t_2 = 0.0001\lambda_o$, $\kappa_{ovp}^{(2)} = \kappa_{ovp}^{(3)} = 80\%$, $w_1 = w_2 = 0.05\lambda_o$, the real and imaginary parts of the input impedance for two different values of δ (distance of the embedded

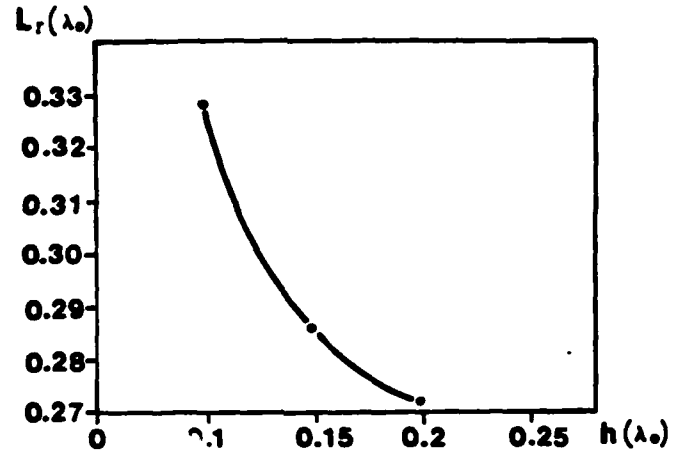

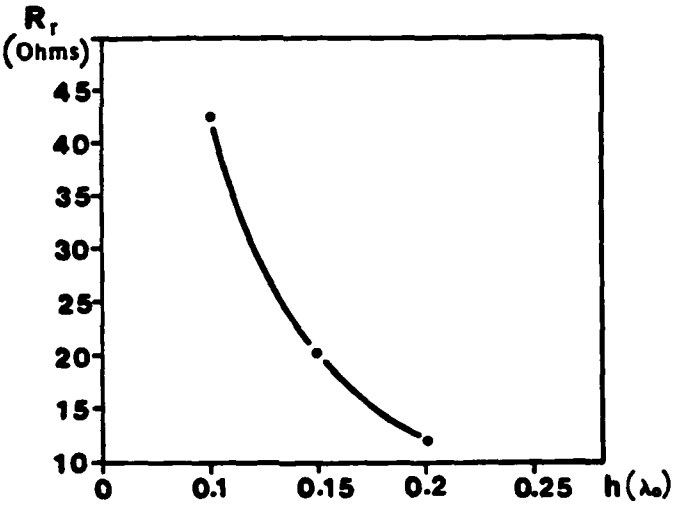

Figure 5.17

Resonant Length and Resonant Resistance of the Excited Dipole as Functions of the Sustrate Thickness $\epsilon_r = 2.35$, $h - b_s = 0.1\lambda_o$, $w = 0.05\lambda_o$ and $t_1 = t_2 = 0.0001\lambda_o$.

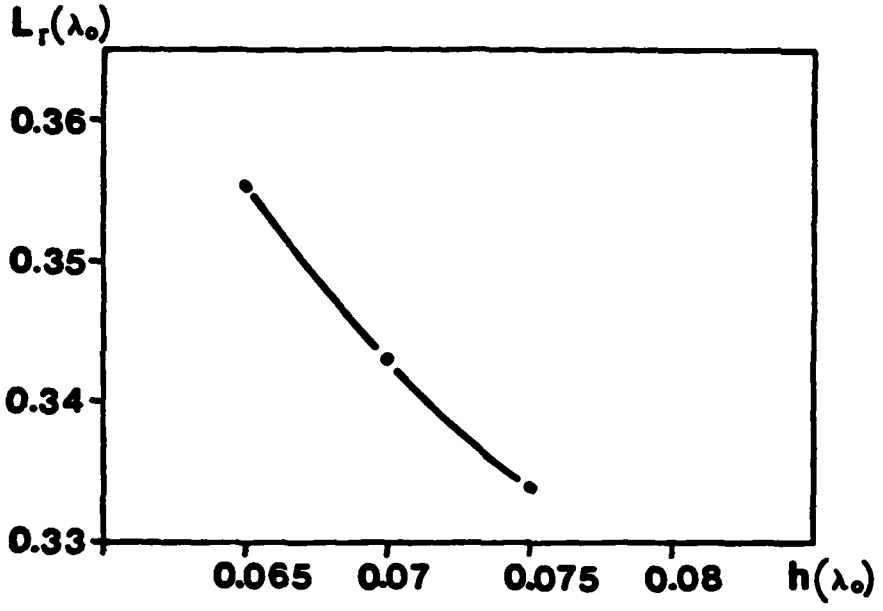

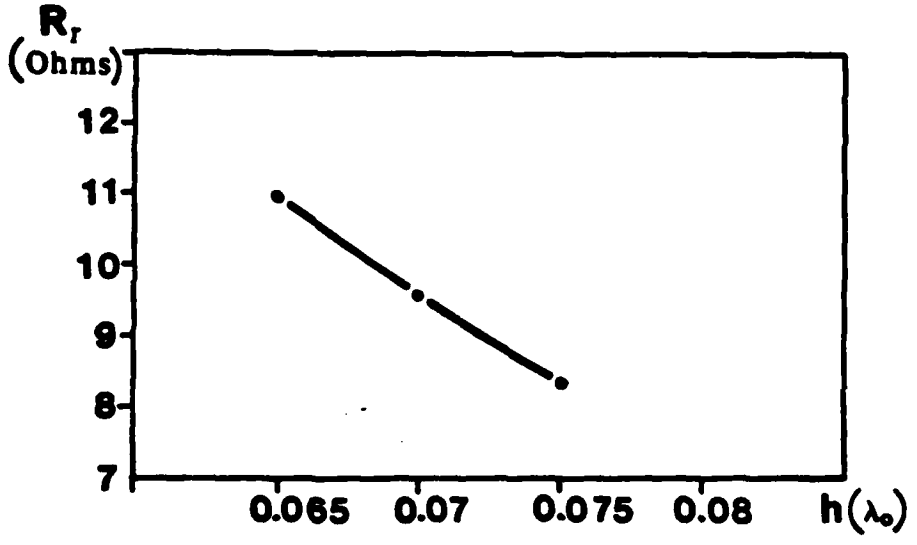

Figure 5.18

Resonant Length and Resonant Resistance of the Excited Dipole as Functions of the Substrate Thickness ϵ_r=2.35, h-b_s= 0.025λ_o , w = 0.05λ_o $\kappa_{ov\beta}$ 23% and t_1= t_2= 0.0001λ_o

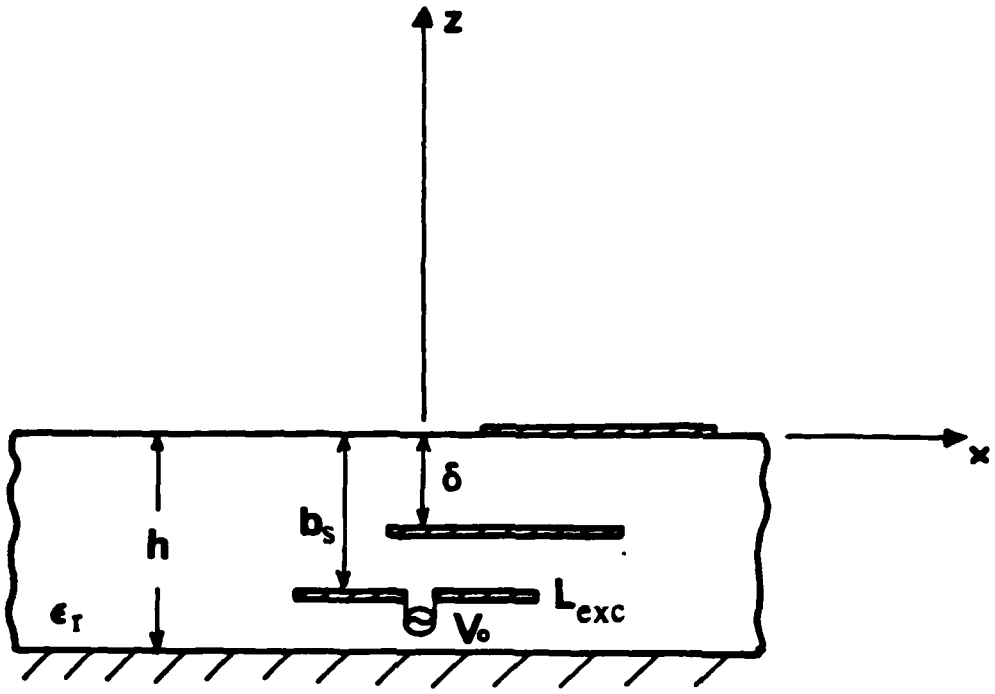

Figure 5.19

Embedded Strip Dipole Excited by a Voltage Gap Generator in the Presence of Two Parasitics. One Embedded in the Dielectric and the Other Printed on the Interface

parasitic from the interface) are given in Figures 5.20 and 5.21. From these two figures, one can see that, as the parasitic approaches the exciter, the resonance occurs at longer lengths of the excited dipole, while the bandwidth decreases and the resonant resistance increases to values above 100 ohms. The resonant length and resonant resistance as functions of the embedding distance δ are shown in Figure 5.22 for two different values of the overlap (50%, 80%).

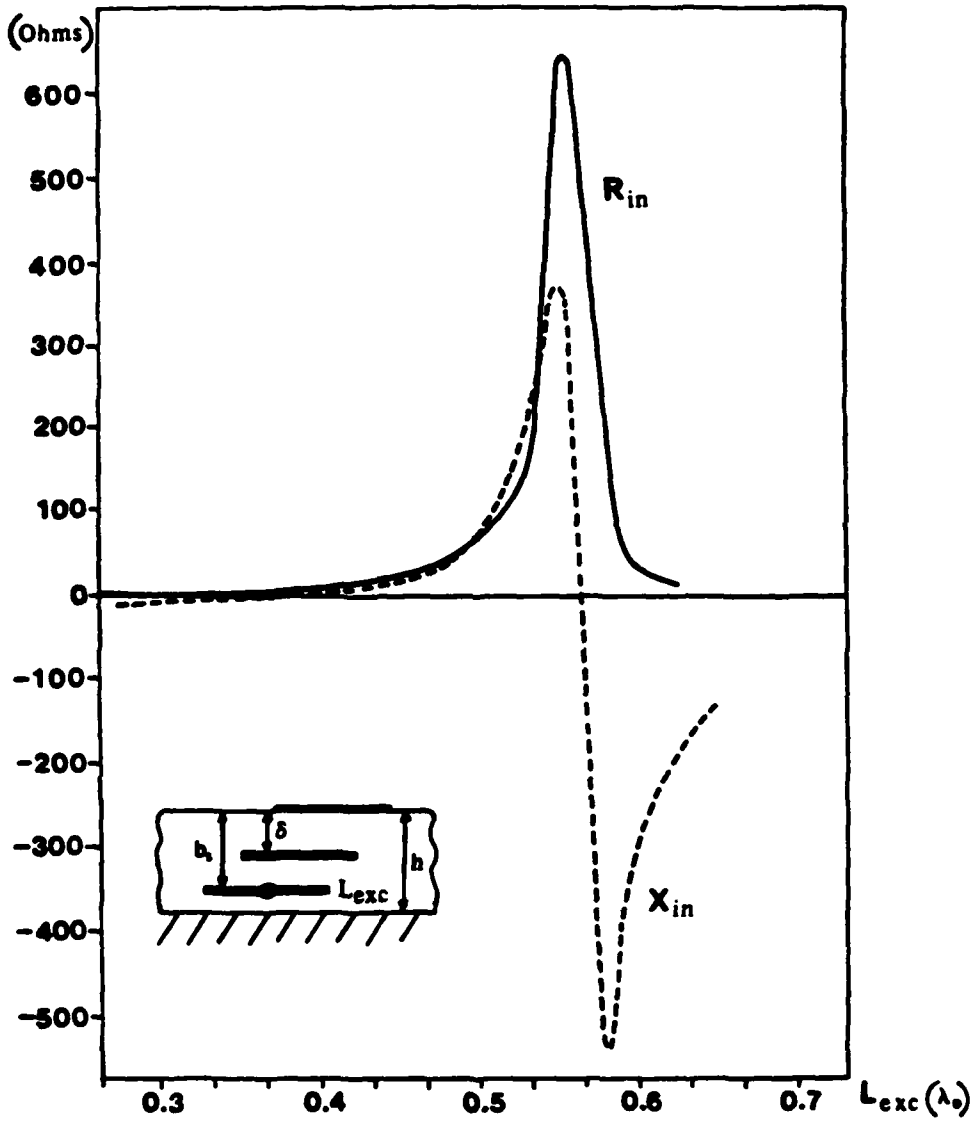

Figure 5.20

Input impedance of the Exciter as a Function of its Length for ϵ_r=2.35, h = 0.065λ. b_1=0.041λ. , w = 0.05λ. t_1=t_2=t_3= 0.0001λ. and δ=0.03λ.

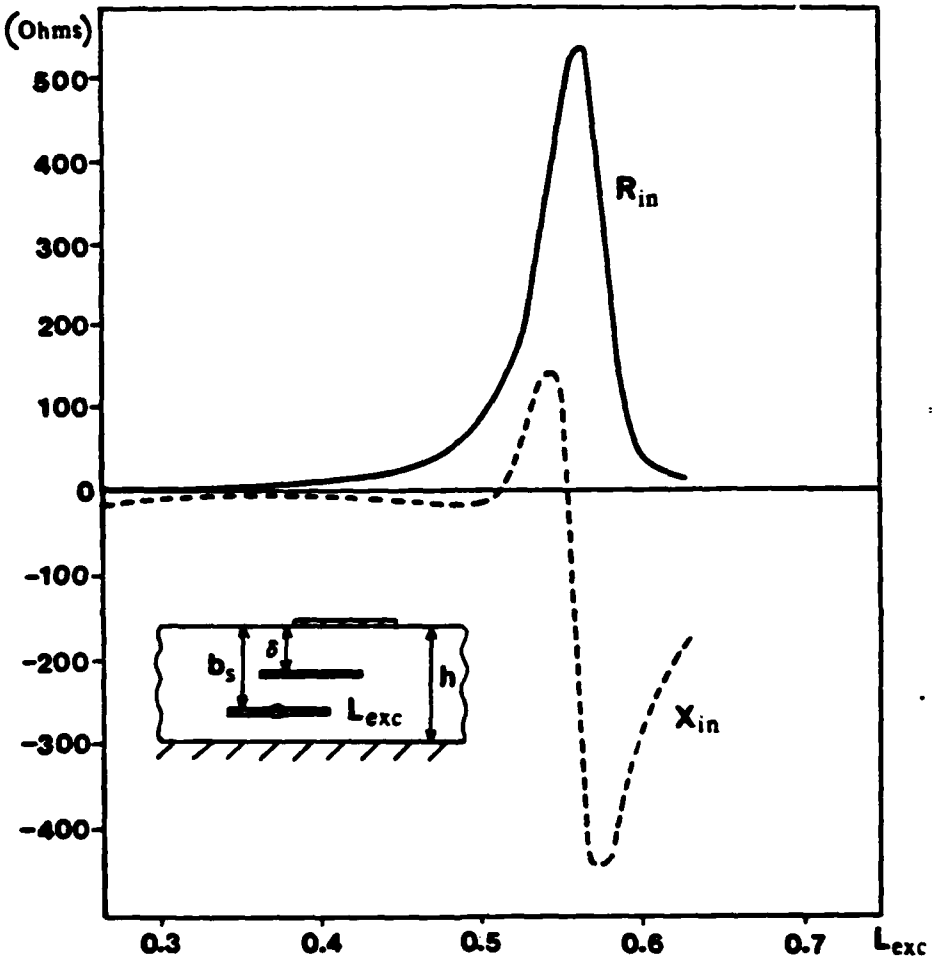

Figure 5.21

Input Impedance of the Exciter as a Function of its Length for $\epsilon = 2.35$, $h = 0.065\lambda_o$, $b_s = 0.041\lambda_o$, $w = 0.05\lambda_o$, $t_1 = t_2 = t_3 = 0.0001\lambda_o$

AD-A145 626 A GENERALIZED SOLUTION TO A CLASS OF PRINTED CIRCUIT ANTENNAS. (U) CALIFORNIA UNIV LOS ANGELES INTEGRATED ELECTROMAGNETICS LAB P B KATEHI-TSEREGOUNIS 15 JUN 84 2/2

UNCLASSIFIED UCLA-ENG-84-14 DAAG29-83-K-0067 F/G 9/5 NL

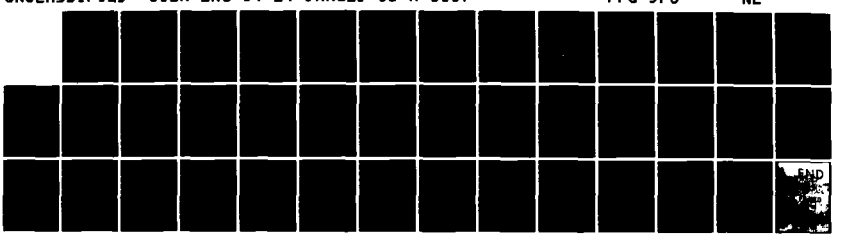

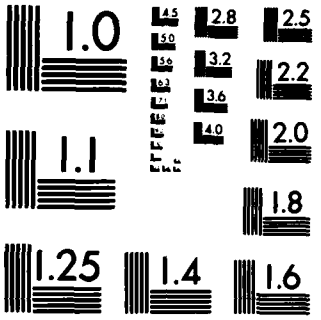

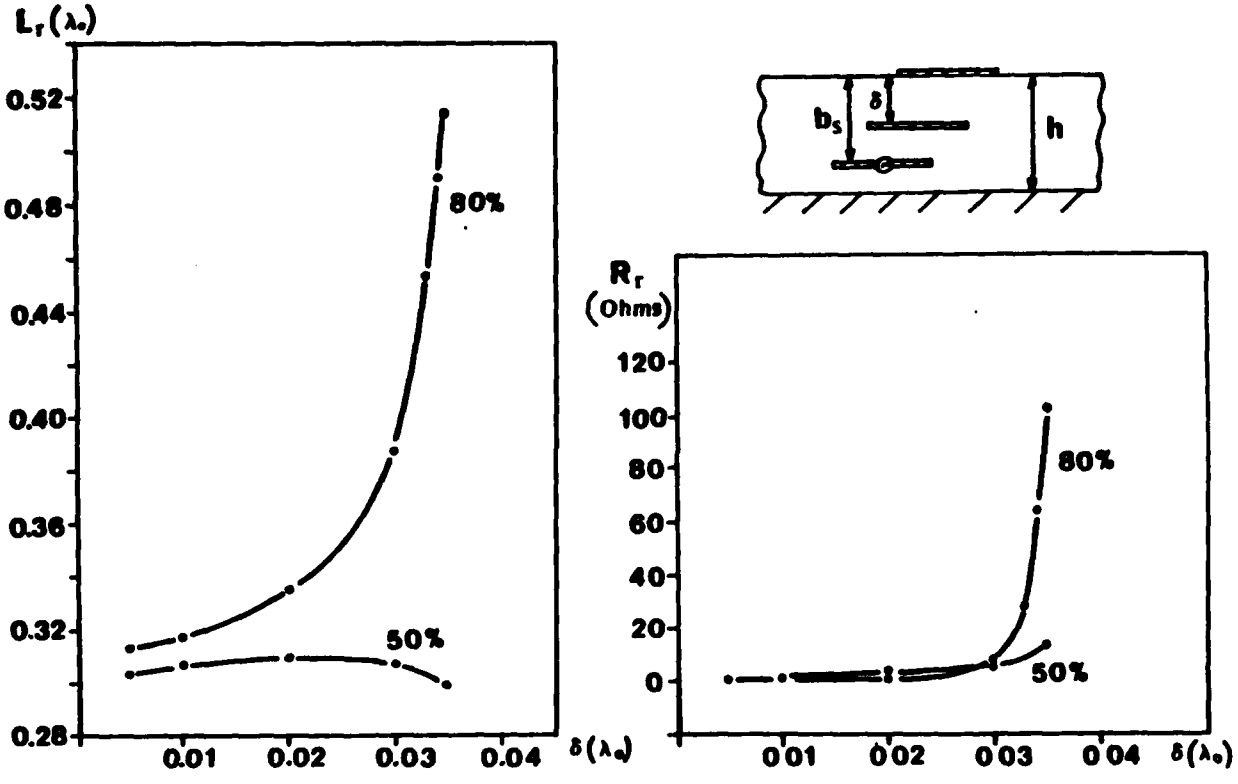

Figure 5.22

Resonant Length and Resonant Resistance of the Exciter as a Function of δ

ϵ_r2.35, h=0.065λ_o, b_s=0.041λ_o, w=0.05$\lambda_o$and t=t=t=0.0001λ_o

CHAPTER 6

RADIATION PATTERN OF PRINTED STRIP DIPOLES

6-1. Formulation of the Equations for the Far-Zone Field

Radiation pattern or far zone fields can be obtained by using a rigorous numerical technique as described in Chapter 2. The numerical technique, although valid for all distances, is quite expensive for the far zone computations. In the calculation of the radiation pattern, only the far zone fields above the air-dielectric interface are required. Hence, the conventional stationary phase method [57]-[58] can be used. The details of the method are covered in Appendix D. When a printed strip dipole is excited either by a gap generator or by a microstrip line embedded in the substrate with $h - b_s << \lambda_o$ (see Figure 6.1), the far-zone field is due totally to the radiation from the dipole. Under this assumption, the far-zone electric field is given by

$$\vec{E}(R,\theta,\phi) = \frac{e^{-jk_1 R}}{R} R_a \vec{R}_s \qquad (6.1)$$

In equation (6.1) R_a is a scalar (called the antenna shape factor) and is given by

$$R_a = j260 \left\{ \frac{\cos(k_1 \ell_x \sin\theta\cos\phi) - \cos(k\ell_x)}{k \sin(k\ell_x) \left[1 - \frac{k_1^2}{k^2} \sin^2\theta\cos^2\phi\right]} \right\} \cdot$$

$$\left\{ J_o\left(k_1 \frac{w_e^1}{2} \sin\phi\sin\theta\right) - \frac{2}{\pi} S(w_e^1,\theta,\phi) \right\} \cdot$$

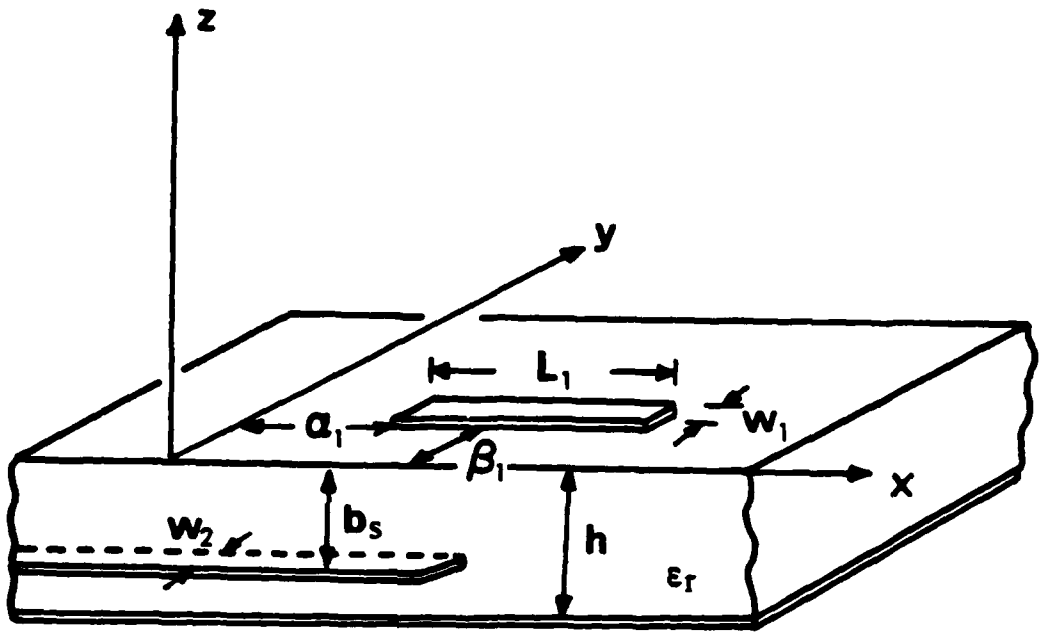

Figure 6.1

Printed Strip Dipole Excited by a Microstrip Transmission Line Embedded in the Dielectric

$$\cdot\, e^{jk_1\beta_1 \sin\phi \sin\theta}\, e^{jk_1 a_1 \sin\theta\cos\phi}$$

$$\sum_{n=1}^{n} I_n e^{jk_1(n\ell_x)\sin\theta\cos\phi} \tag{6.2}$$

where J_o is the zeroth order Bessel function and $S(w_e^1,\theta,\phi)$ is the integral

$$S(w_e^1,\theta,\phi) = \int_o^{\cos^{-1}(w/w_e^1)} \cos\left[k_1 \frac{w_e^1}{2} \sin\phi\sin\theta\cos\sigma\right] d\sigma \tag{6.3}$$

Also, $\vec{R}_s$ is a vector called the substrate factor and has the form

$$\vec{R}_s = \hat{\theta} R_{s\theta} + \hat{\phi} R_{s\phi} \tag{6.4}$$

where

$$R_{s\theta} = -\cos\phi\, \Phi(\varepsilon_r,h,\theta)[\cos\theta + (\varepsilon_r-1)\sin\theta\tan\theta\Lambda(\varepsilon_r,h,\theta)] \tag{6.5}$$

$$R_{s\phi} = \sin\phi\, \Phi(\varepsilon_r,h,\theta) \tag{6.6}$$

and

$$\Phi(\varepsilon_r,h,\theta) = \frac{1}{k_1} \cdot \left\{ \frac{\cos\theta}{\cos\theta - j\sqrt{\varepsilon_r-\sin^2\theta}\, \cot(k_1\sqrt{\varepsilon_r-\sin^2\theta}\, h)} \right\} \tag{6.7}$$

$$\Lambda(\varepsilon_r,h,\theta) = \left\{ \frac{\cos\theta}{\varepsilon_r\cos\theta + j\sqrt{\varepsilon_r-\sin^2\theta}\, \tan(k_1\sqrt{\varepsilon_r-\sin^2\theta}\, h)} \right\} \tag{6.8}$$

6-2. Effect of Substrate Thickness and Permittivity on the Radiation Pattern

An investigation of the expressions given for the far-zone electric field indicates that the effect of the substrate properties on the radiation pattern is controlled by the factors $\Phi(\varepsilon_r,h,\theta)$ and $\Lambda(\varepsilon_r,h,\theta)$. Furthermore, it is verified that $\Phi(\varepsilon_r,h,\theta)$ is a result of the substrate guided TE modes, while $\Lambda(\varepsilon_r,h,\theta)$ is due to the TM modes. A thorough analysis of Φ indicates that it determines the position of the nulls and the principal as well as secondary maxima of the pattern for $\theta < \frac{\pi}{2}$. If one considers the radiation pattern of a strip dipole at resonance, then the number of the lobes and the position of the nulls are totally controlled by the substrate.

A. Number of Lobes

The number of lobes in the radiation pattern can be determined from the equation

$$2\sqrt{\varepsilon_r}\,\frac{h}{\lambda_o} = \left[2\sqrt{\varepsilon_r - 1}\;\;\frac{h}{\lambda_o}\right] + N + a \qquad (6.9)$$

where the brackets indicate the integer value of, N is an integer, and a is an arbitrary real positive number less than one. From equation (6.7), the following cases can be identified:

1) If $N = 0$, there exists a single lobe with maximum at $\theta = 0$.
2) If $N > 0$ and $a > 0$, there exist $2N + 1$ lobes with one of the maxima at $\theta = 0$.

3) If $N > 0$ and $a \to 0+$, there exist 2N lobes with a null at $\theta = 0$.

B. Positions of Nulls ($N > 0$)

From equation (6.9) one can derive the relation

$$\left[2\sqrt{\epsilon_r}\,\frac{h}{\lambda_o}\right] = \left[2\sqrt{\epsilon_r - 1}\,\frac{h}{\lambda_o}\right] + N \qquad (6.10)$$

If it is assumed that

$$\left[2\sqrt{\epsilon_r - 1}\,\frac{h}{\lambda_o}\right] = m$$

then the position of the n^{th} pair of nulls is given by

$$\theta_{n\ 1,2} = \pm\sin^{-1}\sqrt{\epsilon_r - \left(\frac{\kappa}{2h/\lambda_o}\right)^2} \qquad (6.11)$$

where $\kappa = m+n$ and $n = 1,2,\ldots,N$.

The dependence of the $\vec{E}$ and $\vec{H}$-plane normalized radiation power patterns on ϵ_r and h can now be investigated. For a duroid substrate with $\epsilon_r = 2.35$ and for a substrate thickness of $h = 0.2\lambda_o$, equation (6.9) is satisfied for N=0 and $a = 0.613$ and therefore the radiation pattern consists of a single lobe as shown in Figure 6.2a. In light of (6.7), it can be verified that for $h = 0.2\lambda_o$, $0.975\lambda_o$ and $1.05\lambda_o$ the $\vec{E}$ and $\vec{H}$ plane normalized power patterns will have one, two, and three lobes respectively, as shown in Figures 6.2b, 6.3a, 6.3b.

If the substrate thickness h is fixed, e.g., at $h = 0.1016\lambda_o$, then the $\vec{E}$ and $\vec{H}$-plane normalized power patterns are shown in Figures 6.4a, 6.4b and 6.5a for $\epsilon_r = 2$,

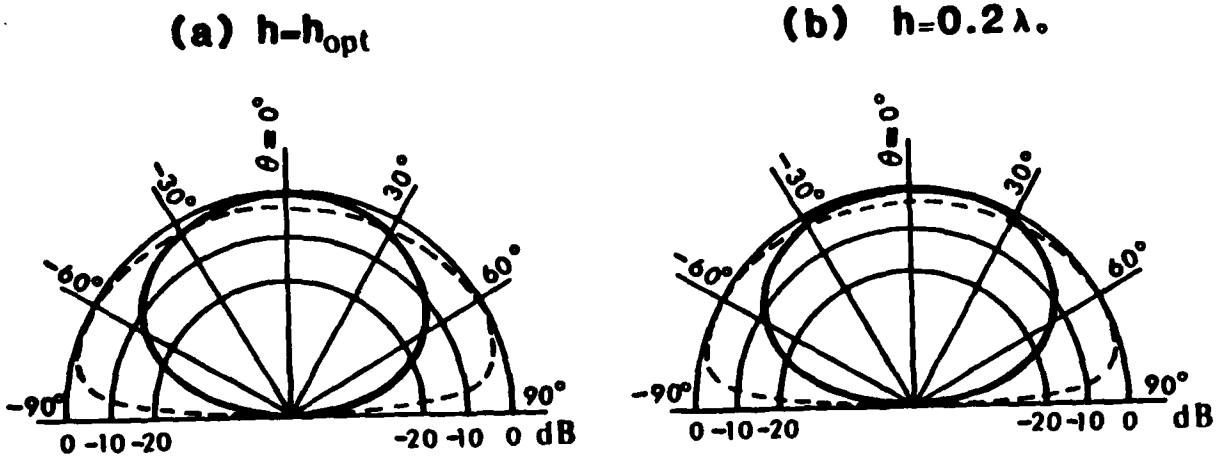

Figure 6.2

Printed Strip Dipole Radiation Patterns.
E- plane, ---- H- plane with ϵ_r=2.35,
w=t=0.0001λ.

(a) h=0.975λ.

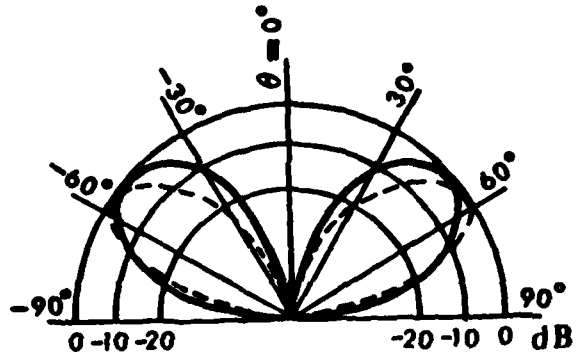

(b) h=1.05λ.

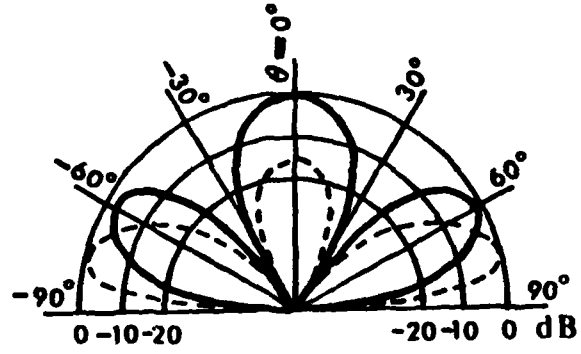

Figure 6.3

Printed Strip Dipole Radiation Patterns
E- plane , ---- H- plane with ϵ_r=2.35,
w=t=0.0001λ.

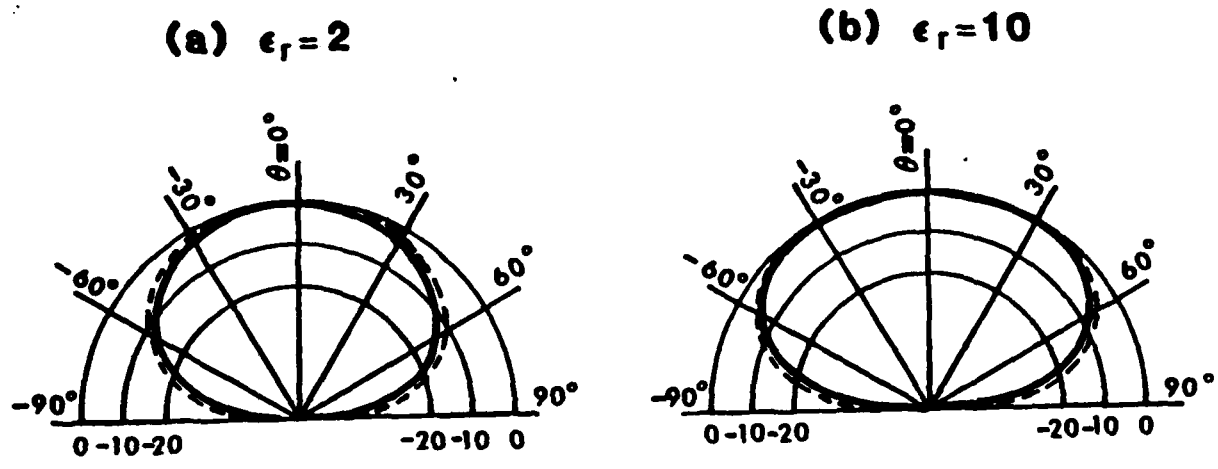

Figure 6.4

Printed Strip Dipole Radiation Patterns
E – plane, ---- H – plane with h=0.1016 λ₀
w=t=0.0001 λ₀

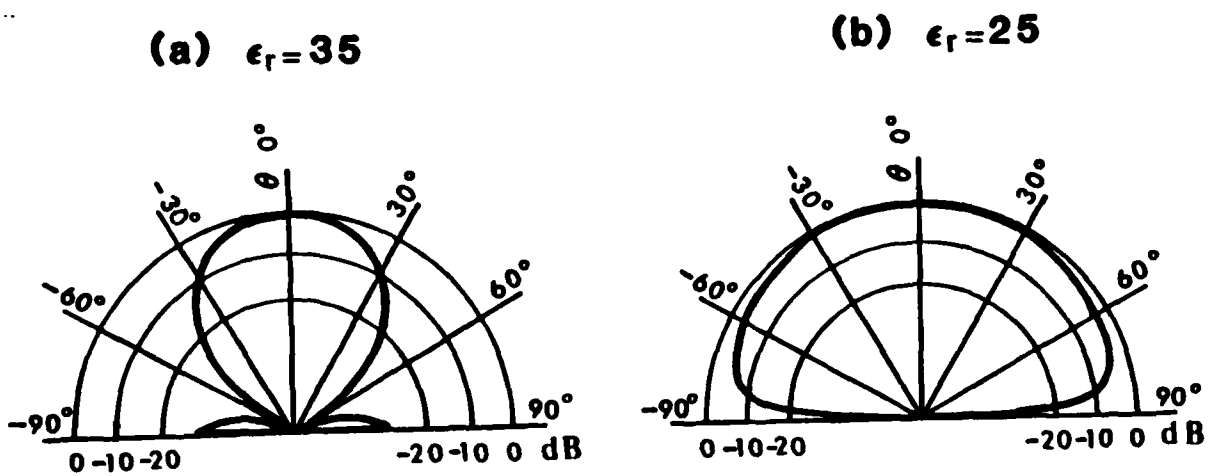

Figure 6.5

Printed Strip Dipole Radiation Patterns

E - plane, ---- H - plane with $h = 0.1016\,\lambda_o$

$w = t = 0.0001\,\lambda_o$

10, 35 respectively. With increasing ε_r, we observe that the PCD directivity is decreased because more energy is radiated close to $\theta = \frac{\pi}{2}$ direction along the length of the antenna as the number of modes guided in the substrate increases. It is further observed in Figure 6.5b that when $\varepsilon_r = 25$ and $h = 0.1016\lambda_o$, there exist three lobes and according to (6.11) the nulls are $\theta = \pm 62.111^{\circ}$. This last case has uncovered an interesting phenomenon which is the radiation at angles θ very close to $\frac{\pi}{2}$. This will be described in the next section.

6-3. Radiation along the Horizon

As mentioned above, an interesting phenomenon is the existence of nonzero radiation close to the horizon in either the $\vec{H}$ or the $\vec{E}$ plane when the electrical thickness of the substrate satisfies specific criteria. In particular, $\vec{H}$-plane radiation along the horizon is seen to occur when a TE surface mode turns on in the substrate and $\vec{E}$-plane radiation close to the horizon is seen to occur when a TM mode is excited and the substrate can support more than one mode. This phenomenon is explained analytically by the coincidence of a pole and a branch point in a Sommerfeld-type integration.

In order to highlight the criteria under which radiation along the horizon takes place, the case of the dipole of Figure 6.1 will be considered in detail. If one studies equations (6.1) - (6.8), it can be seen that the $\vec{H}$- and $\vec{E}$-

plane radiated fields are given by

$$E_\theta(\vec{E}\text{-plane}) = \frac{e^{-jk_1R}}{R} R_a(\phi=0).\ \Phi(\varepsilon_r,h,\theta) \cdot$$

$$\cdot\left[\cos\theta + (\varepsilon_r-1)\ \frac{\sin^2\theta}{\cos\theta}\ \Lambda(\varepsilon_r,h,\theta)\right] \qquad (6.12)$$

and

$$E_\phi(\vec{H}\text{-plane}) = \frac{e^{-jk_1R}}{R} R_a(\phi = \tfrac{\pi}{2})\ \Phi(\varepsilon_r,h,\theta) \qquad (6.13)$$

From equations (6.12) and (6.13), one can obtain

$$\lim_{\theta\to\frac{\pi}{2}} E_\phi = \frac{e^{-jk_1R}}{k_1R} R_a(\phi = \tfrac{\pi}{2}\ ,\ \theta = \tfrac{\pi}{2}) \cdot$$

$$\cdot \lim_{\theta\to\frac{\pi}{2}} \frac{j\cos}{\sqrt{\varepsilon_r-\sin^2\theta}\ \cot(k_1\sqrt{\varepsilon_r-\sin^2\theta}\ h)} \qquad (6.14)$$

In words, the radiated field in the $\vec{H}$-plane tends to zero at the horizon ($\theta\to\pi/2$) unless the denominator also tends to zero as $\theta\to\pi/2$. When $\cot(k_1\sqrt{\varepsilon_r-1}\ h)$ is equal to zero then,

$$2\pi\sqrt{\varepsilon_r-1}\ \frac{h}{\lambda_o} = (2m+1)\ \frac{\pi}{2} \qquad (6.15)$$

$$\sqrt{\varepsilon_r-1}\ \frac{h}{\lambda_o} = \frac{2m+1}{4} \quad m = 0,1,2,\ldots \qquad (6.16)$$

Equation (6.16) is simply the condition for a TE surface wave mode turning on. Equations (6.14) and (6.16) imply that there is nonzero radiation at the horizon in the $\vec{H}$-plane pattern when a TE surface wave mode turns on. For the $\vec{E}$-plane pattern one finds that

$$E_{\substack{\theta \\ \theta \to \frac{\pi}{2}}} = \frac{e^{-jk_1 R}}{k_1 R} R_a(\phi = 0,\ \theta = \tfrac{\pi}{2})\ (\varepsilon_r - 1) \lim_{\theta \to \frac{\pi}{2}} \frac{\cos\theta}{(\varepsilon_r - 1)} = 0 \tag{6.17}$$

Therefore, at $\theta = \frac{\pi}{2}$ the radiation in the $\vec{E}$-plane is always zero. However, it has been observed that for $\theta = \frac{\pi}{2} - b$, where b is a very small angle, the radiation is nonzero when

$$\sqrt{\varepsilon_r - 1}\ \frac{h}{\lambda_o} = \frac{m}{2} \qquad m = 1,2,\ldots \tag{6.18}$$

and when the substrate can support more than one lobe, i.e.,

$$2\sqrt{\varepsilon_r}\ \frac{h}{\lambda_o} = \left[2\sqrt{\varepsilon_r - 1}\ \frac{h}{\lambda_o}\right] + a \tag{6.19}$$

Equation (6.18) combined with (6.19) gives

$$\sqrt{\varepsilon_r - 1}\ \frac{h}{\lambda_o} = \left(\frac{m}{2}\right)^{-} \qquad m=1,2,\ldots \tag{6.20}$$

Equations (6.16) and (6.20) provide a set of curves (see Figure 6.6) which one can use in order to choose the right substrate so that the dipole radiates close to the horizon either in the $\vec{E}$-plane or in the $\vec{H}$-plane. Figure 6.7 shows the $\vec{H}$-plane pattern of a strip dipole at resonance printed on a substrate with $\varepsilon_r = 2.1$ and $h = 0.238\lambda_o$ and Figure 6.8 shows the $\vec{H}$-plane pattern of the same dipole printed on a substrate board with $\varepsilon_r = 2.286$ and $h = 0.6614\lambda_o$. Also, Figure 6.9 shows the $\vec{E}$-plane pattern when $\varepsilon_r = 4$ (Quartz) and $h = 0.285\lambda_o$.

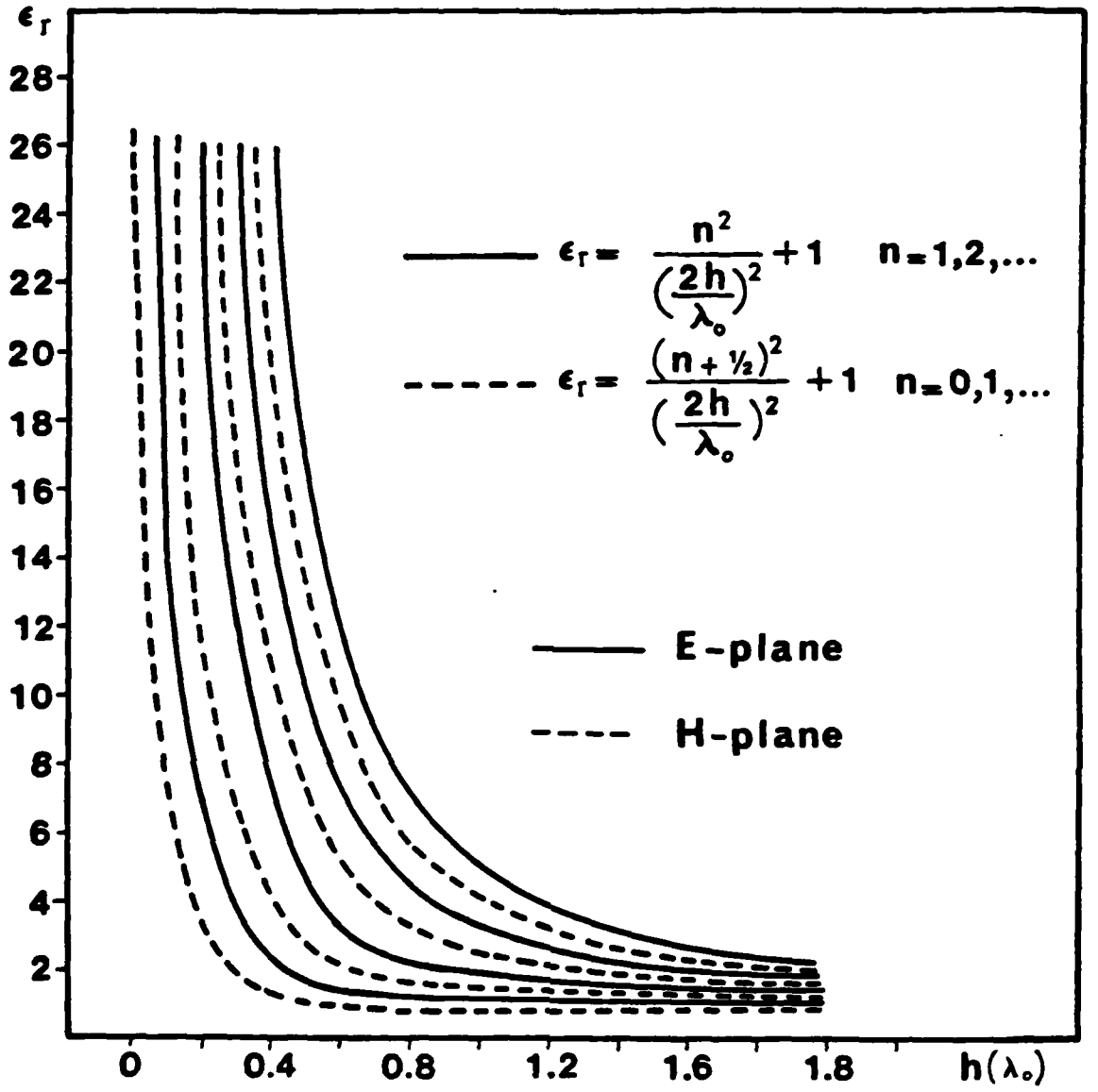

Figure 6.6

Dielectric Constant vs. Substrate Thickness for TE and TM wave Contribution to the H and E - plane Radiation Patterns

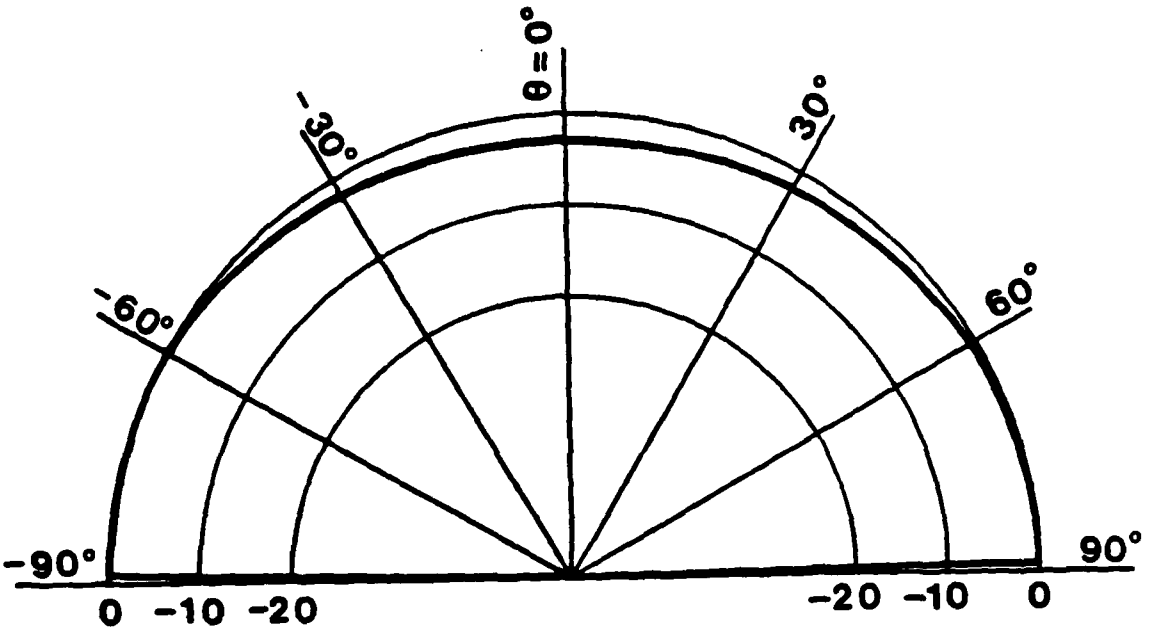

Figure 6.7

H -plane Radiation Pattern of a Printed Strip Dipole with ϵ_r=2.1, h = 0.238 λ_o and w=t=0.0001 λ_o

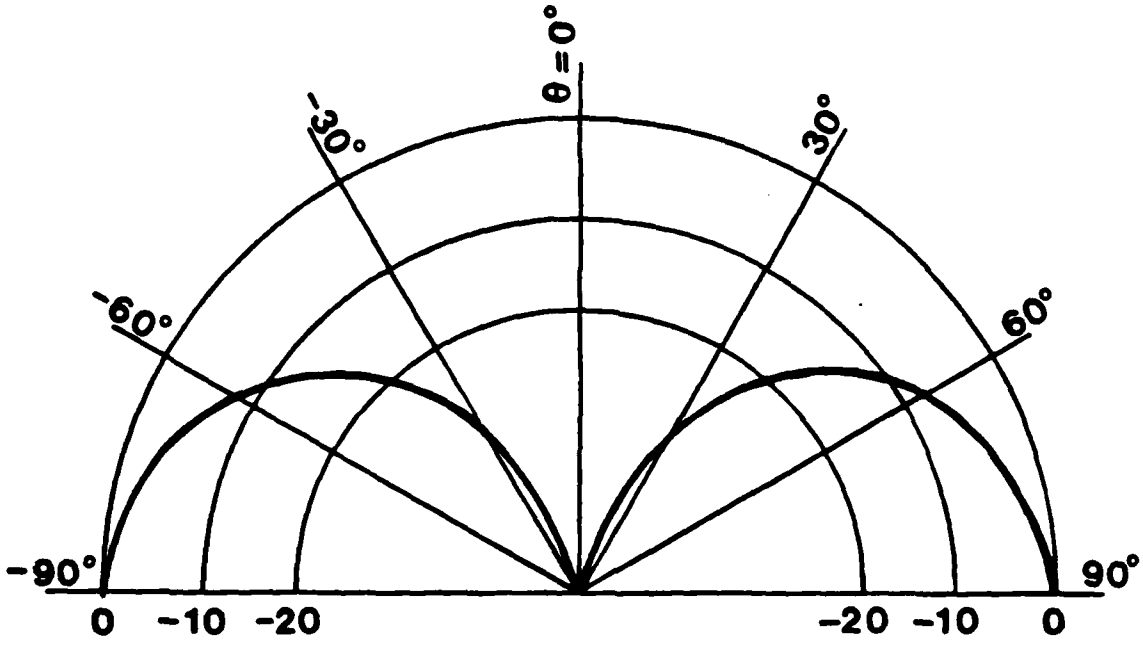

Figure 6.8

H – plane Radiation Pattern of a Printed Strip Dipole with ϵ_r=2.286, h=0.661λ_o and w=t=0.0001λ_o

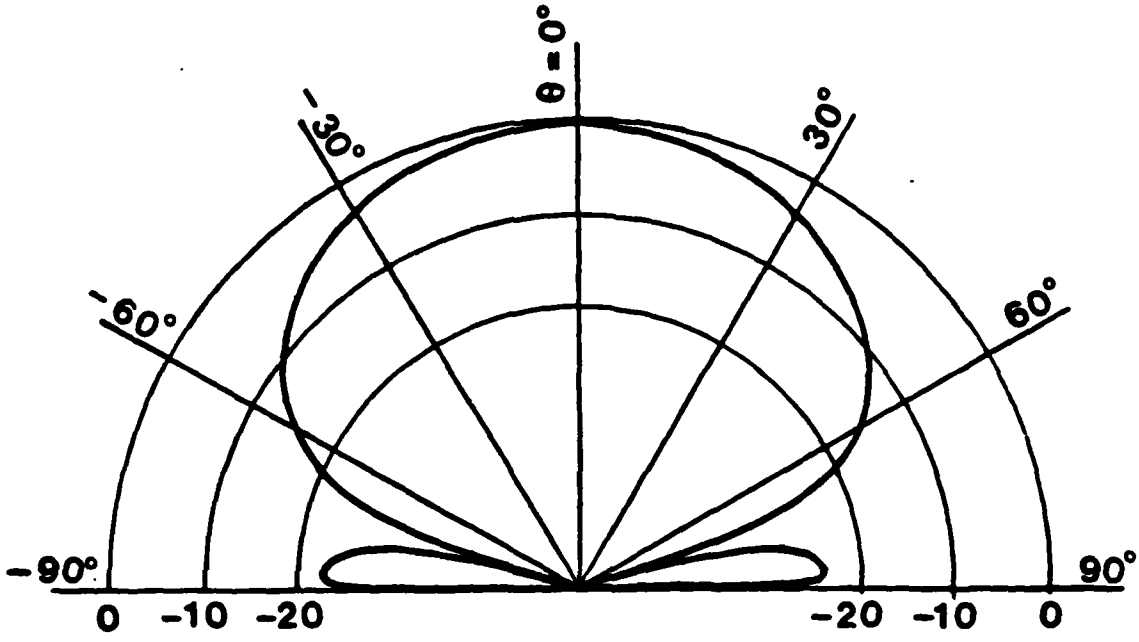

Figure 6.9

E -plane Radiation Pattern of a Printed Strip Dipole with ϵ_r=4 , h=0.285λ_o and w=t=0.0001λ_o

BIBLIOGRAPHY

[1] G. A. Deschamps, "Microstrip Microwave Antennas," 3rd. USAF Symp. on Antennas, 1953.

[2] H. Gutton and G. Baissinot, "Flat Aerial for Ultra High Frequencies," French Patent No. 703113, 1955.

[3] L. Lewin, "Radiation from Discontinuities in Strip Line," in Proc. Inst. Elec. Eng., Vol. 107, Pt. C, Feb., 1960.

[4] E. V. Byron, "A New Flush-Mounted Antenna Element for Phased Array Application," Proc. Phased-Array Antenna Symp., 1970, 1987.

[5] J. Q. Howell, "Microstrip Antennas," Dig. Int. Symp. Antennas Propagat. Soc., Williamsburg, VA, Dec., 1972, 177.

[6] H. D. Weischel, "Progress Report on Development of Microstrip Cylindrical Arrays for Sounding Rockets," Physic. and Sci. Lab., New Mexico State Univ., Las Cruces, 1973.

[7] R. E. Munson, "Single Slot Cavity Antennas Assembly," U.S. Paten No. 3713162, Jan. 23, 1973.

[8] G. G. Sanford, "Conformal Microstrip Phased Array for Aircraft Tests with ATS-6," Proc. Nat. Electronics Conf., Vol. 29, Oct., 1974, 252.

[9] G. W. Garvin, R. E. Munson, L. T. Ostwald, and K. G. Schroeder, "Low Profile Electrically Small Missile Base Mounted Microstrip Antennas," Dig. Int. Symp. Antennas Propagat. Soc., Urbana, IL, June, 1975, 244.

[10] J. Q. Howell, "Microstrip Antennas," IEEE Trans. Antennas Propagat., Vol. AP-23, No. 1, Jan., 1975, 90.

[11] H. D. Weinschel, "A Cylindrical Array of Circularly Polarized Microstrip Antennas," Dig. Int. Symp. Antennas Propagat. Soc., Urbana, IL, June, 1975, 177.

[12] J. R. James and G. J. Wilson, "New Design Technique for Microstrip Antenna Arrays," Proc. 5th European Micro. Conf. Hamburg, Sept., 1975, 102.

[13] R. E. Munson, "Conformal Microstrip Antennas and Microstrip Phased Arrays," IEEE Trans. Antennas Propagat., Vol. AP-22, No. 1, Jan., 1974, 74.

[14] A. G. Derneryd, "Linear Microstrip Array Antennas," Chalmer Univ. Technol. Goteborge, Sweden, Tech. Rep. TR 7505, Oct., 1975.

[15] N. K. Uzunoglu and P. Katehi, "Coupled Microstrip Disc Resonators," IEEE Trans. Microwave Theory and Technique, Vol. MTT-28, No. 2, Feb., 1980, 94.

[16] Y. T. Lo, D. D. Harrison, D. Solomon, G.A. Deschamps, and F. R. Ore, "Study of Microstrip Antennas, Microstrip Phased Arrays and Microstrip Feed Network, Rome Air Development Center, Tech. Rep. TR-77-406, Oct. 21, 1977.

[17] A. G. Derneryd, "A Theoretical Investigation of the Rectangular Microstrip Antenna Element," Rome Air Development Center, Tech. Rep. TR-77-206, June, 1977.

[18] L. C. Shen and S. A. Long, "Low Profile Printed Circuit Antennas," Dept. Elec. Engr., Univ. Houston, Houston, TX, Contract DAAG-29-75-0187, Final Rep., Oct., 1977.

[19] K. R. Carver and E. L. Coffey, "Theoretical Investigation of the Microstrip Antenna," Physic. and Sci. Lab., New Mexico State Univ., Las Cruces, Tech. Rep. PT-00929, Jan. 23, 1979.

[20] A. Waterman and D. G. Henry, "Stripline Strap-on Antenna Array," Abstracts 21st USAF Antenna Symp. Allerton Park, IL, Oct. 12-14, 1971.

[21] K. R. Carver, "A Model Expansion Theory for the Microstrip Antenna," Dig. Int. Symp. AP-S, Seattle, WA, June, 1979, 101.

[22] T.E. Nowicke, "Microwave Substrates, Present and Future," Proc. Workshop Printed Circuit Antenna Tech., New Mexico State Univ., Las Cruces, Oct., 1979, 26/1.

[23] G. R. Traut, "Glad Laminates of PTFE Composites for Microwave Antennas," Proc. Workshop Printed Circuit Antenna Tech., New Mexico State Univ., Las Cruces, Oct., 1979, 27/1.

[24] M. Olyphant, Jr. and T. E. Nowicke, "Microwave Substrates Support MIC Technology," Microwaves, Part 1, Vol. 19, No. 12, Nov., 1980, 74.

[25] I. E. Rana and N. G. Alexopoulos, "Current Distribution and Input Impedance of Printed Dipoles," IEEE Trans. AP, Vol. 29, No. 1, Jan. 1981, 99.

[26] N. G. Alexopoulos and I. E. Rana, "Current Distribution and Input Impedance of Printed Dipoles," Correction, IEEE Trans. on AP, Vol. 30, pp. 822, July, 1982.

[27] N. G. Alexopoulos and I. E. Rana, "Mutual Impedance Computation Between Printed Dipoles," IEEE Trans. AP, Vol. 29, No. 1, Jan., 1981, 106.

[28] E. H. Newman and P. Tulyathan, "Analysis of Microstrip Antennas Using Moments Method, "IEEE Trans. AP, Vol. 29, No. 1, Jan., 1981, 47.

[29] K. K. Mei, "Unimoment Method of Solving Antenna and Scattering Problems," IEEE Trans. AP.

[30] D. B. Rutledge, S. E. Schwarz, and A. T. Adams, "Infrared and Submillimeter Antennas," Infrared Phys., Vol. 18, Dec., 1978, 713.

[31] F. Mizuno, Y. Daiku, and S. Ono, "Design of Printed Resonant Antennas for Monolithic-Diode Detectors," IEEE Trans. MTT, Vol. 25, June, 1977, 470.

[32] D. B. Rutledge, S. E. Schwarz, T. L. Hwang, D. J. Angelako, K. K. Mei, and S. Yokota, "Antennas and Waveguides for Far-Infrared Integrated Circuits," IEEE J-QE, May, 1980, 508.

[33] N. K. Uzunoglu, N. G. Alexopoulos, and J. G. Fikioris, "Radiation Properties of Microstrip Dipoles," IEEE Trans. AP, Vol. 27, Nov., 1979, 853.

[34] R. S. Elliott, "The Green's Function for Electric Dipoles Parallel to and Above or Within a Grounded Dielectric Slab," Hughes Aircraft, Los Angeles, CA, Tech. Rep. 5752.00/072, Feb., 1978.

[35] P. B. Katehi, N. G. Alexopoulos, "On the Effect of Substrate Thickness and Permittivity on Printed Circuit Dipole Properties," IEEE Trans. on AP-S, Vol. AP-31, No. 1, Jan., 1983.

[36] N. G. Alexopoulos, P. B. Katehi, D. B. Rutledge, "Substrate Optimization for Integrated Circuit Antennas," IEEE Trans. on MTT-S, Vol. 31, No. 7, July, 1983.

[37] I. E. Rana, Ph.D. Dissertation, EE, University of California, Los Angeles, 1979, 101.

[38] P. B. Katehi, Master Thesis, Dept. Elect. Engr. University of California, Los Angeles, 1981.

[39] P. B. Katehi, N. G. Alexopoulos, "Real Axis Integration of Sommerfeld Integrals with Applications to Printed Circuit Antennas," J. Math. Phys. (24)3, March, 1983.

[40] D. M. Pozar, "Consideration for Millimeter Wave Printed Antennas," IEEE Trans. on AP, Accepted for Publication.

[41] H. G. Oltman and D. A. Huebner, "Electromagnetically Coupled Microstrip Dipoles," IEEE Trans. on AP-S, Vol. 29, No. 1, Jan., 1981.

[42] R. S. Elliott and G. J. Stern, "The Design of Microstrip Dipole Arrays Including Mutual Coupling, PartI: Theory," IEEE Trans. on AP-S, Vol. 29, No. 5, Sept., 1981.

[43] G. J. Stern and R. S. Elliott, "The Design of Microstrip Dipole Arrays Including Mutual Coupling, Part II: Experiment," IEEE Trans. on AP-S, Vol. 29, No. 5, Sept., 1981.

[44] A. Sommerfeld, "Partial Differential Equations in Physics," Academic Press, New York, 1949.

[45] R. E. Collin, "Field Theory of Guided Waves," McGraw-Hill, New York, 1960.

[46] Chen-To Tai, "Dyadic Green's Functions in Electromagnetics," Intext Educational Publishers, 1971.

[47] L. V. Kantorovich, G. P. Akilov, "Functional Analysis in Normed Spaces," Pergamon Press, Oxford, 1964, pp. 586-587.

[48] R. F. Harrington, "Matrix Methods for Field Problems," Proc. IEEE, Vol. 55, No. 2, Feb. 1967, pp. 136-149.

[49] B. Z. Vulikh, "Introduction to Functional Analysis for Scientists and Technologists," Pergamon Press, Oxford, 1963.

[50] B. Friedman, "Principles and Techniques of Applied Mathematics," John Wiley & Sons, New York, 1956.

[51] J. W. Dettman, "Mathematical Methods in Physics and Engineering," McGraw-Hill Book Co., New York, 1962.

[52] R. F. Harrington, "Field Computation by Moment Methods," Macmillan Company, New York.

[53] T. C. Edwards, "Foundations for Microstrip Circuit Design," John Wiley and Sons Ltd. New York, 1981.

[54] C. N. Kaloi, "Microstrip Antennas, Experimental Results," in Proc. Workshop Printed Circuit Antenna Tech., New Mexico State University, Las Cruces, NM, Oct. 1979, p. 6/1.

[55] D. A. Huebner, "An Electrically Small Microstrip Dipole Planar Array," in Workshop Printed Circuit Antenna Tech., New Mexico State University, Las Cruces, NM, Oct. 1979.

[56] A. A. Oliner, "Microwave Scanning Antennas," Vol. II, Edited by R. C. Hansen, Academic Press, New York, 1966.

[57] N. Bleistein and R. A. Handelsman, "Asymptotic Expansion of Integrals," Holt, Rinehart and Winston, New York, 1975.

[58] L. B. Felsen and N. Marcuvitz, "Radiation and Scattering of Waves," Microwave and Fields Series, Prentice Hall Englewood Cliffs, NJ, 1973.

APPENDIX A

FORMULATION OF POCKLINGTON'S INTEGRAL EQUATION (2.35) IN THE FORM GIVEN BY (2.37)

In Chapter 2 it was shown that the integral equation for the electric field is given by

$$E_x^i(\vec{r}) = \sum_{\nu=1,2} \int_{-w^\nu/2}^{w^\nu/2} dy' \int_0^{L_\nu} dx' \left[k_i^2 F_{\nu xx}^i + \frac{\partial^2 F_{\nu xx}^i}{\partial x^2} + \frac{\partial^2 F_{\nu zx}^i}{\partial x \partial z} \right] J_\nu(x',y',z^\nu). \quad (A.1)$$

If one considers the relationship

$$\frac{\partial F_{\nu zx}^i}{\partial z} = - \frac{\partial F_{\nu z}^i}{\partial x} \quad (A.2)$$

then equation (A.1) can be written as

$$E_x^i(\vec{r}) = \sum_{\nu=1,2} \int_{w^\nu/2}^{w^\nu/2} dy' \int_0^{L_\nu} dx' \left\{ k_i^2 F_{\nu xx}^i + \frac{\partial^2}{\partial x^2} (F_{\nu xx}^i - F_{\nu z}^i) \right\} J_\nu(x',y',z^\nu) \quad (A.3)$$

From equation (A.2) the function $F_{\nu z}^i$ is given by

$$F_{\nu z}^i = -\int dx \frac{\partial}{\partial z} F_{\nu zi}^i = -\int dx \frac{\partial}{\partial z_i} F_{\nu zi}^i \quad (A.4)$$

By substituting (2.28) into (A.4) one can obtain

$$F_{\nu z}^i(\vec{r}/\vec{r}') = 2\left(\frac{j\omega\mu_o}{4\pi k_i^2}\right)(\epsilon_r - 1) \int dx \cos\phi \, \frac{\partial}{\partial z_i} \left\{ \int_0^\infty J_1(\lambda\rho) e^{-u_o z^i \delta_{i1}} \frac{\sinh[u(h - z^\nu + z^\nu \delta_{\nu 1})]}{f_1(\lambda, \epsilon_r, h)} \right.$$

$$\left.\frac{\cos[u(h-z^i+z^i\delta_{i1})]}{f_2(\lambda,\epsilon_r,h)}\right| d\lambda =$$

$$= 2\left(\frac{j\omega\mu_o}{4\pi k_i^2}\right)(\epsilon_r-1)\int dx\,\cos\phi\int_o^\infty J_1(\lambda\rho)e^{-u_o z^i\delta_{i1}} \cdot$$

$$\frac{\left[\delta_{i1}u_o\cosh(uh) - \delta_{i2}u\sinh[u(h-z^i)]\right]}{f_1(\lambda,\epsilon_r,h)} \cdot$$

$$\frac{\left[\delta_{\nu 1}\sinh(uh) + \delta_{\nu 2}\sinh[u(h-z^\nu)]\right]}{f_2(\lambda,\epsilon_r,h)}\lambda^2 d\lambda \quad (A.5)$$

From the relations

$$\rho = [(x-x')^2 + (y-y')^2]^{\frac{1}{2}} \quad (A.6)$$

and

$$\cos\phi = \frac{x-x'}{\rho} \quad (A.7)$$

it is determined that

$$\frac{d\rho}{dx'} = -\cos\phi \quad (A.8)$$

and

$$\frac{dJ_o(\lambda\rho)}{d(\lambda\rho)} = \frac{1}{\lambda}\frac{dJ_o(\lambda\rho)}{dx'}\frac{dx'}{d\rho} =$$

$$= -\frac{1}{\lambda}\frac{dJ_o(\lambda\rho)}{dx'}\frac{1}{\cos\phi} =$$

$$= -J_1(\lambda\rho) \quad (A.9)$$

A substitution of (A.8) and (A.9) into (A.5) yields

$$F^i_{\nu z}(\vec{r}/\vec{r}') = 2\left(\frac{j\omega\mu_o}{4\pi k_i^2}\right)(\epsilon_r-1)\int_o^\infty J_o(\lambda\rho)e^{-u_o z^i\delta_{i1}} \cdot$$

$$\frac{\left[\delta_{i1}u_o\cosh(uh) - \delta_{i2}u\sinh[u(h-z^i)]\right]}{f_1(\lambda,\varepsilon_r,h)}\cdot$$

$$\frac{\left[\delta_{v1}\sinh(uh) + \delta_{v2}\sinh[u(h-z^v)]\right]}{f_2(\lambda,\varepsilon_r,h)}\,\lambda d\lambda \qquad \text{(A.10)}$$

APPENDIX B

EVALUATION OF THE SPACE INTEGRALS IN THE INTERVAL $\lambda\varepsilon[0,A]$

As shown in Chapter 4, the elements of the generalized impedance matrix are given by

$$Z_{mn}^{i\nu} = \int_0^{\nu} \sum_{\nu=1,2} \left[\frac{A^{i\nu}(\lambda,\varepsilon_r,h;z^i,z^\nu)}{f_1(\lambda,\varepsilon_r,h)\cdot f_2(\lambda,\varepsilon_r,h)} \right] \cdot \mathcal{L}_{mn}^{\nu}\{J_o(\lambda\rho)\}d\lambda \tag{B.1}$$

where

$$\mathcal{L}_{mn}\{J_o(\lambda\rho)\} = \frac{\delta(y-y^i)}{[\sin(k\ell_x)]^2} \int_{-w^\nu/2}^{w^\nu/2} dy'\, J_y^\nu(y') \cdot$$

$$\left[E_1 \int_0^{\ell_x} dx \int_0^{\ell_x} dx' \sin[k(\ell_x-x)] \sin[k(\ell_x-x')] \cdot \right.$$

$$[\delta(\rho-\rho_1) + \delta(\rho-\rho_2)+\delta(\rho-\rho_3) + \delta(\rho-\rho_4)] +$$

$$+ E_2 \int_0^{\ell_x} dx \sin[k(\ell_x-x)] \, [\delta(x'+\ell_x) + \delta(x'-\ell_x) -$$

$$\left. -2\cos(k\ell_x)\delta(x')] \cdot [\delta(\rho-\rho_1) + \delta(\rho-\rho_3)] \right] \cdot J_o(\lambda\rho) \tag{B.2}$$

with $\rho_1,\rho_2,\rho_3,\rho_4$ given by equations (4.13) → (4.16) and ρ given by

$$\rho = \{(x-x'+x_m-x_n)^2 + (y-y')^2\}^{\frac{1}{2}} \tag{B.3}$$

The Bessel function in equation (B.2), because of (B.3), can be written as

$$J_o(\lambda\rho) = J_o\{[\lambda^2(x-x'+x_m-x_n)^2 + \lambda^2(y-y')^2]^{\frac{1}{2}}\} =$$

$$= \frac{1}{\pi}\int_o^{\pi} e^{j\lambda(x-x'+x_m-x_n)\cos\theta}\cos(\lambda(y-y')\sin\theta)d\theta \qquad (B.4)$$

If one substitutes (B.4) into (B.2) and interchanges the order of integration, the multiple space integrals $\mathcal{L}_{mn}^{\nu}\{J_o(\lambda\rho)\}$ take the form

$$\mathcal{L}_{mn}^{\nu}\{J_o(\lambda\rho)\} = \frac{\delta(y-y^i)}{[\sin(k\ell_x)]^2}\cdot\frac{1}{\pi}\int_o^{\pi}d\theta\, e^{j\lambda(x_m-x_n)\cos\theta}$$

$$\left[E_1\int_o^{\ell_x}dx\int_o^{\ell_x}dx'\,\sin[k(\ell_x-x)]\sin[k(\ell_x-x')]\cdot\right.$$

$$[e^{j\lambda(x+x')\cos\theta} + e^{j\lambda(x-x')\cos\theta} + e^{j\lambda(-x+x')\cos\theta} +$$

$$+ e^{j\lambda(-x-x')\cos\theta}] + E_2\left[e^{j\lambda\ell_x\cos\theta} + e^{-j\lambda\ell_x\cos\theta} -\right.$$

$$\left.- 2\cos(k\ell_x)\right]\cdot\int_o^{\ell_x}dx\,\sin[k(\ell_x-x)]\,[e^{j\lambda x\cos\theta} +$$

$$\left.+ e^{-j\lambda x\cos\theta}]\right]\cdot\int_{-w^{\nu}/2}^{w^{\nu}/2}dy'J_y^{\nu}(y')\cos(\lambda(y-y')\sin\theta) \qquad (B.5)$$

Equation (B.5), with the use of the equality

$$2\cos a = e^{ja} + e^{-ja} \qquad (B.6)$$

can give

$$\mathcal{L}_{mn}^{\nu}\{J_o(\lambda\rho)\} = \frac{\delta(y-y^i)}{[\sin(k\ell_x)]^2}\cdot\frac{4}{\pi}\int_o^{\pi}d\theta\, e^{j\lambda(x_m-x_n)\cos\theta}\cdot$$

$$\cdot \int_{-w^{\nu}/2}^{w^{\nu}/2} dy'\, J_y^{\nu}(y')\cos(\lambda(y-y')\sin\theta) \cdot$$

$$\int_0^{\ell_x} dx\, \sin[k(\ell_x-x)]\cos(\lambda x\cos\theta) \cdot$$

$$\left| E_1 \int_0^{\ell_x} dx'\, \sin[k(\ell_x-x')]\cos(\lambda x'\cos\theta) \; + \right.$$

$$\left. + E_2[\cos(\lambda\ell_x\cos\theta) - \cos(k\ell_x)] \right| \qquad (B.7)$$

In equation (B.7) if one applies straightforward integration, interchanges the order of integration and assumes that

$$\int_{-w^{\nu}/2}^{w^{\nu}/2} dy' J_y^{\nu}(y') J_o(\lambda\rho_{mn}) = J_o(\lambda x_{mn}) \qquad (B.8)$$

with $x_{mn} = |x_m - x_n|$ and $\rho_{mn} = \{(x_m-x_n)^2 + (y-y')^2\}^{\frac{1}{2}}$, then equation (B.7) can be written as

$$\mathcal{L}_{mn}\{J_o(\lambda\rho)\} = \sum_{\sigma=0}^{\infty} \left| A_{2\sigma}\left(\frac{\ell_x}{\lambda_o}\right)^{2\sigma} \frac{d^{2\sigma}}{d|x|^{2\sigma}} J_o(\lambda x_{mn}) + \right.$$

$$+ B_{\sigma}\left(\frac{\ell_x}{\lambda_o}\right)^{\sigma} \frac{d^{\sigma}}{d|x|^{\sigma}} [J_o(\lambda x_{m(n+1)} + J_o(\lambda x_{mn})$$

$$\left. + J_o(x_{m(n-1)})] \right| \qquad (B.9)$$

where $A_{2\sigma}$, B_{σ} are constant coefficients.

APPENDIX C

FORMULATION OF THE INTEGRAL (4.20) FOR THE TAIL CONTRIBUTION

If we choose A in such a way that

$$\coth[(A^2-k_2^2)^{\frac{1}{2}}h] \doteq 1 \tag{C.1}$$

then in the integral

$$Z_{mn}^{i\nu}(\infty) = \int_A^\infty \sum_{\nu=1,2} \left[\frac{A^{i\nu}(\lambda,\varepsilon_r,h;z^i,z^\nu)}{f_1(\lambda,\varepsilon_r,h)\cdot f_2(\lambda,\varepsilon_r,h)}\right] \mathcal{L}_{mn}^{\nu}\{J_o(\lambda\rho)\} \tag{C.2}$$

with

$$A^{i\nu}(\lambda,\varepsilon_r,h;z^i,z^\nu) = [E_1(k_1^2-k^2)+E_2k]\cdot \mathcal{F}_{\nu xx}^{i}(\lambda,\varepsilon_r,h;z^i,z^\nu)$$

$$+ [E_1k^2-E_2k]\cdot \mathcal{F}_{\nu z}^{i}(\lambda,\varepsilon_r,h;z^i,z^\nu) \tag{C.3}$$

and

$$\mathcal{F}_{\nu xx}^{i}(\lambda,\varepsilon_r,h;z^i,z^\nu) = 2\left(\frac{j\omega\mu_o}{4\pi k_i^2}\right) e^{-u_o z^i}\delta_{i1} \cdot$$

$$\cdot \{1-\delta_{i2}\delta_{\nu2}+\delta_{i2}\delta_{\nu2}[u\cosh(uz^\nu) + u_o\sinh(uz^\nu)]\} \cdot$$

$$\cdot \sinh[u(h-z^\nu + z^\nu\delta_{i1}\delta_{\nu1})] \cdot f_2(\lambda,\varepsilon_r,h)\lambda \tag{C.4}$$

$$\mathcal{F}_{\nu z}^{i}(\lambda,\varepsilon_r,h;z^i,z^\nu) = 2\left(\frac{j\omega\mu_o}{4\pi k_i^2}\right) e^{-u_o z^i}\delta_{i1}\,(\varepsilon_r-1) \cdot$$

$$\{\delta_{i1}u_o\cosh(uh) - \delta_{i2}u\sinh[u(h-z^i)]\}\cdot$$

$$\{\delta_{\nu1}\sinh(uh) + \delta_{\nu2}\sinh[u(h-b_s)]\}\,\lambda \tag{C.5}$$

the functions $f_1(\lambda,\varepsilon_r,h)$, $f_2(\lambda,\varepsilon_r,h)$ can be approximated by

$$f_1(\lambda,\varepsilon_r,h) = \sinh(uh)(u_o+u) \tag{C.6}$$

and

$$f_2(\lambda,\varepsilon_r,h) = \sinh(uh)(\varepsilon_r u_o+u) \tag{C.7}$$

In equations (C.2) → (C.5), the z-coordinate for the source currents (z^ν) and observation points (z^i) is given by

$$z^i = \begin{cases} t & i=1 \\ -b_s+t & i=2 \end{cases} \qquad z^\nu = \begin{cases} 0 & \nu=1 \\ -b_s & \nu=2 \end{cases} \tag{C.8}$$

If one substitutes (C.6) and (C.7) into (C.4), then the function $\mathcal{F}^i_{\nu xx}(\lambda,\varepsilon_r,h;z^i,z^\nu)$ can be written as

$$\begin{aligned} \mathcal{F}^i_{\nu xx}(\lambda,\varepsilon_r,h;z^i,z^\nu) = 2\left(\frac{j\omega\mu_o}{4\pi k_i^2}\right)\Bigg\{ & \delta_{i1}\delta_{\nu1}\,\frac{\lambda}{u_o}\,\frac{e^{-u_o t}}{1+\frac{u}{u_o}} + \\ & + (\delta_{i1}\delta_{\nu2}+\delta_{i2}\delta_{\nu1})\frac{\lambda}{u}\,\frac{e^{-u_o t}\,e^{-ub_s}}{1+\frac{u_o}{u}} + \\ & + \delta_{i2}\,\delta_{\nu2}\,\frac{\lambda}{u}\left\{e^{-ut}+\frac{1-\frac{u_o}{u}}{1+\frac{u_o}{u}}\,e^{-u(2b_s-t)}\right\}\Bigg\} f_1(\lambda,\varepsilon_r,h) \end{aligned} \tag{C.9}$$

Similarly, the function $\mathcal{F}^i_{\nu z}(\lambda,\varepsilon_r,h;z^i,z^\nu)$ can be approximated by

$$\mathcal{F}^i_{\nu z}(\lambda,\varepsilon_r,h;z^i,z^\nu) = 2\left(\frac{j\omega u_o}{4\pi k_i^2}\right) \cdot$$

$$\left\{ \delta_{i1}\delta_{\nu 1} \frac{\lambda}{u_o} e^{-u_o t}\left(\frac{1}{1+\frac{u}{u_o}} - \frac{1}{\varepsilon_r + \frac{u}{u_o}}\right) + \right.$$

$$+ (\delta_{i1}\delta_{\nu 2} + \delta_{i2}\delta_{\nu 1})\frac{\lambda}{u} e^{-u_o t} e^{-ub_s}\left(\frac{1}{1+\frac{u_o}{u}} - \frac{1}{1+\varepsilon_r \frac{u_o}{u}}\right) +$$

$$\left. + \delta_{i2}\delta_{\nu 2} \frac{\lambda}{u} e^{-u(2b_s - t)}\left(\frac{1}{1+\frac{u_o}{u}} - \frac{\varepsilon_r}{1+\varepsilon_r \frac{u_o}{u}}\right)\right\} \quad (C.10)$$

In equations (C.9) and (C.10) u_o,u are functions of λ given by

$$u_o = (\lambda^2 - k_1^2)^{\frac{1}{2}} \quad (C.11)$$

$$u = (\lambda^2 - k_2^2)^{\frac{1}{2}} \quad (C.12)$$

Because of (C.10) and (C.11), the functions $1 + \frac{u_o}{u}$, $1 + \frac{u}{u_o}$, $\varepsilon_r + \frac{u}{u_o}$, $1 + \varepsilon_r \frac{u_o}{u}$ in (C.9) can be written as

$$1 + \frac{u}{u_o} = \frac{1}{2}\{1 - e_2(\lambda)\}^{-1} \quad (C.13)$$

$$1 + \frac{u_o}{u} = \frac{1}{2}\{1 + e_4(\lambda)\}^{-1} \quad (C.14)$$

$$\varepsilon_r + \frac{u}{u_o} = \frac{1}{\varepsilon_r + 1}\{1 - e_3(\lambda)\}^{-1} \quad (C.15)$$

$$1 + \varepsilon_r \frac{u_o}{u} = \frac{1}{\varepsilon_r + 1}\{1 + e_6(\lambda)\}^{-1} \quad (C.16)$$

where

$$0 \leq e_2(\lambda) \leq \frac{1}{4} \frac{k_2^2 - k_1^2}{A^2 - k_1^2} \quad (C.17)$$

$$0 \leq e_3(\lambda) \leq \frac{1}{2(\epsilon_r+1)} \cdot \frac{k_2^2-k_1^2}{A^2-k_1^2} \tag{C.18}$$

$$0 \leq e_4(\lambda) \leq \frac{1}{4} \cdot \frac{k_2^2-k_1^2}{A^2-k_2^2} \tag{C.19}$$

$$0 \leq e_6(\lambda) \leq \frac{2\epsilon_r}{1+\epsilon_r} \cdot \frac{k_2^2-k_1^2}{A^2-k_2^2} \tag{C.20}$$

Also, in equations (C.9) and (C.10), the function $e^{-(u_o t + ub_s)}$ can be approximated by

$$e^{-(u_o t + ub_s)} = e^{-ut^*} \tag{C.21}$$

where

$$t^* = b_s + t[1+2e_4(\lambda)] \tag{C.22}$$

If one substitutes (C.13) - (C.16) and (C.21) into (C.9) and (C.10), equation (C.2) takes the form

$$Z_{mn}^{i\nu}(\infty) = \left(\frac{j\omega\mu_o}{4\pi k_i^2}\right) \sum_{\nu=1,2} \left\{ \int_{(A^2-k_1^2)^{1/2}}^{\infty} D_1(\lambda) e^{-u_o t} \cdot \right.$$

$$\cdot \mathcal{L}_{mn}^{\nu}\{J_o(\lambda\rho)\}du_o + \int_{(A^2-k_2^2)^{1/2}}^{\infty} D_2(\lambda) e^{-ut^*} \cdot$$

$$\cdot \mathcal{L}_{mn}^{\nu}\{J_o(\lambda\rho)\}\, du + \int_{(A^2-k_2^2)^{1/2}}^{\infty} D_3(\lambda) e^{-u(2b_s-t)} \cdot$$

$$\left. \cdot \mathcal{L}_{mn}^{\nu}\{J_o(\lambda\rho)\}\, du \right\} \tag{C.23}$$

where

$$D_1(\lambda) = \left| [E_1(k_1^2-k^2)+E_2k] \frac{\delta_{i1}\delta_{\nu 1}}{1-e_2(\lambda)} + [E_1k^2-E_2k] \cdot \delta_{i1}\delta_{\nu 1} \cdot \left(\frac{1}{1-e_2(A)} - \frac{2}{\varepsilon_r-1} \cdot \frac{1}{1-e_3(A)}\right)\right| \tag{C.24}$$

$$D_2(\lambda) = \left| [E_1(k_1^2-k^2) + E_2k] \cdot \frac{\delta_{i1}\delta_{\nu 2}+\delta_{i2}\delta_{\nu 1}+\left(1+e_4(\lambda)\right)\delta_{i2}\delta_{\nu 2}}{1 + e_4(\lambda)} + \right.$$

$$+ [E_1k^2-E_2k](\delta_{i1}\delta_{\nu 2}+\delta_{i2}\delta_{\nu 1}) \cdot \left. \cdot \left(\frac{1}{1+e_4(\lambda)} - \frac{2}{\varepsilon_r+1} \cdot \frac{1}{1+e_6(\lambda)}\right)\right| \tag{C.25}$$

$$D_3(\lambda) = \left| - [E_1(k_1^2-k^2) + E_2k] \frac{e_4(\lambda)\delta_{i2}\delta_{\nu 2}}{1+e_4(\lambda)} + \delta_{i2}\delta_{\nu 2} \cdot \left(\frac{1}{1+e_4(\lambda)} - \frac{2\varepsilon_r}{1+\varepsilon_r} \cdot \frac{1}{1+e_6(\lambda)}\right)\right| \tag{C.26}$$

From all the equations above one can conclude that

$$|D_1(\lambda)-D_1(A)| \leq |D_1(\infty)-D_1(A)| = O(A^{-2}) \tag{C.27}$$

Therefore, equation (C.25) can be written as

$$Z^i_{mn}(\infty) = \left(\frac{j\omega\mu_o}{4\pi k_i^2}\right) \sum_{\nu=1,2} \left| D_1(A) \int_{(A^2-k_1^2)^{\frac{1}{2}}}^{\infty} e^{-u_o t} \mathcal{L}^{\nu}_{mn}\{J_o(u_o\rho_1^*)\}du_o \right.$$

$$+ D_2(A) \int_{(A^2-k_2^2)^{\frac{1}{2}}}^{\infty} e^{-ut^*} \mathcal{L}_{mn}^{\nu} \{J_o(u\rho_2^*)\}\, du +$$

$$+ D_3(A) \int_{(A^2-k_2^2)^{\frac{1}{2}}}^{\infty} e^{-u(2b_s-t)} \mathcal{L}_{mn}^{\nu} \{J_o(u\rho_2^*)\} du +$$

$$+ 0\left(A^{-2}\, Z_{mn}^{i\nu}(\infty)\right) \qquad \text{(C.28)}$$

where

$$\rho_1^* = \rho\left(1 + e_1(A)\right) \qquad \text{(C.29)}$$

and

$$\rho_2^* = \rho\left(1 + e_5(A)\right) \qquad \text{(C.30)}$$

APPENDIX D

FAR-ZONE ELECTRIC FIELD OF A PRINTED STRIP DIPOLE

The far-field due to a printed strip dipole (see Figure 6.1) is given by

$$E_\theta \sim k_1^2[\cos\theta\cos\phi\Pi_x - \sin\theta\Pi_z] \tag{D.1}$$

and

$$E_\phi \sim k_1^2[-\sin\phi\Pi_x] \tag{D.2}$$

where

$$\Pi_x = -\frac{j\omega\mu_o}{4\pi k_1^2}\int_{a_1}^{L+a_1}dx'\int_{-w/2+b_1}^{w/2+b_1}dy'\,J(x',y')\cdot$$

$$\int_{-\infty}^{+\infty}H_o^{(2)}(\lambda\rho)e^{-u_o z}\frac{\sinh(uh)}{f_1(\lambda,\epsilon_r,h)}\lambda d\lambda \tag{D.3}$$

and

$$\Pi_z = -\frac{j\omega\mu_o}{4\pi k_1^2}(1-\epsilon_r)\cos\phi\int_{a_1}^{L+a_1}dx'\int_{-w/2+b_1}^{w/2+b_1}dy'\cdot$$

$$\cdot\,J(x',y')\int_{-\infty}^{+\infty}H_1^{(2)}(\lambda\rho)\,e^{-u_o z}\cdot$$

$$\cdot\frac{\sinh(uh)}{f_1(\lambda,\epsilon_r,h)}\cdot\frac{\cosh(uh)}{f_2(\lambda,\epsilon_r h)}\lambda^2 d\lambda \tag{D.4}$$

In equation (D.3) and (D.4), $J(x',y')$ is the current density on the strip dipole

$$J(x',y') = \frac{\pi}{2w_e^1} \frac{1}{\sqrt{1-\left(\frac{2y'}{w_e^1}\right)^2}} \sum_{n=1}^{N} I_n J_{nx}(x') \qquad (D.5)$$

with $J_{nx}(x)$ given by equation (3.21) and $f_1(\lambda,\varepsilon_r,h)$, $f_2(\lambda,\varepsilon_r,h)$ given by equations (2.31), (2.32). If the substitutions $\lambda = k_1 \sin a$, $z = r\cos\theta$, $\rho = r\sin\theta$ are introduced (where r,θ,ϕ describe the far-field in spherical coordinates) together with the large argument asymptotic expansions for $H_o^{(2)}(\lambda\rho)$, $H_1^{(2)}(\lambda\rho)$, Equations (D.3) and (D.4) can be written as

$$\Pi_x = -\frac{j\omega\mu_o}{4\pi} \sqrt{\frac{2j}{\pi r k_1}} \int_{a_1}^{L+a_1} dx' \int_{-w/2+b_1}^{w/2+b_1} dy' J(x',y') \cdot$$

$$\int_{-\infty}^{+\infty} f(\varepsilon_r,h,a) e^{-jrk_1\cos(\theta-a)} da \qquad (D.6)$$

$$\Pi_z = -\frac{j\omega\mu_o}{4\pi} \sqrt{\frac{2j}{\pi r k_1}} (1-\varepsilon_r)\cos\phi \int_{a_1}^{L+a_1} dx' \int_{-w/2+b_1}^{w/2+b_1} dy' \cdot$$

$$\cdot J(x',y') \int_{-\infty}^{+\infty} g(\varepsilon_r,h,a)\, e^{-jrk_1\cos(\theta-a)} da$$

(D.7)

where

$$f(\varepsilon_r,h,a) = j \frac{\sin a \cos a}{\sqrt{\sin\theta \sin a}} \frac{\sin(k_1\sqrt{\varepsilon_r-\sin^2 a}\, h)}{f_1(a,\varepsilon_r,h)} \qquad (D.8)$$

and

$$g(\varepsilon_r,h,a) = -k_1 \frac{\sin^2 a \cos a}{\sqrt{\sin\theta \sin a}} \cdot \frac{\sin(k_1\sqrt{\varepsilon_r-\sin^2 a}\ h)}{f_1(a,\varepsilon_r,h)} \cdot$$

$$\cdot \frac{\cos(k_1\sqrt{\varepsilon_r-\sin^2 a}\ h)}{f_2(a,\varepsilon_r,h)} \qquad (D.9)$$

The integrals with respect to a in equations (D.6) and (D.7) have a stationary point at a = θ. Therefore, one can apply the stationary phase technique for the evaluation of these integrals and Π_x, Π_z are given by

$$\Pi_x = -\frac{j\omega\mu_o}{4\pi}\sqrt{\frac{2j}{\pi r k_1}} \int_{a_1}^{L+a_1} dx' \int_{-w/2+b_1}^{w/2+b_1} dy' J(x',y') \cdot$$

$$\cdot f(\varepsilon_r,h,\theta) \int_{-\infty}^{+\infty} e^{-jrk_1\cos(\theta-a)}\, da \qquad (D.10)$$

$$\Pi_z = -\frac{j\omega\mu_o}{4\pi}\sqrt{\frac{2j}{\pi r k_1}}\,(1-\varepsilon_r)\cos\phi \int_{a_1}^{L+a_1} dx' \int_{-w/2+b_1}^{w/2+b_1} dy' \cdot$$

$$\cdot J(x',y')\, g(\varepsilon_r,h,\theta) \int_{-\infty}^{+\infty} e^{-jrk_1\cos(\theta-a)}\, da \qquad (D.11)$$

If the substitutions $r = R - x'\sin\theta\cos\phi - y'\sin\phi\sin\theta$, $\frac{1}{r} \sim \frac{1}{R}$ then the stationary phase method yields (D.12)

$$\Pi_x = -\frac{j\omega\mu_o}{2\pi}\,\frac{e^{-jk_1R}}{k_1R}\,\Phi(\varepsilon_r,h,\theta) \cdot I \qquad (D.13$$

and

$$\Pi_z = \frac{j\omega\mu_o}{2\pi}\,\frac{e^{-jk_1R}}{k_1R}\,(\varepsilon_r-1)\cos\phi\tan\theta\,\Phi(\varepsilon_r,h,\theta) \cdot \Lambda(\varepsilon_r,h,\theta) \cdot I \qquad (D.14)$$

where

$$\Phi(\varepsilon_r,h,\theta) = \frac{1}{k_1} \cdot \left| \frac{\cos\theta}{\cos\theta - j\sqrt{\varepsilon_r - \sin^2\theta}\,\cot(k_1\sqrt{\varepsilon_r - \sin^2\theta}\,h)} \right| \tag{D.15}$$

$$A(\varepsilon_r,h,\theta) = \left| \frac{\cos\theta}{\varepsilon_r\cos\theta + j\sqrt{\varepsilon_r - \sin^2\theta}\,\tan(k_1\sqrt{\varepsilon_r - \sin^2\theta}\,h)} \right| \tag{D.16}$$

and

$$I = \frac{2}{\pi w_e^1} \int_{a_1}^{L+a_1} dx'\, e^{jk_1x'\sin\theta\cos\phi} \int_{-w/2+b_1}^{w/2+b_1} dy'\, e^{jk_1y'\sin\phi\sin\theta} \cdot$$

$$\cdot \frac{1}{\sqrt{1-\left(\frac{2y'}{w_e^1}\right)^2}} \cdot \sum_{n=1}^{N} I_n J_{nx}(x') \tag{D.17}$$

After straightforward integration the integral I takes the form

$$I = 2\left\{ \frac{\cos(k_1\ell_x\sin\theta\cos\phi) - \cos(k\ell_x)}{k\sin(k\ell_x)\left[1 - \frac{k_1^2}{k^2}\sin^2\theta\cos^2\phi\right]} \right\} \cdot$$

$$\cdot \left| J_o\left(k_1 \frac{w_e^1}{2}\sin\phi\sin\theta\right) - \frac{2}{\pi} S(w_e^1,\theta,\phi) \right| \cdot$$

$$\cdot e^{jk_1b_1\sin\phi\sin\theta}\, e^{jk_1a_1\sin\theta\cos\phi} \cdot$$

$$\sum_{n=1}^{n} I_n e^{jk_1(n\ell_x)\sin\theta\cos\phi} \tag{D.18}$$

where

$$S(w_e^1,\theta,\phi) = \int_o^{\cos^{-1}(w/w_e^1)} \cos\left[k_1 \frac{w_e^1}{2}\sin\phi\sin\theta\cos\sigma\right] d\sigma \tag{D.19}$$

From all the above, one can conclude that

$$\vec{E}(R,\theta,\phi) = \frac{e^{-jk_1 R}}{R} R_a \vec{R}_s \tag{D.20}$$

where

$$R_a = j\ 60\ I \tag{D.21}$$

and

$$\vec{R}_s = \hat{\theta} R_{s\theta} + \hat{\phi} R_{s\phi} \tag{D.22}$$

with

$$R_{s\theta} = -\cos\phi\ \Phi(\varepsilon_r,h,\theta)[\cos\theta + (\varepsilon_r-1)\sin\theta\tan\theta \cdot \cdot \Lambda(\varepsilon_r,h,\theta)] \tag{D.23}$$

and

$$R_{s\phi} = \sin\phi\ \Phi(\varepsilon_r,h,\theta) \tag{D.24}$$

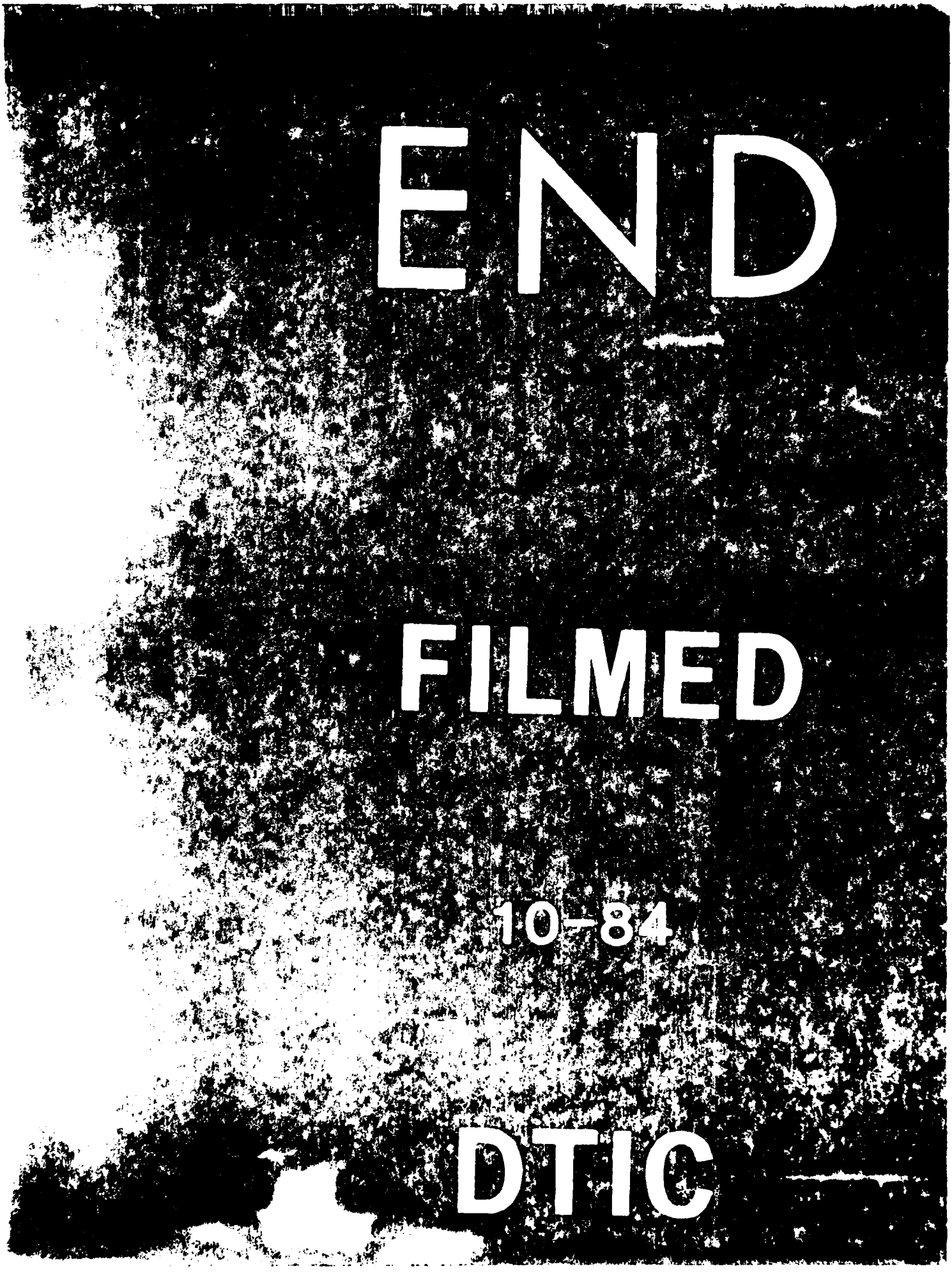
END
FILMED
10-84
DTIC